Modeling Bio-Dust Combustion in Suspension Firing

Leth-Espensen, Anna

Publication date:
2019

Document Version
Publisher's PDF, also known as Version of record

Modeling Bio-Dust Combustion in Suspension Firing

Ph.D. Thesis
by
Anna Leth-Espensen

April 2019

DTU Chemical Engineering
Department of Chemical and Biochemical Engineering

DTU Chemical Engineering
Center for Combustion and Harmful Emission Control
Department of Chemical and Biochemical Engineering
Technical University of Denmark

Søltofts Plads 229
2800 Kongens Lyngby
Denmark
Phone +45 4525 2800

www.kt.dtu.dk

Abstract

During the past decades there has been an increasing focus on climate change, and consequently also a demand for energy production methods with a lower net CO_2 emission. One possible options is suspension firing of biomass. The focus in this thesis has been to model the biomass devolatilization as happening in pulverized fuel fired boilers. The aim has been to add to the knowledge on suspension firing and consequently allow for an increased scientific basis for development of new biomass boilers and optimization of already exciting plants.

The thesis is divided into a literature study and three main parts. The literature review briefly covers the basics of biomass particle devolatilization. Devolatilization is a subprocess happening during combustion of a biomass particle. It is the release of volatiles from the particle after heat up and evaporation of water and before the oxidation of said volatiles and the remaining char. Devolatilization can also happen concurrently with evaporation and oxidation processes, but for simplicity, the phenomena are often considered and modeled separately. The literature study also describes suspension firing equipment and conditions, which include high heating rates ($>$ 10^3 K/s), high maximum temperatures ($>$ 1300 K), and small particle diameters ($<$ 3 mm).

The first model presented in the thesis is based on multivariate data analysis, and estimates the char yield obtained from high heating rate pyrolysis. The char yield differs markedly when performing devolatilization at low and high heating rates, so the heating rate is an important factor to include, if one wants a model, which can adequately predict char yield obtained under suspension firing conditions. The model presented here is simple yet accurate and validated against experimental data. It can be used to define important input parameters for computational fluid dynamics (CFD) or other rigorous devolatilization models.

The second model presented in this thesis revolves around the influence of biomass particle morphology on devolatilization under suspension firing conditions. Biomass particles are typically more elongated than the historically combusted coal particles, which have often been modeled as spheres. Spheres are one dimensional in nature and thus easier to implement in models, consequently this has typically also been the approach for biomass particles. The best simple geometry to mimic the shape of elongated biomass particles is, however, the cylinder. Here a model is presented, which accounts for gradients in temperature and mass, and can describe the devolatilization of both spherical and cylindrical particles. Thereby, differences in devolatilization of different particle morphologies can be compared. The model has been compared to relevant experimental data from literature and shows good agreement.

The third model presented in this thesis is also based on multivariate data analysis and aims to include the gradient effects in the cylindrical model without adding to the computational costs in a CFD simulation. This is done by including the heat transfer limitations in the parameters of the kinetic scheme. By lumping the kinetic and the heat transfer limitations in one single first order reaction (SFOR) a simple isothermal particle model can describe the devolatilization

of cylindrical biomass particles under suspension firing conditions without putting a strain on computational resources.

In conclusion, this work contributes to the knowledge on devolatilization and gives an insight into how it can be modeled using multivariate data analysis. The developed simple models can be implemented into CFD without adding to the computational costs. Furthermore, the morphology model is a tool for investigating the effect of particle morphology and for assessing to which degree biomass particle characterization is necessary.

Resumé (Danish)

Gennem de sidste årtier er der kommet et stigende fokus på klimaforandringer og dermed også et krav om metoder til energiproduktion med en lavere nettoudledning af CO_2. En mulighed er suspensionsfyring af biomasse. Fokus i denne afhandling er at modellere biomassedevolatilisering, som det sker i pulverfyrede anlæg. Formålet har været at øge den eksisterende viden om suspensionfyring og dermed muliggøre en øget videnskabelig tilgang til udvikling af nye biomassekedler og optimering af allerede eksisterende anlæg.

Afhandlingen er inddelt i et litteraturstudie og tre hovedkapitler. Litteraturstudiet gennemgår kort det grundlæggende inden for biomassepartikeldevolatilisering. Devolatilisering er en underproces, der sker under forbrænding af biomassepartikler. Det er frigivelsen af gasser fra partiklen efter opvarmning og fordampning af vand og før oxidationen af føromtalte gasser og det tilbageværende koks. Devolatilisering kan også foregå samtidigt med vandfordampning og oxidationsprocesserne, men for forenklingens skyld er fænomenerne ofte beskrevet og modelleret enkeltvis. Litteraturstudiet beskriver også anlæg til suspensionsfyring og suspensionsfyringsbetingelser, der inkluderer høje opvarmningshastigheder ($> 10^3$ K/s), høje maksimumtemperaturer (> 1300 K) og små partikeldiametre (< 3 mm).

Den første model, der bliver præsenteret i denne afhandling, er baseret på multivariat dataanalyse og estimerer koksudbyttet fra pyrolyse under høje opvarmningshastigheder. Koksudbyttet er markant forskelligt for pyrolyseprocesser med lave og høje opvarmningshastigheder, så opvarmningshastigheden er en afgørende faktor at inkludere i en model, hvis den skal kunne prædiktere koksudbyttet under suspensionsfyrede betingelser med tilstrækkelig nøjagtighed. Den præsenterede model er simpel, men nøjagtig, og er valideret med eksperimentel data. Modellen kan bruges til at definere vigtige inputparameter til numeriske beregninger af fluidmekanik (computational fluid dynamics, CFD) og andre komplicerede devolatiliseringsmodeller.

Den anden model, der præsenteres i denne afhandling, omhandler effekten af biomassepartikelmorfologi på devolatiliseringsprocessen. Biomassepartikler er typisk mere aflange end de historisk afbrændte kulpartikler, der ofte er blevet modelleret som kugler. Kugler kan beskrives vha. én variabel og er dermed nemmere at implementere i modelarbejde, hvilket dermed også har været almen praksis for biomassepartikler. Den bedste simple geometri til at beskrive biomassepartiklers aflange facon er dog en cylinder. Her præsenteres en model, der indregner temperatur- og massegradienter, og som kan beskrive devolatiliseringen af både kugleformede og cylindriske partikler. Dermed kan forskelle i devolatiliseringen af forskellige partikelmorfologier sammenlignes. Modellen er sammenlignet med relevant eksperimentel data og er i god overensstemmelse hermed.

Den tredje præsenterede model er også baseret på multivariat dataanalyse og søger at inkludere effekterne af gradienterne i den cylindriske partikelmodel uden at øge de computermæssige beregningsomkostninger i en fluidmekanisk numerisk beregning. Det er gjort ved at inklud-

ere effekten af varmetransmissionsbegrænsingerne i kinetikparametrene. Ved at slå effekterne af kinetik- og varmetransmissionsbegrænsningerne sammen i én førsteordensreaktion (SFOR) kan devolatiliseringen af en cylindrisk biomassepartikel devolatiliseret under suspensionsfyrede forhold beskrives i en simpel model, der ikke øger behovet for beregningsmæssige ressourcer.

Alt i alt bidrager dette studium til viden om devolatilisering og giver en indsigt i, hvordan denne kan modelleres ved brug af multivariat dataanalyse. De udviklede simple modeller kan implementeres i numeriske fluidberegninger uden at øge beregningsomkostningerne. Desuden er morfologimodellen et værktøj til at studere effekten af partikelmorfologi yderligere og til at bestemme i hvilken grad biomassepartikelkarakteristik er nødvendig.

Preface and Acknowledgment

This thesis is written as partial fulfillment of the doctors degree in philosophy (PhD) at the Technical University of Denmark (DTU), Department of Chemical and Biochemical Engineering (KT), Center for Combustion and Harmful Emission Control (CHEC). The project was carried out from May 2016 to April 2019. Part of the study was conducted at the Norwegian University of Science and Technology (NTNU), Department of Energy and Process Engineering, Group of Combustion Kinetics (ComKin). The work has been financed as a Nordic PhD fellowship, funded by the Nordic Five Tech alliance, DTU, and Ørsted A/S. Additionally Ørsted A/S, Burmeister & Wain Scandinavian Contractors (BWSC) A/S, and Rambøll A/S have all assisted with guidance and an eagerness to share knowledge, which highly benefitted the project.

Many people deserve to be thanked for their help and support through the last three years. Firstly, I would like to thank my colleagues at DTU. To my academic supervisors, professor and head of department Kim Dam-Johansen, PhD; professor Peter Glarborg, lic. techn.; and senior researcher Peter Arendt Jensen, thank you for inspiring discussions, for reading through my manuscripts, and for your dedication to the field of combustion. Furthermore, to my fellow PhD candidates, previous and present, thank you for the good moments, both fun and serious, we have had over the last three years, thank you for the "lunch club", and for understanding the occasional frustrations. You'll always be my band of brothers. A huge thanks also goes to the administrative staff for saving the day more than once. Hanne Mikkelsen, Klaus Kirstein Haubroe, and Gitte Rossen-Jørgensen you are the true backbones of CHEC and KT.

Secondly, I would like to thank the extended ComKin Group at NTNU. You made Trondheim a home away from home and turned my Norwegian adventure into one, which I remember with fondness and gratitude. Thanks for including me in your group, for an amazing cabin trip, and for teaching me cross country skiing. I enjoyed it all, and I will be back!

I would also like to thank Søren L. Hvid, PhD, from Rambøll A/S, Lisbeth Myllerup, PhD, from BWSC A/S, and Bo Sander, PhD, from Ørsted A/S for ideas and for enthusiastic, fruitful discussions. Your help and guidance has been invaluable, and I hope we'll one day be colleagues.

Finally, a huge thank you to my family and friends. Thank you for listening, for being there, when the project didn't go as planned, and thank you for asking about my project, even if the answer didn't make much sense at times. And to Kasper, thank you for your love and support. You are the loveliest, most honest and caring person, I have ever met, and all that one could ask for, both through the course of a Ph.D. project and in life in general.

Anna Leth-Espensen
Technical University of Denmark
Spring 2019

Table of Contents

Nomenclature

Abbreviations

AR	aspect ratio
C	center
CFD	Computational fluid dynamics
CHP	Combined Heat and Power Plant
CRDF	Carbonized refuse derived fuel
CY	Char Yield
cyl	cylinder
daf	dry ash free basis
db	dry basis
DTR	Drop Tube Reactor
EFR	Entrained Flow Reactor
ESH	Captive sample electrical screen heater reactor
EV	Explained Variance
ExpVar	Explained Variance
FFB	Flat Flame Burner
FSP	Fiber Saturation Point
FT	Final Temperature
HR	Heating Rate
IRZ	Internal Recirculation Zone
KC	Potassium content
LHV	Lower Heating Value
LV	Latent Variables
PC	Principal Component
PCA	Principal Component Analysis
PF	Pulverized Fuel
PLS	Partial Least Squares regression
PSD	Particle Size Distribution
RCV	Root Mean Squared Error of Cross Validation
RDF	Refuse derived fuel
RMSE	Root Mean Squared Error
RMSECV	Root Mean Squared Error of Cross Validation
RMSEP	Root Mean Squared Error of Prediction
S	surface
SEM	Scanning electron microscopy
SFOR	Single first order reaction
sph	sphere
TFC	Down-fired Turbulent Flow Combustor
TGA	Thermogravimetric Analysis
wb	wet basis

WMR	Wire Mesh Reactor
wt	weight

Greek Characters

α	thermal diffusivity	[m^2/s]
ϵ	emissivity coefficient	[-]
γ	char yield	[-]
μ	dynamic viscosity	[Pa·s]
ω	reaction rate	[kg/s]
ρ	density	[kg/m^3]
σ	Stefan-Boltzmann constant	[$J/(s\ m^2\ K^4)$]
Υ	volatile fraction	[-]

Roman Characters

ΔH	Enthalpy	[J/kg]
$\mathcal{L}$	Latent heat	[J/kg]
A	Arrhenius preexponential factor	[s^{-1}]
A	Surface area	[m^2]
C_p	specific heat capacity	[J/(kg K)]
D	initial diameter	[m]
d_p	diameter	[mm/μm]
E_a	Arrhenius activation energy	[J/mol]
F	Evaporation heat function	[]
g	gravity acceleration constant	[m^2/s]
h	convective heat transfer coefficient	[J/(s·m^2·K)]
k	reaction rate	[s^{-1}]
k	thermal conductivity	[J/(s·m·K)]
L	initial particle length	[mm or μm]
l	particle length	[mm or μm]
m	mass	[kg]
n	number of datapoints	
Nu	Nusselt Number	
Pr	Prandtl Number	
Q	Heat flow	[J/s]
R	initial particle radius	[m]
r	particle radius	[mm or μm]
R_g	gas constant	[J/(mol K)]
Re	Reynolds Number	
T	temperature	[K]
t	time	[s]
V	Volume	[m^3]
v	velocity	[m/s]
Y	mass fraction	[-]
y	measured char yield value for experiment i	[wt%]
y	moisture content	[wt fraction db]
$\hat{y}$	predicted char yield value for experiment i	[wt%]
X	Matrix of independent parameters	
Y	Matrix of dependent parameters	

Sub- and Superscripts

*	initial value
b	boundary
boil	boiling

desorp	desorption
devo	devolatilization
end	final or maximum value of e.g. the temperature
g	gas
H	high
i	index number
ini	initial value
j	integer
L	low
l	layer
m	moisture
p	particle
ref	reference
rxn	reaction
th	thermal
w	radiation temperature

1 Introduction

Climate change has gradually received an increased interest over the past decades, and now ranks as one of the most prominent topics in political discussions. The indisputable need for action and how increased sustainability should be obtained is a political discussion and will not be accounted for here. In this context, it is merely stated that the world needs a more sustainable approach to energy production, and attention is drawn to the UN Sustainable Development Goals as an example of the prominent position energy production has on the list of major worldwide challenges. The most relevant UN sustainability for a more sustainable energy production are goals 7, 11, 12, and 13, which can be seen in figure 1.1. They all deal directly with energy production, but many of the others can also be indirectly linked to this topic.

Figure 1.1: The four UN Goals most relevant for a more sustainable energy production. Modified from[1].

In order to accommodate to the needs for a greener self-sufficient energy production the EU has developed the "20-20-20" goals,[2] where, among others, the Danish government has committed Denmark to cover at least 20 % of the energy consumption with renewable energy sources.[3] Additionally, the government has set the long-term goal for Denmark to be independent of fossil fuels by 2050. A political settlement signed by all parties in the Danish parliament[4] means that the focus on climate change and fossil fuel free power production is likely to stand regardless of

the outcome of the upcoming national election.

There are many means by which renewable energy can be defined, but combustion of biomass is usually characterized as carbon neutral, since the CO_2 emissions can be balanced by the CO_2 uptake from new plants growing up within a defined period of years.[5] A large fraction of biomass combustion in Denmark is done in combined heat and power plants, which converts up to 90 % of the energy stored in the biomass to heat and electricity.[5] Biomass fuels are often used in boilers previously used for coal combustion utilizing the method of suspension firing, where the biomass is comminuted and combusted as particles. Furthermore, the Danish government has decided that coal should be phased out of the energy production by 2030[3] and Ørsted, which is the largest energy company in Denmark, has announced to be coal free in all Danish combustion facilities by 2023.[6] The only feasible way forward regarding these existing facilities is thus suspension firing of woody biomass. In 2012, the total biomass consumption amounted to 136.5 PJ, and it is expected to increase to 173 PJ in 2020,[7] thus optimizing this process may have a large potential for decreasing CO_2 emissions.

In order to study and optimize the combustion of biomass in suspension fired units research revolving around biomass combustion has been conducted at DTU Chemical Engineering continuously for decades. In the later years focus has been on suspension firing.[8] Many experimental studies have been conducted,[9–13] and some modeling studies.[14,15] None of the modeling studies do, however, deal with the morphology of particles, and the increased focus on computational fluid dynamics (CFD) modeling of suspension firing has also revealed a need for a simple model estimating the char yield at high heating rate devolatilization. Thus, in order to expand the knowledge on particle devolatilization products and particle morphology a new Ph.D. project was initiated in May 2016.

1.1 Aim of Present Work

To model a suspension firing unit one needs to consider wood particles of different sizes and morphologies in a complicated turbulent flow with large temperature and concentration gradients for multiple gas species. A typical model approach is to use CFD. As part of the CFD biomass pulverized fuel (PF) boiler modeling, submodels of the wood particle combustion process are needed. They should provide accurate descriptions of the heating, drying, devolatilization, and char combustion processes, and at the same time be implementable into CFD without adding substantially to the computational costs.

The main focus in this project has been on devolatilization of biomass particles in the relevant temperature and size ranges. The topic of devolatilization is vastly described in the literature, but primarily for larger particles at low temperatures, where results are not applicable to suspension firing units. Studies regarding biomass devolatilization under suspension firing conditions are, in contrast, scarce.

This work aims at diminishing the knowledge gap regarding suspension firing, by supplying simple, yet accurate devolatilization submodels. The models both illuminate important factors

regarding biomass devolatilization, and can additionally be implemented into CFD or other complicated model schemes.

The main foci have been determining the char yield from biomass devolatilization, describing the effect of particle morphology on the devolatilization process for different, relevant particle sizes, and providing a simple equation, which can account for particle morphology in more complicated models. These foci are described in individual chapters in this thesis. The thesis outline is presented below.

1.2 Outline of Thesis

- **Chapter 1** is a literature review, which gives a general introduction to biomass, combustion in a suspension firing units, and an introduction into the combustion process for a single fuel particle. A more in depth description is given of pyrolysis of biomass particles at suspension firing conditions, as this is the main focus of the subsequent chapters.

- **Chapter 2** is a published, peer-reviewed article with the title *"Predicting Biomass Char Yield from High Heating Rate Devolatilization using Chemometrics"* about how to empirically model char yield obtained from biomass devolatilization under suspension firing conditions. The model is put forward using multivariate data analysis.

- **Chapter 3** is a paper submitted to a peer-reviewed journal. The article has the title *"The Influence of Size and Morphology on Devolatilization of Biomass Particles"*. It presents a 2D model, which can predict the course of pyrolysis for cylindrical and spherical biomass particles under conditions relevant for suspension firing.

- **Chapter 4** is a manuscript in preparation. It has the title *"Determination of Zero Dimensional, Apparent Devolatilization Kinetics for Elongated particles at High Heating Rates"*. It present a simple model for estimating Arrhenius Parameters for a zero dimensional, isothermal particle model, where the effects of heat transfer limitation and kinetics are lumped together.

- **Chapter 5** presents the concluding remarks and a section for further work.

- **Appendix A** is a paper in press in the popular science Danish Chemistry journal, *"Dansk Kemi"*, in Danish. The title is *"Bestemmelse af koksindholdet i biomasse"*, which translates to *"Determination of the char yield in biomass"*. The paper will be published in the Summer of 2019.

- **Appendix B** is the paper presented in chapter 2 in its original formatting as published in Energy & Fuels, 2018, 32, 9572-9580. The appendix also contains the supplementary material available online.

- **Appendix C** is the supplementary material for the paper presented in chapter 4.

1.3 Financial Support and Collaboration Partners

The PhD project presented in this thesis was funded partly by the Nordic Five Tech alliance (N5T), Ørsted A/S and DTU. All are gratefully acknowledged for their economical support. Moreover, the project was conducted in close collaboration with Ørsted A/S, Burmeister & Wain Scandinavian Contractors A/S (BWSC), and Rambøll A/S, who all generously shared their knowledge on particle combustion and provided insight into challenges and solution methods in industry, which has been most appreciated.

2 Literature Review

This chapter contains a short introduction to combustion of biomass particles under suspension firing conditions. First a short definition of suspension firing is given, then a description of biomass and biomass particle characteristics, which are relevant for suspension firing, is presented. Flame characteristics for suspension firing is then briefly covered before an overview of single particle biomass combustion is introduced as the final part of this chapter.

2.1 Introduction to Suspension Firing

Suspension firing, also known as pulverized fuel (PF) combustion, is combustion of small particle sizes pneumatically transported into a combustion chamber by streams of hot air. The combustion of the particles starts as they enter the combustion chamber, which induces a flame at the chamber inlet.[16] Fuel/air ratios and flame conditions can vary, but a rapid combustion usually occurs due to the small particle sizes.

Suspension firing units were originally constructed for coal combustion,[16] but the method has subsequently been used for biomass, both in newly designed facilities and in rebuilt coal combustion boilers. The inlet of the particle/air streams is located as part of the burner. The design and location of burners in a suspension firing unit vary considerably. In the large suspension firing units in Denmark, Amagerværket, Herningværket, and Avedøreværket, there are horizontally

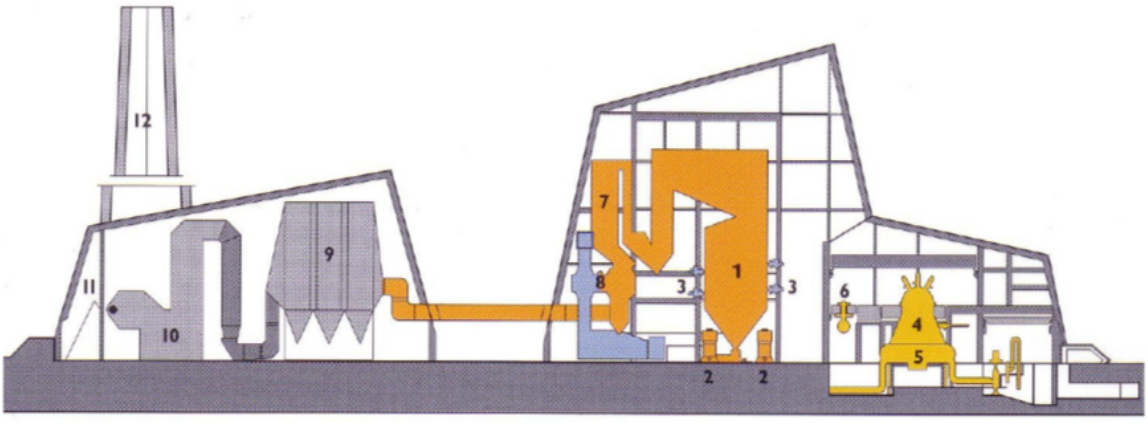

Figure 2.1: Avedøre power plant, Denmark.[17] The boiler chamber is unit number 1.

located burners, which require each individual burner to be designed to give a self-supporting swirl stabilized flame[18] A typical combustion chamber has 10-50 burners, which are typically mounted in a grid pattern.[19] A sketch of Avedøreværket can be seen in figure 2.1. The PF boiler chamber is the unit numbered 1 in the figure. The remaining units are for controlling outlets and emissions from the power plant, and for converting the energy from the combustion into steam.

Suspension firing requires that the particles are sufficiently small to be transported by air. For biomass combustion that means that the vast majority of the particles are below 3 mm.[12,20] Small particles entail high heating rates in the magnitude of 10^3 K/s or higher[21,22] in a combustion chamber with temperatures above 1300 K.[23] These conditions are more extreme, with respect to temperature than other biomass combustion technologies such as fluid bed or grate firing. The focus of this thesis is suspension firing, and a more detailed description of the particle characteristics and combustion conditions under such conditions, will be presented in the subsequent parts of this chapter.

2.2 Biomass Used for Suspension Firing

Biomass originates from animals or plants and is used as fuel. It has been used for energy generation since mankind started to control fire and is partly still combusted this way today in some regions of the world. However, due to an increased awareness of climate change, the interest in biomass as a CO_2 neutral energy source has increased. Thus, biomass combustion has developed into a technologically demanding discipline in large power plants generating heat and electricity to millions of people. In this report the biomass of main interest is wood as this is the primary sources of biomass fuel in suspension firing units in Denmark. As herbaceous material may also be used for suspension firing some attention will also be diverted hereto.

2.2.1 Chemical Properties of Biomass and Coal

A thorough database for chemical composition of biomass samples is made by the Energy Research Centre of the Netherlands.[24] A few representative examples of chemical compositions are given in table 2.1. It can be seen that soft- and hardwood have similar composition, with a slightly higher fixed carbon content in hardwood. The ultimate analysis also reveals that the ash fractions of the two wood types have differences; of special interest is the potassium content, which is higher in hardwood. Compared to herbaceous biomass, per contra, the potassium content in both wood types is generally low, and the amount of fixed carbon is generally higher. The chemical composition of coal is also included in table 2.1 for comparative reasons. A more thorough comparison of biomass to coal is described in section 2.2.3.

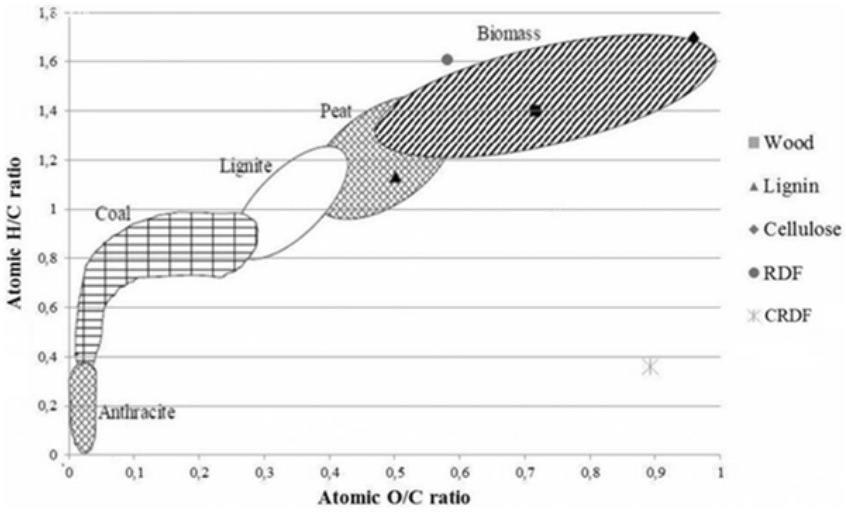

Figure 2.2: Van Krevelen diagram showing differences in chemical composition for different biomass types.[25] RDF = refuse derived fuel, CRDF = carbonized RDF.

Organic Constituents

Biomass primarily consists of C, H, and O organized in macromolecular structures called cellulose, hemicelluloses, and lignin.[26] This gives biomass a fibrous structure. In contrast, coal primarily consists of carbon,[27] and is more brittle. Differences in chemical composition can be sen in a Van Krevelen diagram as the one presented in figure 2.2, which shows the H/C atomaic ratio as a function of the O/C atomic ratio for different fuels. The lower H and O content in coal results in coal being in the lower left corner of the diagram, which can easily be distinguised from biomass, which with its higher H and O content is in the upper right corner in a Van Krevelen diagram.

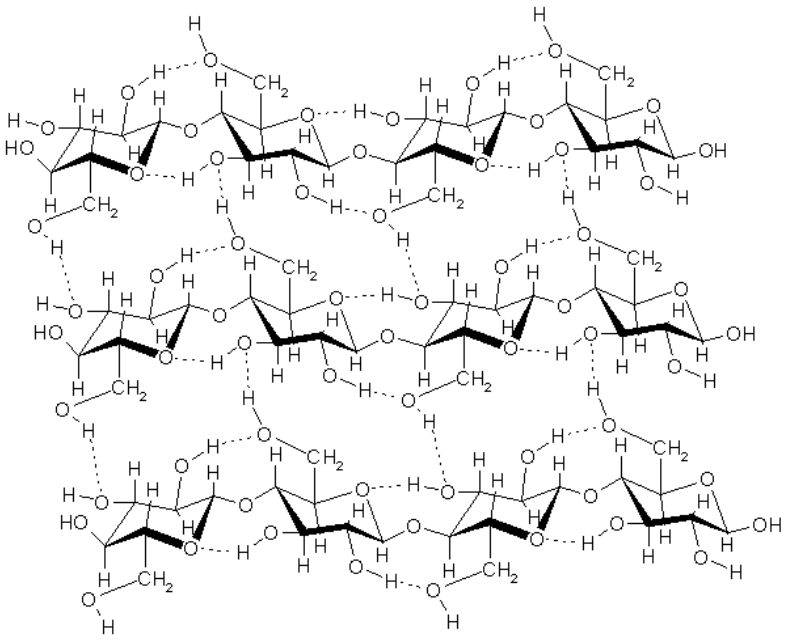

Figure 2.3: Structure of cellulose.[28]

Cellulose is an unbranched polymer consisting of glucose units linked by a β-1,4 linkage.[29] The β-linkage (in contrast to the α-linkage) results in long straight polymer chains. The chains are interlinked by hydrogen bonding resulting in a rigid polymer structure with high tensile strength. Cellulose is an important structural part of plant cell walls. The structure of cellulose can be seen in figure 2.3.

Hemicellulose is a collective name for a number of heteropolymers, most commonly polysaccharides.[30] Hemicellulose is present in plant cell walls, where it aids in holding the cellulose in place.[31] Due to the random structure of the sugar monomers in hemicellulose, it does not have the same mechanical strength as cellulose. The most abundant monomers in hemicellulose are xylose, arabinose, mannose, glucose, galactose, glucuronic acid, methylglucuronic acid, galacturonic acid, and to a smaller extent rhamnose, and fucose.[32] The monomers can be seen in figure 2.4.

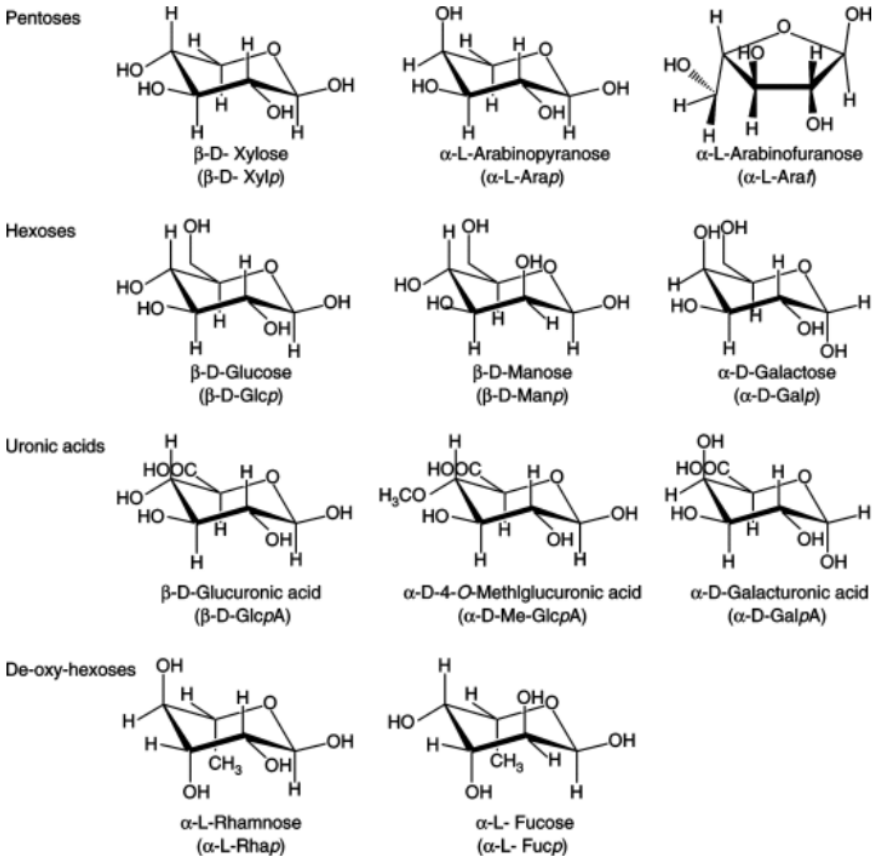

Figure 2.4: Structure of some of the monomers abundant in hemicellulose.[32]

Lignin is a collective term for a three dimensional polyphenolic polymer consisting of primarily coumaryl alcohol, coniferyl alcohol, and sinapyl alcohol monomers.[33] The structure of the three components can be seen in figure 2.5. Lignin is adding to the structural strength of plants both in and outside the cell walls. Since lignin is such a diverse and structurally different matter it decomposes over a wider range of temperatures than cellulose and hemicellulose.[34] Usually cellulose, hemicellulose, and lignin are interweaven within cell walls and no clear boundaries between the three can be defined.

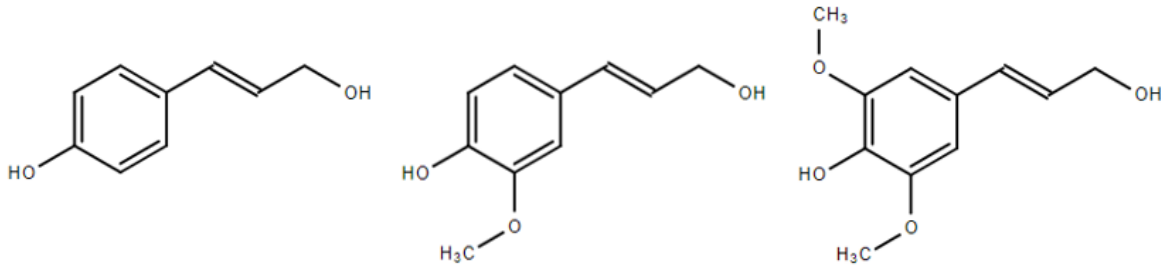

Figure 2.5: Structure from left to right of p-coumaryl alcohol, coniferyle alcohol, and sinapyl alcohol.

Inorganic Constituents

Biomass also contains a large number of inorganics and trace elements. When biomass is combusted in an oxidative environment above 1023 K a number of mineral oxides are present. It is typically oxides of calcium, magnesium, iron, potassium, sodium, silicium, copper, zinc, manganese, chlorine, sulfur, and aluminum.[24] In wood the typical ash content on dry basis is 0.5 wt%, and rarely above 1 wt%. For grasses the ash content is usually 2-5 wt%, and for straw it might be as high as 15 wt%.[35] The inorganic compounds may cause problems in the combustion equipment, because they are the reason for deposits and corrosion.[36,37] The degradation temperatures as well as the final relative fractions of char, tar, and gas will be influenced by the amount and type of inorganics.[38] Typical values for the content of inorganics can be seen in table 2.1.

2.2.2 Biomass Types for Suspension Firing

Wood

Wood as a biomass can come from whole trees or from sawdust which is residue from sawmills etc. Wood applied in PF plants is mainly received as wood pellets. The pellets are produced in a pellet facility, where the wood is dried, pulverized, and pelletized to produce pellets, which can be transported to the power plants.

The chemical and physical properties of wood pellets depend on a multitude of factors. A few will be mentioned here. Wood is a natural product, which comes from trees. A tree roughly consists of a trunk, roots, and branches, which serve different needs of the tree.[41] Each of these is again divided into layers with special subfunctions. The trunk consists of two layers of bark, the cambium, which is a cell layer intended for plant growth, the sapwood, which facilitates the transport of water to the branches and leaves, and the heartwood, which is the oldest, innermost wood in a tree trunk. A sketch of the structure of a tree trunk can be seen in figure 2.6. The varying purposes of the different parts of the tree also mean that the chemical composition and physical properties vary within a single tree.[42]

Table 2.1: Chemical composition of biofuels. All weight percentages are on dry bases except the moisture content which is percentage "as received". The ash content is from fuel pre-treated to 550 °C except for the Beech which has been heated to 600 °C. All data is found in the "Phyllis 2, database for biomass and waste" made by the "Energy research Centre of the Netherlands".[24] Beech data originally from[39], pine, wheat, and miscanthus from[40], coal from the Energy and research Centre of the Netherlands.

Fuel Type	**Beech (hardwood)**	**Pine (softwood)**	**Wheat Straw**	**Miscanthus**	**Coal**
	Partially w/ bark Wood chips	Whole tree Wood chips	Straw Parts	Whole Plant	Bituminous coal Taldinsky Mine
Land of origin	Denmark	Finland	Denmark	Italy	Russia
Proximative analysis (%)					
Moisture content	14.2	3.87	10.25	5.74	5.39
Ash content	0.56	0.6	4.71	3.31	13.17
Volatile matter	75.2	80	77.7	78.5	32.33
Fixed carbon	24.24	19.4	17.59	18.19	54.5
Ulitimate analysis (%)					
C	48.1	51.8	47.3	47.9	68
H	6.4	6.1	5.87	6	4.09
N	0.08	0.3	0.58	0.6	2
S	0	0.01	0.07	0.55	0.36
O	44.9	41.2	41.5	41.6	11.7
Cl	0.0001	0.004	0.17	0.33	0.005
K	0.16	0.10	0.55	0.97	0.16
Na	0.01	0.004	0.01	0.03	0.04
Ca	0.14	0.14	0.25	0.18	0.43
Mg	0.04	0.02	0.05	0.10	0.11
P	0.01	0.01	0.05	0.08	0.04
Fe	0.01	0.01	0.02	0.01	0.46
Si	0.01	0.07	1.32	0.66	3.40

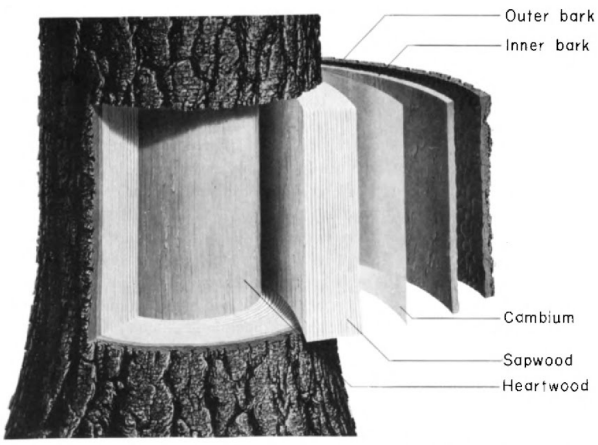

Figure 2.6: Schematic overview of tree trunk.[41]

Roughly tree species can be divided into two groups, hardwood and softwood, depending on the system for transporting water to the upper parts of the tree.[41] Hardwood is wood from angiosperm trees. Angiosperm means "cased seeds" and are trees, where the seeds are covered, e.g. like beech masts from the beech tree. Examples of hardwood include birch, beech, and oak. Hardwood type trees have vessels or pores to transport and distribute water to different parts of the tree. Typically, hardwood trees grow at a slower pace, than softwood species. Softwood is wood from gymnosperm trees. Gymnosperm means "naked seeds", and are trees, where the seeds are not covered, like e.g. the pine nuts from pines. Typical examples of softwood are pines, firs, and spruces. Water transport in softwood species is, in contrast to hardwood, facilitated in the walls of vertically oriented cells (tracheids) in the sapwood. A diagram showing the different cell structures in hardwood and sapwood can be seen in figure 2.7. Additionally, the water transport facilities in a tree, regardless of whether it is hard- or softwood, means that wood is not isotropic. The differences in main constituents of hardwood and softwood can be seen in table 2.2. Here it can be seen that the cellulose content is similar, whereas the lignin content is a little lower and the hemicellulose content is typically a little higher for hardwood.

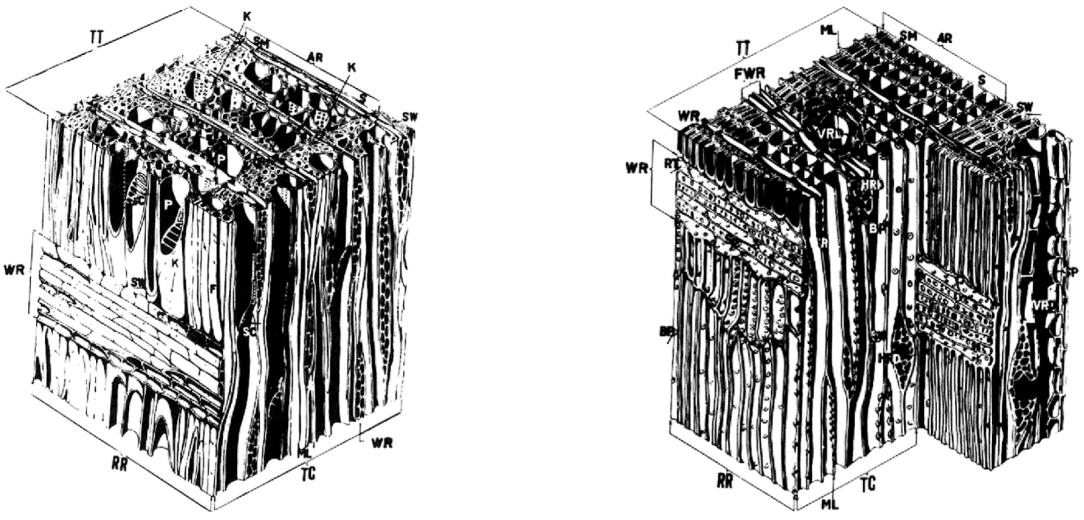

Figure 2.7: Schematic overview of cellular structure in Hardwood (left) amd Softwood(right).[41]

The properties of wood also depend on the season, location, storage facilities and the individual tree specie will have an influence.[43,44] Especially the inorganic content in the soil might effect tree growth and the inorganic content in the trees.[45]

Table 2.2: The composition of plant stem from soft- and hardwood.[46–48] All percentages are wt%.

		Softwood	**Hardwood**
Cellulose			
	Typical Values[a]	40-44 %	40-45 %
	Interval[b]	30-61 %	31-64 %
Hemicellulose			
	Typical Values[a]	28-30 %	20-35 %
	Interval[b]	17-47 %	31-73 %
Lignin			
	Typical Values [a]	25-35 %	18-25 %
	Interval[b]	22-37 %	14-35 %

[a] From[46,47]. Both have given typical values, and a combined interval is given, this means some wood types will be outside these intervals. Total include ashes but no extractives (extractive free wood).

[b] From[48]. An interval for 153 samples is given. Gives a broader interval. Total includes both ash and extractives.

Herbaceous Material

Herbaceous material include by-products from agricultural industries and some energy-crops. Straw is an example of a by-product and has been investigated as a potential biofuel due to its abundance and status as a waste product, when producing wheat, rye, barley, rape, etc. Straw is an annual herbaceous crop which can be shredded or milled and used as pulverized biofuel.[49] The alkali content in straw is high and especially the higher K and Cl contents can result in corrosion and slagging. In order to prevent damage to the equipment straw is sometimes pretreated. A typical method is leaching.[50] During leaching the straw is soaked in water in order to decrease the alkali content. Leaching can happen either at the combustion site or as natural leaching, leaving the straw exposed to weather changes at the field in order to let some of the nutrients return to the soil. Apart from reducing the alkali content considerably the leaching method also results in a disadvantageous lowering of the biomass yield due to degradation, and an increase in fuel water content.[51] Straw also has the advantage that it is cheaper than wood. In Denmark straw costs approximately 5.6 euro/GJ compared to approximately 8.4 euro/GJ for wood pellets.[52]

An example of an energy-crop is miscanthus (*Miscanthus giganteus*), also known informally as elephant grass. It has been tested in smaller scale facilities (78 MW fluidized Bed in Denmark, co-firing 50 wt% coal),[53] but a few challenges with respect to major scale production are remaining. The advantages of miscanthus is the high amount of biomass produced per area. Under optimal

growth conditions miscanthus has produced as much as 2.5 kg dry weight/m^2 at the end of the growing season in the fall.[53] However, miscanthus is usually left unharvested for several months on the field until early spring in order to decrease the moisture content and allow some nutrients/inorganics as K and Cl to be recycled back to the soil. This procedure results in 1.5 kg dry weight/m^2 under optimal growth conditions. The reduction in dry biomass yield is allowed, because the crop does not need further drying, has a lower K content and is easier to transport after this process. Miscanthus is also advantageous because the need for fertilizer is low and the water consumption is relatively efficient. The disadvantages are among others that even despite a high efficiency the water consumption is still high and the crop is sensitive to the water supply during the growth phase. Furthermore the content of inorganics (see table 2.1) is still high compared to wood, but reasonable low for perennial crops. Also the miscanthus has no other function than being an energycrop.

2.2.3 Comparison of Biomass and Coal

Biomass is primarily chosen over coal, because biomass is considered to be CO_2 neutral. The combustion of coal was a major contributor to the industrial revolution and has been used for large scale energy production since.[54] The tradition for and knowledge on coal combustion is thus plentiful. The choice of biomass is comparatively new and the technology is not as developed as that for coal. In addition to this, there are some technological challenges added when combusting biomass in PF boilers compared to coal, some of which will shortly be mentioned here.

Some of the physical properties for coal and biomass are summarized in table 2.3. Differences include that the lower heating value (LHV) for coal is higher than that for biomass.[27] Thus a smaller volume of coal needs to be brought to the plant site, which again means less energy used on transportation. In addition, the storage facilities can be smaller in size and hold the same amount of energy when using coal.

Secondly, coal is more brittle, so it can be ground or crushed more easily than biomass, which with its fibrous structure requires a higher energy consumption for milling.[55] Still the coal particles used in PF burners are smaller by at least an order of magnitude.

Table 2.3: Physical Properties of Biomass and Coal. Modified from Demirbas[27]

Property	**Biomass**	**Coal**
Fuel density [kg/m^3]	$\sim$ 500	$\sim$ 1300
Particle Diameter in PF boiler [µm]	$\sim$ 1500	$\sim$ 100
Dry Heating Value [kJ/kg]	14-21	23-28
Dry Heating Value [GJ/m^3]	7-11	30-36

An additional issue, when using biomass, is the inorganic composition that causes corrosion and deposits, which may give problems with downtime of the combustion equipment.[56] Typical inorganic contents of wood and coal can be seen in table 2.1. Other differences between coal and biomass chemistry include the biomass' ability to bind water.

2.3 Pretreatment of Biofuels

Biomass used for PF combustion is transported and sold as pellets, which is subsequently milled at the power plants. The pelletizing process is a huge research topic in itself and only a short recap will be given here. The dried and pelletized biomass is more valuable and have several benefits including longer storage time, easier transport, more energy per unit mass, and easier control over combustion process due to lower fluctuations i moisture content.[57] Before pelletizing, the biomass must be sufficiently dry. A schematic overview of the pelletization process from reception of raw material to packaging of pellets can be seen in figure 2.8.

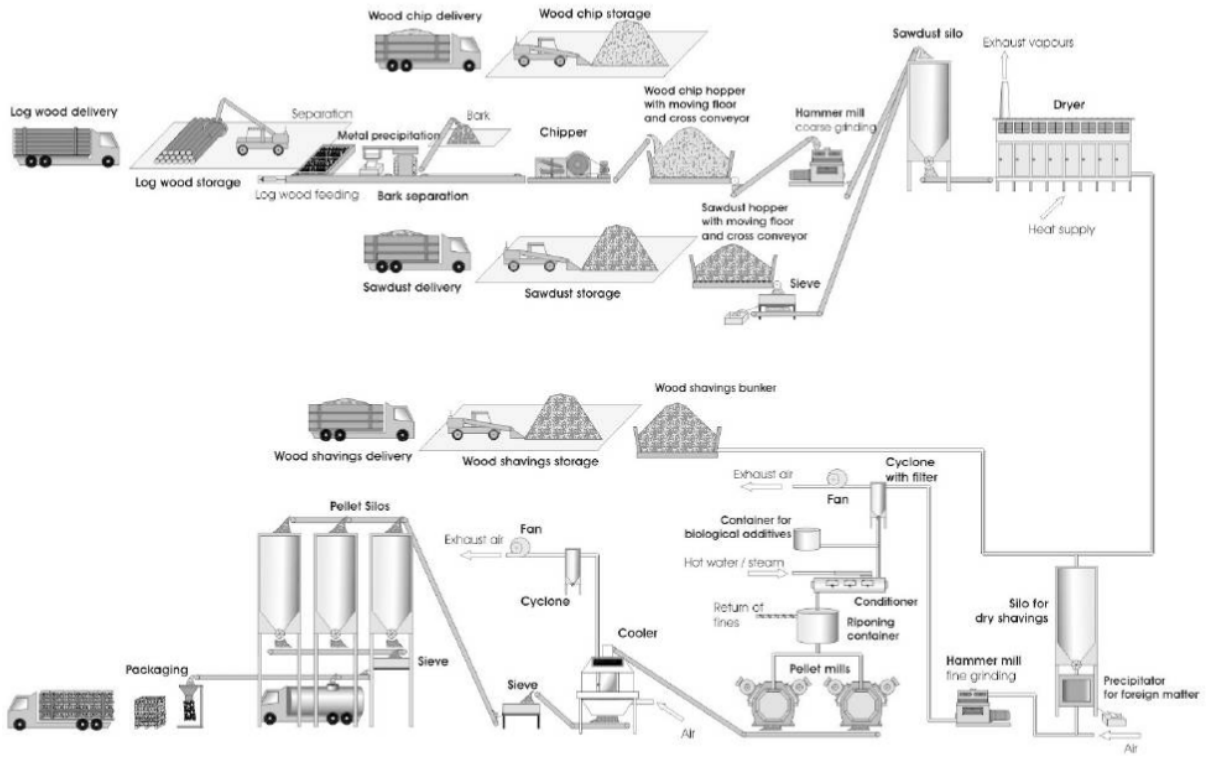

Figure 2.8: Schematic drawing of the pelletization process from milling of raw material to packaging.[58]

2.3.1 Drying and Milling Before Pelletization

Biomass typically contains 50 to 63 wt% water at time of harvest depending on the biomass type, weather, and season.[57] Water can exist in biomass in three forms; in bound liquid form, in free liquid form, and in gaseous form. The bound liquid form is water molecules chemically bound to some of the macromolecules in the biomass, e.g. to the hydroxyl groups in cellulose. The percentage of water which can be bound in this fashion is depending on the fuel properties and is called the fiber saturation point (FSP). Typically the FSP at room temperature is between 21 and 32 wt% for wood grown in temperate regions.[59] Any additional liquid water present will be present in the free form, where it is held within the pores in the particle by capillary forces. The gaseous water is likewise only present in porous particles and is part of the gas phase. At

ambient temperature the equilibrium moisture content in wood is around 9-16 % depending on the relative humidity.[60]

The particles must be heated and the majority of the water evaporated before the pelletizing process can take place. Drying the biomass is of high importance for the milling. Biomass at 30 wt% H_2O can require up to 8 % of the calorific value for milling.[61] Typically, the biomass has a moisture content of 8-12 wt% wb, when it enters the pelletization in the pellet mill.[62]

Biomass is ground before pelletization. For 6 mm pellets, which are typical for suspension firing units a 4 mm screen in often used in a hammer mill.[58] A schematic drawing of a hammer mill can be seen in figure 2.9. For larger pellet sizes, a larger screen size may be used. The grinding can take place in different mill types. Hammer mills are the most typical, but for some applications cutting mills are preferable, e.g. if the moisture content is too high.

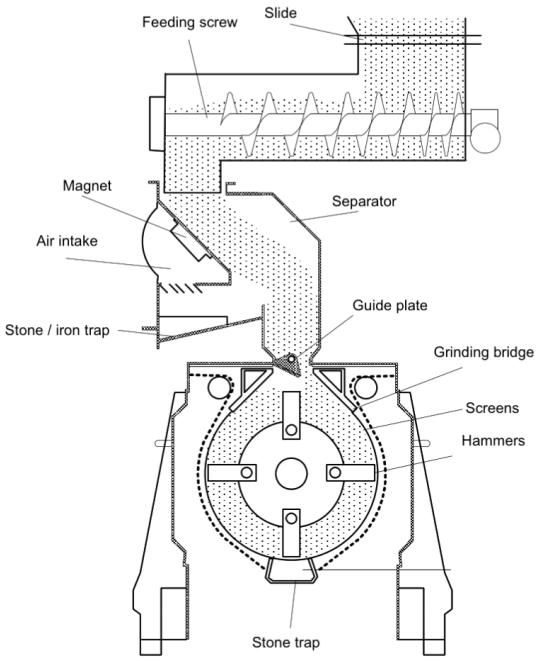

Figure 2.9: Schematic drawing of a hammer mill.[58]

2.3.2 Pelletization

Biomass pellets are produced in a pellet mill[63] and the dimensions of the pellets are typically diameters in the range of 6-25 mm and lengths in the range of 3-50 mm.[64] Standards for pellet quality, dimensions and composition are defined in the EU in classification EN 14961-1, EN 14961-2, and 14961-6. The pellets are formed in dies designed specifically for the given biomass at hand.[65] In figure 2.10 the pelletization of a pellet can be seen. During pelletization the die is filled with ground biomass, where the particle size distribution indicates particles, which are, on average, smaller than the final pellet diameter.[66] The biomass is then pressed into the die by a roller. The heat of the process aids in softening the lignin in the biomass, which is responsible for the cohesion in the pellet. The pellet is not stabilized until it has cooled.

Pellet bulk density for baled (herbaceous) biomass can be increased from around 150 kg/m^3 to about 650 kg/m^3 through pelletization.[67,68] The increase in density as a result of pelletization is smaller albeit still significant for wood. The typical heating value for wood pellets is 17 MJ/kg[65] and the typical moisture content is $<$ 10 wt% wb.

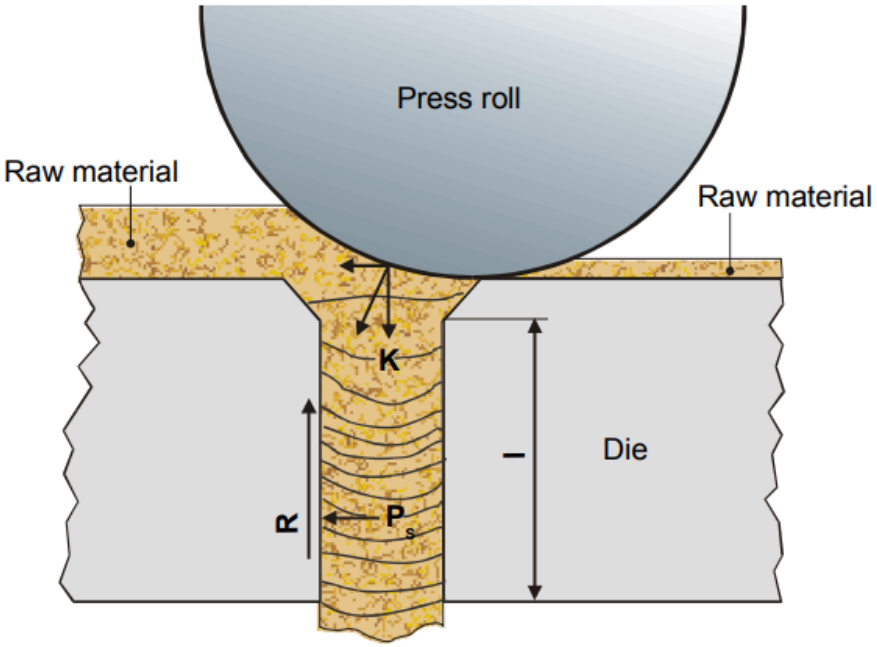

Figure 2.10: Schematic drawing of pelletization. Modified from Alakangas and Paju.[65]

2.3.3 Milling of Biomass Pellets

Milling of biomass pellets is necessary for the pneumatic transport of biomass into the combustion chamber, and to decrease the ignition time in order to ensure full combustion. Preferably, the particle size should be small. For coal over 70 wt% of the particles should have a diameter below 75 µm,[69] but reducing the size of the biomass particles is comparatively more energy consuming than coal comminution. The fibrous nature of biomass makes it more energy consuming to mill it, and, consequently, biomass fired burners typically accept larger particle sizes. For wood particles, diameters are typically in the range from 200-3000 µm.[70,71] Odd shapes and elongated particles are typical due to the fibrous nature of biomass and aspect ratios ($AR = L/d_p$) for wood[72] are 2-3 and up to approximately 14 for herbaceous material.[73]

Different types of mills exist. As suspension firing typically is utilized at plants constructed for coal combustion many mills are retrofitted coal mills. Roller mills require less energy for grinding than hammer mills.[74] And hammer mill needs less energy than cutting mill.[61] On the other hand cutting mills can be more versatile and accept higher moisture contents in the biomass.[58] The particle size after milling is dependent on the obtained sizes from the pre-pelletization grinding,[72] but also on load, biomass type,[75,76] and mill type.[77]

2.4 Power Plant Burners

After the milling the fuel is carried by hot air, called the primary air, through a burner into the boiler chamber. The burner can have two different designs; jet burner and swirl burners. The focus here will be on swirl stabilized burners as they are the ones mainly used in PF boilers. The purpose of the burner is to ensure a stable flame, a high burnout of the fuel, and a low formation of NO_x. An example of a swirl stabilized burner can be seen in figure 2.11.

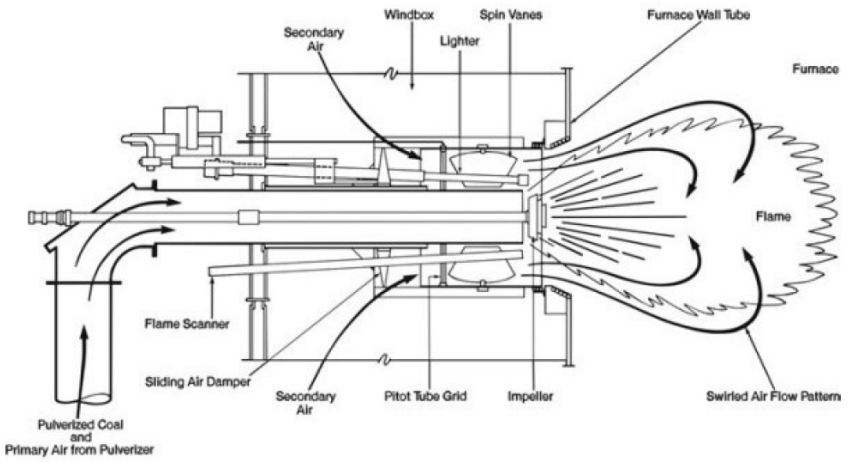

Figure 2.11: A schematic depiction of a swirl stabilized burner.[18]

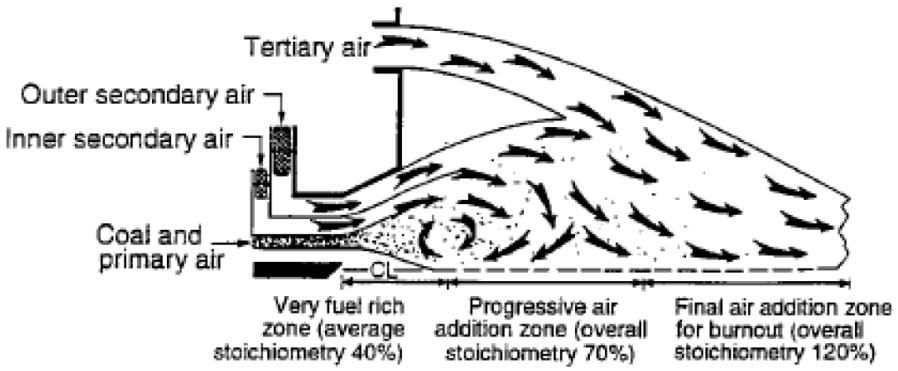

Figure 2.12: A schematic depiction of a distributed mixing burner, where the tertiary air and the internal recirculation zones are visualized.[17]

The mixture of fuel and primary air enters the burner at 15-25 m/s.[71] Secondary air heated to approximately 550 K is fed through an annular ring around the primary air inlet.[18] The amount of secondary air exceeds the amount of primary air. The secondary air is introduced to the furnace in a swirling motion. The amount of air and degree of swirling can be regulated by adjustable air vanes. The adjustments should be made so that a recirculation zone of hot air towards the burner throat is formed in order to provide sufficient energy for ignition of the

fuel feed.[78] Some newer types of swirl stabilized burners also have a tertiary air inlet in order to reduce the NO_x emissions. An example of such a burner can be seen in figure 2.12. A large PF boiler usually has 20-50 burners each with its own flame envelope, i.e. burners are largely independent.[18] Flames can have different outlines, as described by Syred and Beér[79] and the flame pattern will depend on operating conditions.

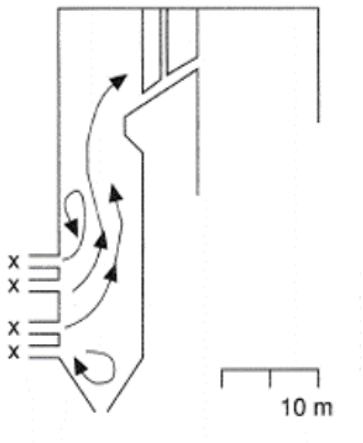

Figure 2.13: A schematic depiction of horizontal firing in the combustion chamber.[80]

The constellation of the burners can vary. PF boilers may have tangential firing, wall firing (=horizontal firing), opposed wall firing, and down firing. In the Danish power plants, Amagerværket and Herningværket, wall firing is used. Wall firing has all the burners on one side in the boiler chambers. See figure 2.13. Steam in the boiler is produced to drive turbines which produce electricity. The steam after the turbine is condensed and the heat from the condensation process can be used for district heating.

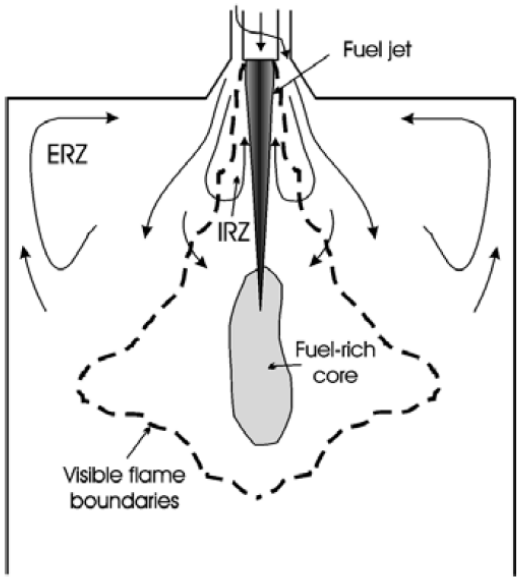

Figure 2.14: Schematic outline of PF flame.[78]

Swirl burners work by imposing a pressure gradient, i.e. forming low pressure regions in the vicinity of the quarl.[81] This causes the hot combustion air to recycle back towards the fuel/primary air nozzle. The area of returned air/fuel is known as the internal recirculation zone (IRZ). An outline of a PF flame can be seen in figure 2.14. The purpose of the recirculation is to ensure a stable combustion and a rapid heat release. Furthermore it has been shown that staged combustion techniques where the air inlet is divided into two or three separate inlet streams can reduce the formation of NO_x.[81]

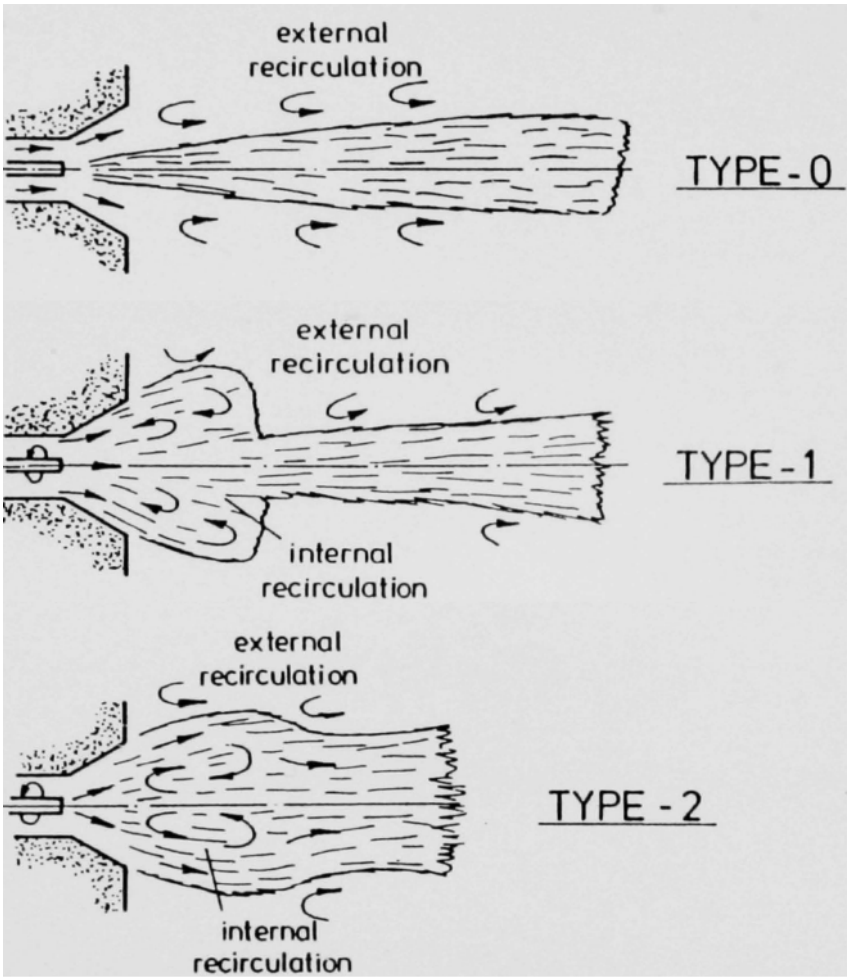

Figure 2.15: The flame types as defined by the IFRF. Modified from Smart and Weber.[82]

2.4.1 Flame Types

The combustion in PF fired burners is primarily a turbulent mixing phenomenon.[82] Flame types are categorized by the international flame research foundation. Different flame types are given in figure 2.15. There are two major flame types and combinations thereof. Flame type 0 is a long jet flame. Flame type 0 has the elongated shape since the air inlet flow is high enough to pierce through the recirculation zone and create a long narrow flame. Flame type II is a shorter and broader flame. Here the inlet air velocity is lower or the swirl number is higher resulting in most of the fuel being trapped in the recirculation zone.[16,82] Both flame types have advantages

and flame types of an in-between length and width are sometimes desired depending on the burner design and purpose of the burner. The in-between flame is classified as flame type I. The flame configuration can be adjusted by changing the degree of swirling and the primary air inlet velocity.

2.4.2 Biomass Flames

Since biomass particles are typically larger than coal particles, biomass flames and the particles within them sometimes behave differently than coal in coal flames. The calorific value of biomass is also lower than for coal; typically around a factor of 2. In order to supply the same amount of energy the amount of biomass must thus be correspondingly higher. This again requires a higher air influx, which also alters the flame structure.[83] The flame structure is also affected by the higher amount of volatiles in biomass. The higher amount of volatiles and the larger particle size increase the risk of an unstable flame and a lower degree of particle burnout.

Experiments[11] conducted in a 30 MW_{th} full scale suspension firing swirl stabilized burner at Amagerværket (Amager Power Station, Unit 1) in Denmark, with a fuel inflow of 1.87 kg/s showed a biomass flame, closely attached to the burner quarl, and where fluctuations in the flame resulted in slight flame detachments from the quarl. The flame and the quarl can be seen in figure 2.16. The flame matches the structure outlined in figure 2.14.

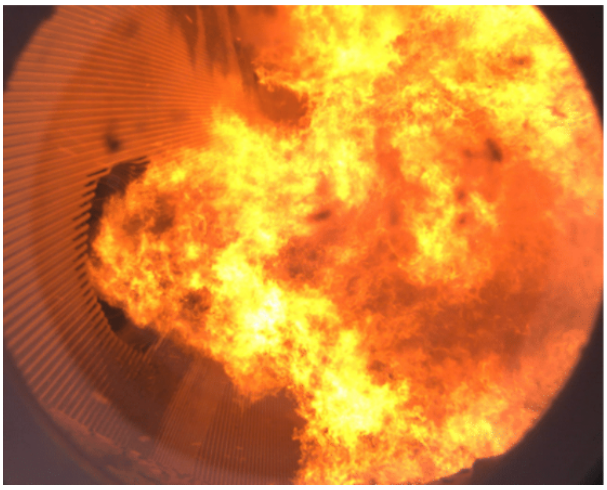

Figure 2.16: Picture of biomass PF flame from Amagerværket.[11]

Experiments[84] conducted in a swirl-stabilized, down-fired, dual-feed burner flow reactor comparing a coal flame (particle size Rosin-Rammler mean = 110 µm, fuel inflow 15.3 kg/h) and a biomass flame (particle size Rosin-Rammler mean = 451 µm, fuel inflow 26.5 kg/h) show differences in burnout. The larger biomass particles are less likely to be affected by the swirling motion and is carried straight through the core of the flame resulting in diminished residence time and less contact with the higher O_2 concentration zones in the outer regions of the flame. Furthermore the amount of volatiles in the biomass is higher, thus increasing the need for O_2 in order not to risk too high volumes of unreacted off-gas.

Comparison[61] of pure biomass and coal flames in a top-fired vertical burner shows that biomass combustion also may lead to an increase in CO emissions from 50 to 75 mg/m^3, which can possibly be explained by a decreased degree of burnout of the large biomass particles.

Other experiments,[78] conducted in a semi-industrial furnace, proved biomass flames to result in a larger amount of volatiles in the near-burner region compared to coal flames, an increase in the radial flame dimension, and a second combustion region downstream in the burner chamber. The two latter phenomena have also been observed for co-firing coal and biomass.[83] The two combustion zones in the boiler chamber can be explained by the larger size range for biomass particles. The small particles release volatiles close to the quarl, whereas the larger particles release volatiles further down in the burner chamber. The large particles thus may results in a large fraction of unburned hydrocarbons late in the burner chamber compared to coal flames.

Co-combustion experiments[61] in a top-fired vertical burner of biomass and coal additionally suggest that the NO_x emissions can be reduced by replacing coal partly with biomass fines. Co-firing biomass also results in lower SO_2 release due to the typically lower content of S in biomass. Furthermore the typically higher alkaline-earth metal content in biomass can capture some S in the ash.

2.5 Combustion of a Single Particle

The structure, time scale, and degree of burnout in biomass flames depend on the combustion process for each individual biomass particle blown into the combustion chamber. This section serves as an introduction to biomass particle combustion. The literature on this subject is extensive, so the focus here has been limited to particle combustion related to suspension firing, where the amount of literature is more restricted.

For structure the combustion process is divided into five sub-processes; heating, drying, devolatilization, char combustion, and gas phase oxidation.[85] A schematic overview can be seen in figure 2.17. It is a general description applicable to all types of biomass particle combustion. The extend and details of each sub-process vary and is dependent on a multitude of biomass characteristics and process parameters. Furthermore the sub-processes can occur subsequently or simultaneously depending on combustion conditions and biomass type.

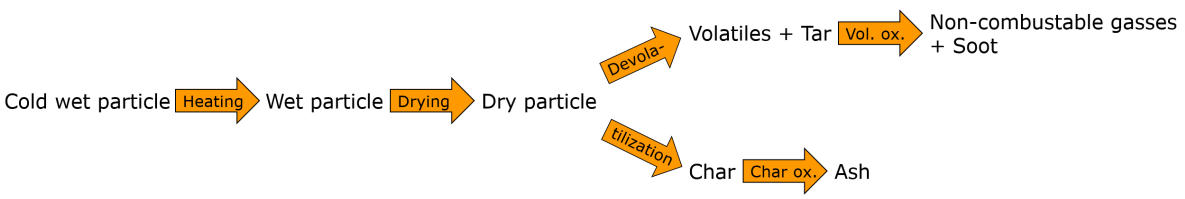

Figure 2.17: Schematic overview of biomass combustion.

2.5.1 Heating

The temperature of the particle increases, when it is admitted to the combustion chamber. The heating phase is here defined as the time from the particle is blown into the combustion chamber until it reaches the temperature, where water evaporation is prevalent; around 373 K at ambient pressure. External heat is supplied to the particle by means of convection of hot flue gas and by radiation from the flame, combustion chamber walls, and surrounding particles. The heating is primarily done by convection for small particles, but since the heat supplied by radiation scales with surface area, the contribution from radiation is important for larger particles.

The heating of the interior parts of the particle is typically due to intraparticular conduction, either through the solid material or through the gas or liquid in the particle pores. In porous particles the radiation between pore walls will also contribute to the energy flux.

2.5.2 Drying

When the particles enter the combustion chamber some remaining moisture will be present. The energy for evaporation of the water can be supplied either by convection, conduction or radiation. Water is evaporated due to differences in the partial water vapor pressure and the equilibrium partial pressure of free water. The transport of water out of the particle is controlled by a combination of pressure gradient between the inside of the particle and the surface, diffusion due to differences in chemical potential of sorbed water molecules, and diffusion due to differences in the mole fraction of water in different regions of the particle.[86] Experiments[86] conducted at an ambient temperature of 398 K show that drying is primarily heat transfer controlled at this temperature. It is externally heat transfer controlled in the beginning of the drying process, but as water evaporates from the particle and the wet film boundary moves inwards, the heat transfer becomes internally limited. Water moving outwards towards the particle surface has a cooling effect on the exterior parts of the particle as the water from inside the particle is colder than the surface. The pressure gradient outwards is created by water leaving the surface as a result of the particle heat up on the surface.

As the free water is evaporated the temperature will start to increase also in the inner parts of the particles, which again will evaporate more water. In this process the free liquid water is evaporated before the bound water is desorped. Both evaporation of water and desorption are energy consuming reactions and they will consequently affect the particle temperature. The drying time is dependent on particle size, but model results[87] show that drying takes approximately 0.3 second for a $d_p = 1.5$ mm particle with 4 wt% wb moisture as shown in Paper B.

2.5.3 Devolatilization

Devolatilization is a collective term for the chemical degradation of solid particles due to heating with no or limited amounts of oxygen. It is often used interchangeably with the term pyrolysis,

and this will also be the case in this thesis. Sometimes, pyrolysis is defined to be degradation in inert or practically inert atmospheres, whereas devolatilization is defined as thermal degradation in oxidative or unspecified atmospheres. However, even if the surroundings are generally oxidative, the local environment around the biomass particle may be inert/reductive so in practicality it is difficult to differentiate.

The degradation of biomass particles through devolatilization yields a mixture of gasses, liquid, and solid material;[88] called gas, tar, and char respectively. The relative fractions of the three depend very much on heating rate, final temperature and operating conditions in general. Multiple experiments conducted under low heating rate condition have been performed, but high heating rate devolatilization experiments, relevant for suspension firing, are more scarce. The higher temperatures and extremely high heating rates results in a higher complexity of the experiments and more demanding requirements for the experimental equipment.

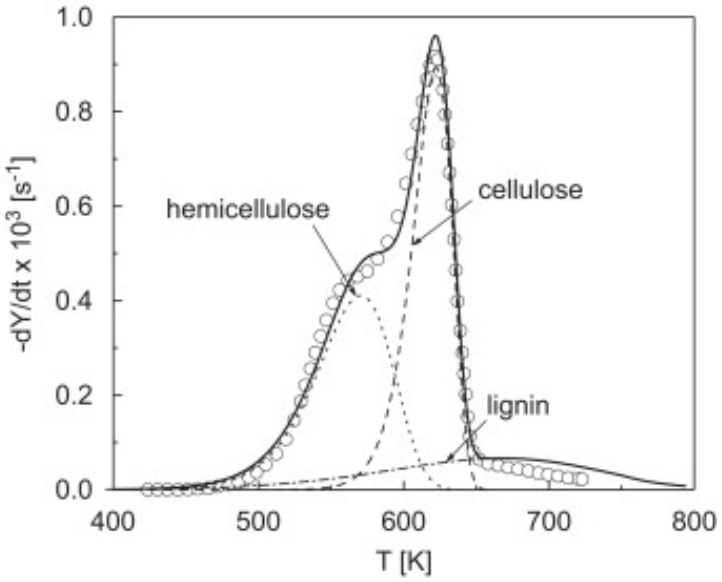

Figure 2.18: The degradation through pyrolysis for hemicellulose, cellulose and lignin at a heating rate of 5 K/min.[34]

Low Heating Rate Devolatilization

In low heating rate biomass pyrolysis, thermogravimetric analysis (TGA) is widely used. The low heating rate experiments yield a level of detail explaining some of the phenomena occuring during devolatilization, which can be hard to observe under high heating rate experiments, and which aid in explaining the complex phenomenon of devolatilization. In brief, TGA experiments have shown that the different components of biomass decomposes at different temperatures during pyrolysis.[89] The hemicellulose decompose at 470-598 K, cellulose at 510-648 K, and lignin at 523-773 K.[34,89] These temperatures vary with operating conditions, but suggests that lignin is decomposing over a much wider temperature span than cellulose and hemicellulose. For experiments[34] conducted at low heating rates, 5 K/min, an example of the degradation of the three primary components in biomass can be seen in figure 2.18.

High Heating Rate Devolatilization

The remainder of this section deals with high heating rate devolatilization, which is relevant for suspension firing. An overview of some of the literature addressing high heating rate devolatilization can be seen in table 2.4. Here the experimental equipment, the maximum temperature, particle size, residence time and heating rate is stated. All these factors influence the course of the devolatilization process, and the relative fractions of the pyrolysis products, gas, tar, and char, are dependent on these. Below is first a description of the biomass particle morphology both during and as a result of devolatilization. Secondly, comes a short description of the three main pyrolysis products, gas, tar, and char and their respective yields. Lastly, is a description of the devolatilization kinetics and the parameters, which affect the kinetic scheme.

Particle morphology

Devolatilization and particle morphology are interdependent, and the resulting char particle morphology depends both on devolatilization characteristica and the original structure and chemical composition of the wood particle. A comparative study[90] of pyrolysis at low and high heating rates with pine saw dust (50-200 µm) showed that the particles change and get a more "melted" appearance and spherical pores in the surface, when the heating rates were high. SEM images of low and high heating rate chars can be seen in figure 2.19. The "melted" appearance is characteristic of a metaplast produced during devolatilization. Metaplast is the state of the biomass during devolatilization, which release some pyrolysis gasses and where the remaining material is the predecessor for the char particle.[91] Similar results were obtained by Lewis and Fletcher[92] in a flat flame burner with small (d_p = 45-75 µm) particles at high temperatures (T =1163-1433 K). Comparatively, low heating rate biochar retains the original fibrosity and morphology. Experiments by Trubetskaya et al.[12,13,93] showed that char plasticization was diminished for biofuels with a high potassium content.

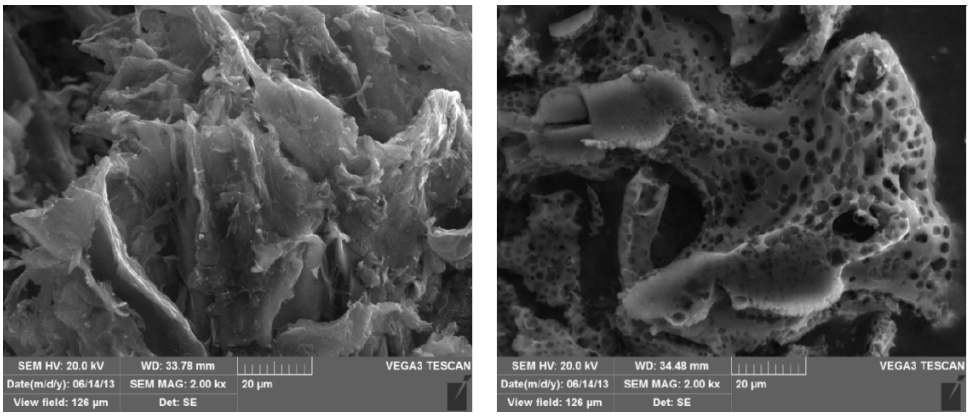

Figure 2.19: SEM images of chars obtained at low (left) and high (right) heating rates at a maximum temperature of 1123 K. Low heating rate chars are produced in a TGA with a heating rate of $\sim$ 1 K/s, and high heating rate chars are produced in a WMR at $\sim$ 4400 K/s.[90]

Furthermore, devolatilization is a transient phenomenon, so physical and chemical particle properties change over time. As time progresses, the porous structure is changed and consequently also density, thermal radiation properties, and diffusion rates change. Additionally, cracking,

shrinking, and swelling can also change particle size and size distribution. Tree dust and straw typically contain their three dimensional fibrous structure, but shrink and become more porous during devolatilization.[94]

Pyrolysis Products

The products from the pyrolysis process can generally be divided into gas, tar and char. **Gas yield** depends, as the other pyrolysis products, on experimental conditions. High heating rates and residence times will lead to a higher gaseous yield and more porous particles. For wood at suspension firing conditions a yield of 92-98 wt% gas is possible.[37,94,101,105] The gaseous products are usually H_2O, CO,CO_2, H_2, CH_4 C_2H_4, and C_2H_6.[96,112] Experiments by Septien et al.[97] performed in a drop tube reactor at T $>$ 1273 K with beech wood particle of two sizes (d_p = 350/800 µm) furthermore showed that the gas yield and composition do not depend on particle size as long as $T > 1273$ K and the residence time is high enough to obtain fully pyrolyzed particles. The two particle sizes experienced reasonably similar heating rates. Experiments by Zanzi et al.[104] in a free-fall reactor at 1073-1273 K showed that the volatile yield is higher for smaller particles. In this experiment it was not ensured that the particles were fully pyrolyzed, and the heating rates seem to differ more than in the experiments by Septien et al.[97]

At pyrolysis temperatures, **Tar** remains in the gas phase, but condenses at room temperature forming a very viscous liquid, which consists of phenols, ethers, polyaromatic hydrocarbons (PAH), and other heavy compounds. The tar can also undergo secondary reactions which create a mixture of non-condensable gases and soot.[113] At high temperatures relevant for suspension firing, the tar decomposes into light gasses and soot. Tar yields are in the range of approximately 1-2 wt % daf for temperatures relevant for suspension firing.[92]

The **Char Yield** is also dependent on a myriad of factors. First of all, the biomass char yield is dependent on pre-treatment of the biomass. Experiments conducted in a DTR by McNamee et al[114] show that torrefaction results in a slower devolatilization and a higher char yield compared to untreated woody material. In the remainder of the thesis only untreated woody material will be described as this is most typical in suspension firing units. The char yield can vary between 2 and 80 wt% (daf) depending on heating rate, pyrolysis temperature, and residence time.[13,21,101] For fast pyrolysis in suspension firing units, char yields are low, and down to around 2-6 wt% are typical.[101]

One of the factors influencing char yield is the heating rate of the biomass particle. Experiments[90] show that high heating rates during pyrolysis yields a char with an increased oxidation reactivity. Additionally, at high heating rates the fraction of char is lower than for identical samples pyrolyzed under low heating rate conditions.[13,89,93] The same conclusion was drawn by Hajaligol et al.[115] for cellulose samples at maximum temperature up to 1273 K and a heating rate of 1000 K/s in a laboratory scale batch reactor. The experiments showed that both heating rate and final temperature of the sample are important. The effect of the peak temperature is shown in figure 2.20. It can be seen that the char yield decreases when the peak temperature is high. The effect of the combination of heating rate and particle residence time for cellulose can be seen in figure 2.21. The plots for tar and gasses show corresponding results and can be seen in the paper by Hajaligol et al.[115] In figure 2.21 the char yield as wt% of cellulose is given as a function of peak temperature for different heating rates. The holding time at the final tem-

Table 2.4: Literature overview over literature concerning pyrolysis under high heating rate conditions. DTR = drop tube reactor, EFR = entrained flow reactor, ESH = Captive sample electrical screen heater reactor, FFB = flat flame burner, TFC = down-fired turbulent flow combustor. WMR = wire mesh reactor.

Equipment	**Size** [μm]	**Res. Time** [s]	**Biomass Type**	**Max. T** [K]	**Heating r.** [K/s]	**Volatiles** [wt %]	**Char** [wt %]	**Ref.**
DTR	<1000	N/A	pine shells, olive, wheat	1373	high			[95]
DTR	<500	3	Hinoki cypress	873-1673	high	88 wt% db	3 wt% db	[96]
DTR	350-800	<5	beech wood	1273-1673	N/A	96 wt % db	4 wt % db	[97]
DTR	90-150	<0.6	cacao shells	673-1073	1000	N/A	10 %	[98]
DTR	112-1000	<1.5	wood (no specification)	873, 1173	1500-4000	<94.2 % wt db	N/A	[99]
FFB	45-75	0.020-0.100	saw dust (soft wood)	1163-1433	10^5	87-96 wt% daf	5 wt% db	[92]
FFB	500-1000	5-500	hardwood, palm, straw	1500, 2200	10-1000		>5 wt %	[20]
EFR	300-500	N/A	*Cynara cardunculus* thistle	1073-1448	10000	83-88 wt% wb		[100]
EFR	90-355	1.5-2	pine wood, beech wood	873-1573	10^4-10^5		>1% daf	[101]
EFR	355-1250	0.7-3.5	sylvester pine, spruce	1073-1273	> 500	>75 %wt	<10 % wt	[102]
EFR	<180	0.2-1	Bark free white oak	723-1223	1000		165 m/z	[103]
EFR	125-1000	<10	Norwegian spruce (stem)	1073-1273	N/A	N/A	>2 wt%	[91]
free fall	500-1000	1-2	wood/straw/olive waste	1073-1273	N/A	N/A	7/13/20-27 wt%	[104]
single part.	300-15000	up to 80	poplar	1050-1275	high	<97 wt %	N/A	[105]
Heat. foil	<90	10 at max T	Softwoods/reed	1273	6000	71/52.5 wt % db	14/32 %wt db	[106]
plate reac.	90	0-50	bark pine (*P.Sylvestris*)	708-1373	up to 1000		6 % wt db	[107]
ESH	45-88	0 at max T	sweet gum	600-1400	1000	87 wt % db	7 wt db	[108]
WMR	150-250	1	pine wood	773	7000	92 wt % db	5 % wt db	[109]
WMR	50-2000	1-4	wood, wheat, rice, alfalfa	623-1673	10-3000		>5 % wt daf	[12]
Fluid. bed	300-800	N/A	mallee (hardwood)	N/A	1000		4-5 wt %	[110]
TFC	710-840	N/A	alfalfa / red oak	1523	N/A	82/93 wt % daf	-/7 wt%	[111]

perature is 0 s. In other words, the sample is cooled immediately when the final temperature is reached, thus when the heating rate is low, the sample has more time to release volatiles, and, consequently, the char yield becomes lower. When holding times are sufficient to reach fully pyrolyzed particle, the char yields are lower for higher heating rates and higher maximum temperatures.[12,13]

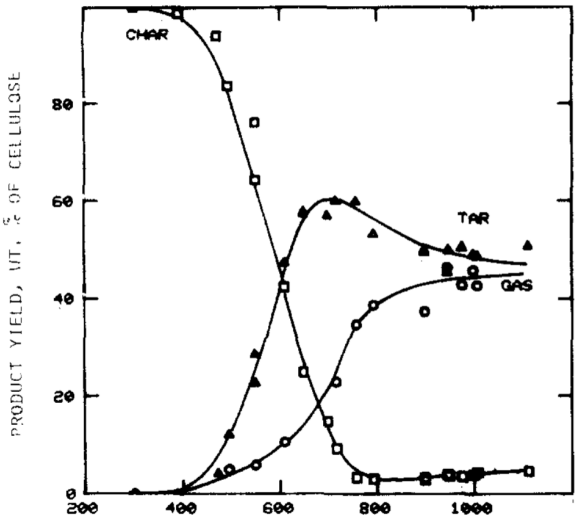

Figure 2.20: Effect of peak temperature on yield of char, tar, and gas (including water), from pyrolysis of cellulose strips. Points experimental data; curves: trendlines; pressure 5 psig (He); heating rate 1000 K/s; sample thickness = 0.101 mm.[115]

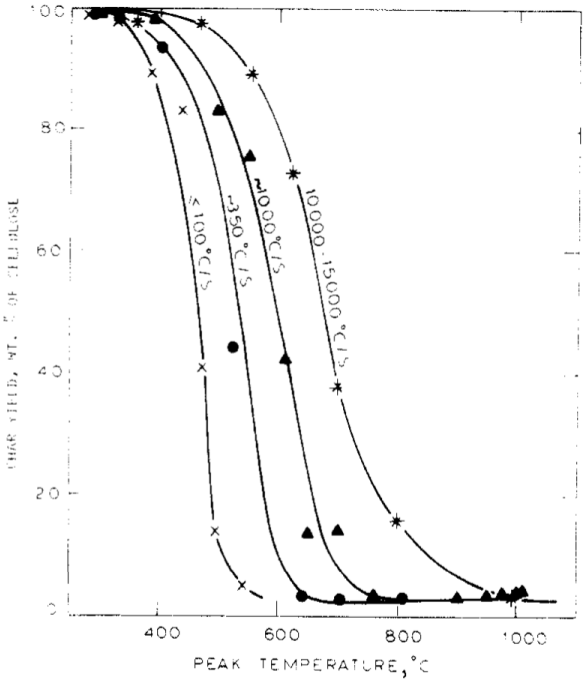

Figure 2.21: Effect of heating rate (specified on curves), to the peak temperature indicated on the abscissa, on char yield from pyrolysis of cellulose strips. (Points: experimental data; curves: trendlines; pressure 5 psig (He); sample thickness = 0.101 mm.[115]

The potassium content in the biomass sample has also been shown to have great influence on the char yield. Trubetskaya et al[12,13,93] have measured the char yield under high heating rate conditions in a wire mesh reactor (WMR) and a drop tube reactor (DTR) and found that the relative fractions of cellulose, hemicellulose, and lignin are of minor importance with respect to char yield compared to the potassium content, which has catalytic effects. The char yield is lower for biomass with a low potassium content, thus combustion of low potassium wood species gives a comparatively lower char yield than herbaceous material.

Devolatilization Kinetics

Devolatilization kinetics are among other dependent on heating rate and gas temperature,[116,117] and can be characterized both trough modeling work and experiments. Modeling pyrolysis kinetics can be done in numerous ways, see e.g. these excellent descriptive papers and reviews.[118–121] In its simplest form, pyrolysis can be modeled using a single global reaction as described in equation 2.1.

$$Biomass \rightarrow Products \tag{2.1}$$

Here the reaction can be described as in equation 2.2, assuming the reaction order is one.

$$\frac{d\Upsilon}{dt} = k(\Upsilon^* - \Upsilon) \tag{2.2}$$

Here k is the reaction rate, Υ^* is the amount of available reactant at $t = 0$, and Υ is reactant concentration. The above equations constitute a single first order reaction (SFOR) for devolatilization of biomass. The rate of reaction for this mechanism, k, is typically modeled using an Arrhenius equation as seen in equation 2.3.

$$k = A\,exp\Big(\frac{-E_a}{RT}\Big) \tag{2.3}$$

The Arrhenius parameters A and E_a vary considerably. Obtaining accurate high heating rate Arrhenius kinetics is often complicated, as it can be difficult to determine both the residence time and the heating rate of particles at very high temperatures accurately. The influence of intraparticle heat transfer limitations relevant for all biomass particle sizes further complicates the problem. Examples of high heating rate, high temperature SFOR pyrolysis constants from literature are given in table 2.5 and depicted in the Arrhenius plot in figure 2.22. It can be seen that though the Arrhenius parameters vary considerably, the reaction rates match reasonably a high temperatures. At lower temperatures the variation in the reaction rates suggests that high heating rate kinetics are not applicable at these temperatures without careful consideration.

Table 2.5: Arrhenius parameters for single first order devolatilization reaction rate at high heating rates and temperatures.

#	**Biomass**	**Max. T** [K]	**HR** [K/s]	**A** [s^{-1}]	**Ea** [kJ/mol]	**Ref.**
A	Bagasse	1373	10^4	$1.1 \cdot 10^4$	59.5	[113]
B	Beech wood	1273	10^4	$2.6 \cdot 10^5$	83.7	[122]
C	Cacao shells	1073	10^4	625	20.4	[98]
D	Cellulose	1273	10^3	$20.0 \cdot 10^7$	133	[115]
E	Cellulose	1273	10^4	$6.8 \cdot 10^9$	139.75	[123]
F	*Cynara Cardunculus* thistle	1448	10^4	47.2	11	[100]
G	Lignin (from wood)	1400	10^3	$3.4 \cdot 10^5$	82.01	[124]
H	Mischanthus	1667	10^5	$20.5 \cdot 10^3$	17.9	[10]
I	Mischanthus (leached)	1667	10^5	$13.7 \cdot 10^3$	13.5	[10]
J	Pine	1667	10^5	$18.9 \cdot 10^3$	21.3	[9]
K	Pine (KCl doped)	1667	10^5	$14.8 \cdot 10^3$	14.4	[10]
L	Sweet Gum hard wood	1400	10^3	$3.4 \cdot 10^4$	69.04	[108]
M	Wood	1173	$4 \cdot 10^3$	5880	42.7	[99]

Experiments by Johansen et al.[9] conducted in a laminar entrained flow reactor at high temperatures (T = 1405-1667 K), high heating rates (HR $\approx 10^5$ K/s), with small pine particles (sieve size < 125 µ) have showed a dependence on heating rate and temperature for the pyrolysis kinetics. The same results were repeated with other biomass types (doped pine, mischanthus, leached mischanthus) with similar results.[10] The latter study showed that the potassium content does not influence pyrolysis kinetics at high heating rates, even if it influences char yield. Radlein et al.[125] also underlined a strong dependence of the kinetics on the heating rate.

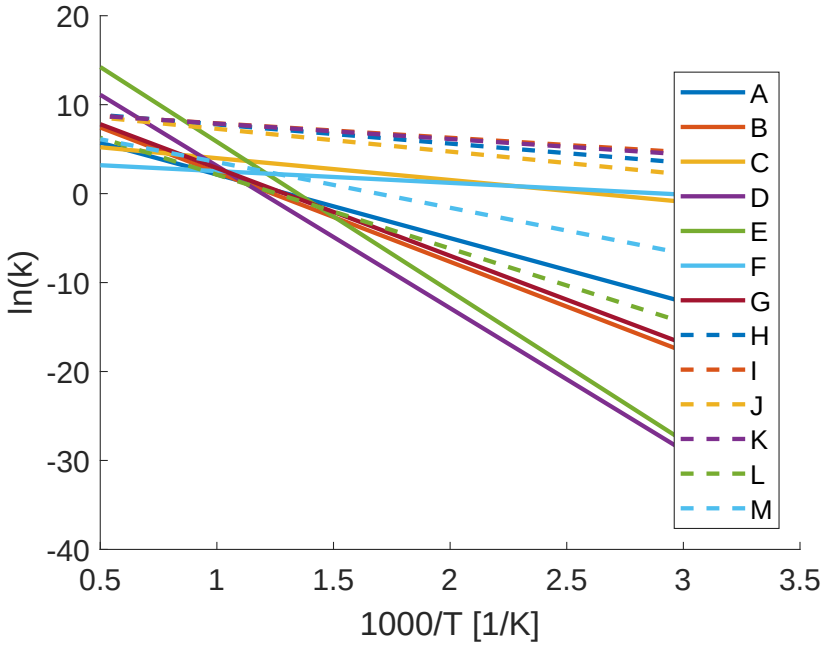

Figure 2.22: Arrhenius plot for SFOR devolatilization kinetics for high heating rate experiments from literature.[9,10,98–100,108,113,115,122–124] Letters explained in table 2.5.

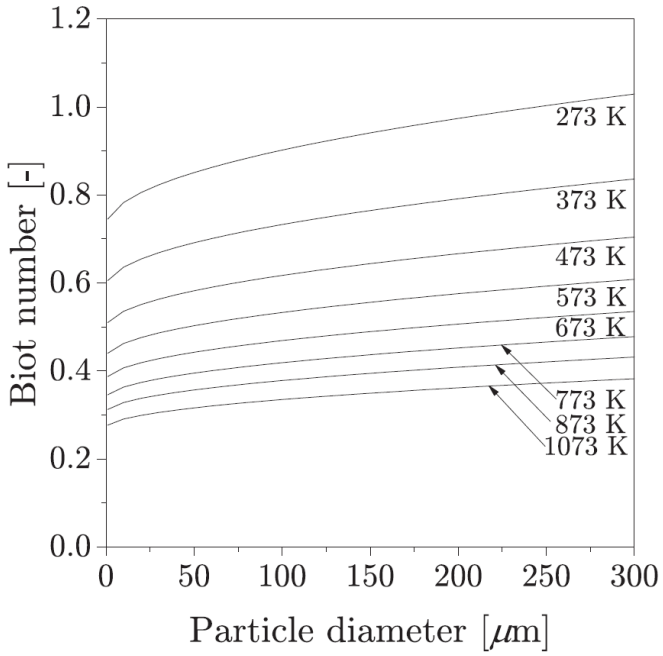

Figure 2.23: The Biot number as a function of particle size for different temperatures.[14]

Demirbas[89] reports that the activation energy rises as the pyrolysis reactions progress (which consequently means a rise in particle temperature), thus further underlining the pyrolysis kinetics' dependence on temperature.

When determining biomass pyrolysis kinetics it should further be taken into account that biomass particles are typically regarded as thermally thin, and the intraparticle heat transfer limitations

are ignored for small particles (typically $d_p < 75$ µm). Thermally thin is mathematically defined as $Bi \ll 1$, where the Biot number is defined as in equation 2.4. This assumption may be a necessity due to the difficulties in obtaining accurate pyrolysis kinetics data for very high heating rate experiments, but does not hold for conditions relevant for suspension firing as reported by Johansen et al.[14] and shown in figure 2.23

$$Bi = \frac{hd_p}{2k_p} \tag{2.4}$$

Where h is the convective heat transfer coefficient and k_p is the thermal conductivity.

2.5.4 Volatile Oxidation

Combustion of pyrolysis gasses takes place in the gas phase where combustible volatiles are oxidized. The gasses produced by devolatilization are mainly light hydrocarbon gasses, hydrogen, CO and CO_2.[126] The volatile oxidation rate depends on the amount of oxidizer, the extent of mixing, and the temperature. The oxidation process increases the temperature in the flame. The flames from volatile oxidation have been observed cinematographically and tend to be spherical in lab scale equipment[126,127] and elongated in full scale.[128] The oxidation of combustion gasses is significantly faster than char oxidation, whereas char tends to burn at higher temperatures than pyrolysis gasses.[127]

2.5.5 Char Combustion

Char from both biomass and coal consists roughly of carbon, some O and H, and ashes/inorganics.[129] The carbon can be directly oxidized by O_2 following one of the two reactions seen below in equation (2.5) and (2.6),[130] where temperatures above 1000 K, typical for suspension firing, favor reaction equation (2.6).

$$C + O_2 \rightarrow CO_2 \tag{2.5}$$

$$C + \frac{1}{2}O_2 \rightarrow CO \tag{2.6}$$

Char can also be oxidized indirectly through gasification.[130–133] The C will then first react with CO_2 and water, and subsequently the generated H_2 and CO will be further reacted in the gas phase to the final combustion products as described in reaction (2.7), (2.8) and (2.9).

$$C + CO_2 \rightarrow 2CO \tag{2.7}$$

$$C + H_2O \rightarrow CO + H_2 \tag{2.8}$$

$$C + 2H_2 \rightarrow CH_4 \tag{2.9}$$

The reaction rate of char combustion depends on both operating conditions and particle properties. Experiments by Tilghman and Mitchell[134] for small biomass char particles ($d_p = 42$ µm) obtained under high temperatures and heating rates, show that the reactivity increases for

increasing temperature and O_2 concentration, whereas presence of H_2 decreases reactivity.[134] Other experiments[135] for char particles ($d_p < 150$ µm before devolatilization) obtained under high heating rates showed that oxidation of the particles was influenced by mass transfer limitations at temperatures as low as 673 K, meaning that mass transfer limitations must be included for all practical application in suspension firing units. Char from biomass typically burns at temperatures 100-200 K lower than coal char.[126]

2.6 Concluding Remarks

This literature review seeks to introduce the topic of combustion of biomass particles under condition typical in suspension firing units, i.e. high heating rates ($> 10^3$ K/s), high temperatures (> 1000 K), and small particles ($d_p = 0.1$-3 mm). Typical biomass properties are covered, as well as how the biomass goes from raw product to become a biofuel through milling, pelletization, and subsequently milling again at the power plant. The structure of biomass flames in suspension firing units is also briefly touched upon. The remainder of the chapter deals with the subprocesses taking place during single particle combustion; heating, drying, devolatilization, volatile, and char oxidation.

In order to model combustion in suspension firing each of these subprocesses must be adequately described. Modeling suspension firing can aid in the design process[136] for large suspension firing units as well as in retrofitting of already existing combustion facilities, so that the amount of antropogenic CO_2 emissions can be diminished. The large amount of particles in suspension firing units can be modeled using computational fluid dynamics (CFD)[15], but the accuracy of the simulation is directly dependent on the quality of the particle conversion models.

The following chapters seek to add to the knowledge of devolatilization of biomass under high heating rates. As mentioned, the relative ratio of char, tar, and gas, after devolatilization is dependent on operating conditions and biomass properties. As of yet, the char yield from devolatilization of particles under suspension firing conditions has been investigated in several experimental studies. However, a simple and accurate model determining char yield is presently not available. In this thesis a simple, empirical formula for the char yield is defined for a number of operating parameters.

Furthermore the morphology of biomass particles and its influence on devolatilization time is an underexposed subject. Particle morphologies are difficult to define in experiments and likewise difficult to treat in simple models. The transition from coal to biomass particles in suspension firing boilers has induces the necessity for dealing with non-spherical morphologies as biomass particles are generally larger and particle morphologies vary more for biomass. It has been the effort in this work to describe the effect of morphology for different particle sizes, and to propose a method of dealing with morphology effects in a simple single first order devolatilization kinetic model.

Paper A

This chapter contains the paper "Predicting Biomass Char Yield from High Heating Rate Devolatilization Using Chemometrics"[137] by Leth-Espensen, A; Glarborg, P.; and Jensen, P.A. It was published in Energy & Fuels, 2018, 32, 9572-9580. The supplementary material can be seen in appendix together with the original formatting in the journal.

3 Predicting Biomass Char Yield from High Heating Rate Devolatilization Using Chemometrics

3.1 Abstract

This study provides a simple model for biomass char yield obtained under conditions relevant for suspension firing. Using the multivariate data analysis methods, principal component analysis (PCA) and partial least squares regression (PLS regression), an equation is presented, which predict the char yield for wood and herbaceous biomass. The model parameters are heating rate (0.1-10 $\cdot 10^3$ K/s), average particle size (0.13-0.93 mm), maximum temperature (873-1673 K), potassium content (from 0.02 wt% db and upwards), and char yield (1-15 wt% daf). The model is developed based on wood biomass data and subsequently expanded to include straw and other herbaceous biomass. It is validated against experimental data from the literature and in general it exhibits the same characteristics. Independent data sets of wood are predicted with an average error (RMSEP) of 0.9 wt%point daf, and straw with an RMSEP = 0.9 wt% daf for the model, when a slope/intercept correction is applied, or RMSEP = 1.1 wt% daf otherwise. To include herbaceous biomass, the model introduces a potassium cut off level at 0.53wt%db, because the catalytic effect of potassium on the devolatilization process levels off above this concentration. The model consists of one equation, making implementation into CFD and devolatilization models possible without adding to the computational costs.

3.2 Introduction

The increased awareness of climate change has resulted in a demand for a more sustainable power and heat production. One possible option is suspension firing of biomass, which is often economically advantageous, because biomass particles can be utilized in existing boilers originally constructed for coal combustion. Combustion of single particles, regardless of whether it is coal or biomass, in suspension fired boilers includes devolatilization followed by volatile and char combustion. The combustion of the released volatiles happens relatively fast within the visual flame, while the char combustion is a more time consuming process.[138,139] Consequently, it is important to know the fractions of volatiles and char for prediction of the burnout of the fuel. The

volatile and char fractions are also often used as input parameters in combustion models.[14,140,141] Differences between coal and biomass particles include e.g. particle size, chemical composition, and volatile fraction[142]; which influence the obtainable char yield. Since so many parameters influence the process, char yield fractions are often determined experimentally for each individual fuel batch, but this is time-consuming and laborious under suspension firing conditions.

Several experimental studies[12,13,96,97,101,143] have investigated how typical suspension fired conditions influence the char yield of different types of biomass. Typical condition for suspension firing include high heating rates ($>$ 1000 K/s), high final temperatures ($>$ 1000 K), and small particles ($<$ 3 mm). For fully devolatilized wood particles char yields in the range 1-15 wt% dry ash free basis (daf) have been observed.[12,101] Experimental results obtained under suspension firing conditions have shown that particle size,[12,97,101] final temperature,[12,13,96,101] heating rate,[12] and alkali content[12,101,143] influence the obtained char yield. Higher values for both particle size and potassium content result in a higher char yield for suspension firing conditions. For an increase in particle size the tendency is weak,[12] whereas the potassium content shows a strong correlation to char yield up to approximately 0.5 wt% db of the biomass.[12] Values above 0.5 wt% db seem not to change the char yield further. An increase in final temperature and/or heating rate yields an exponentially decreasing correlation with char yield.[12]

In this study, the influence of different experimental and material parameters on biomass char yield has been examined through multivariate data analysis. The use of multivariate data analysis to determine biomass thermal conversion properties is limited, but a few examples have been found in literature. Acquah et al.[144] have made a chemometric analysis for predicting the results of thermogravimetric analysis (TGA) experiments, Kim et al.[145] used principal component analysis (PCA) to study biomass properties after exposure to CO_2, and wood pellet properties have been studied using PCA by both Toscano et al.[146] and Mancini et al.[147]. To the knowledge of the authors, no papers predicting the char yield of high heating rate experiments with the help of multivariate data analysis have been published. Neves et al.[148] made an empirical model for char yield obtained from devolatilization at final temperatures up to 1273 K and heating rates in the order 1-100 K/s. Trubetskaya et al.[93] made a one dimensional kinetic model of the char yield, fitting a set of differential equations.

This paper has two main purposes. First, it presents an exploratory investigation into data from devolatilization of biomass under suspension firing conditions using the key input parameters; particle size, final temperature, heating rate, and potassium content. This investigation is conducted through a principal component analysis (PCA). Subsequently, a model using aforementioned data to predict char yield is presented. The prediction model is calculated using partial least squares regression (PLS). The model is interpreted; evaluating the importance of the input parameters in a quantifiable way. The prediction model is simple, so it can be implemented into more complicated models and CFD simulations without adding substantial computational time.

3.3 Method

Chemometrics is the subject of extracting information from chemical measurements with a statistical approach. Commonly used methods within chemometrics are PCA and PLS.[149–151] In depth descriptions of PCA and PLS is beyond the scope of this paper, but can be found in the literature.[149–154] The PCA and PLS models presented here are made in PLS Toolbox version 8.1.1, Matlab version 9.3.0 (R2017b). The data have been extracted from the relevant papers using WebPlotDigitizer version 4.1.

3.3.1 Definitions of Parameters used for Model Development

The input parameters to the models are particle size, final temperature, heating rate, and potassium content, as they affect char yield from high heating rate biomass devolatilization.[12,148] In the scope of this paper **particle size** is defined as the average between the upper and the lower sieve sizes used for determination of biomass particle size. The sieve size average is used because it is frequently available and for simplicity. As biomass can vary in size and shape, more complicated measures exist.[155] **Final temperature** is the final or maximum temperature of the applied reactor. **Heating rate** can be obtained, e.g., via a thermocouple in a wire mesh reactor. Otherwise the heating rate is estimated as described in supplementary material. The **potassium content** is here defined as the potassium content in wt% dry basis (db) of the original biomass. In papers where the potassium content is not published it is estimated as described in the supplementary material. The **Char yield** is defined as the percentage of ash free char from a dry ash free biomass sample.

3.3.2 Selection of Data Applicable for Model Development

The interest of this study is the final char yield after suspension firing, hence only data for fully devolatilized particles have been used both for model development and model evaluation. The data set used for developing the model is obtained in a wire mesh reactor (WMR) and a drop tube reactor (DTR), originates from Trubetskaya et al.[12,13] and will be referred to as the calibration set. Any data, which fulfills the requirements indicated below will be used for independent validation of the model, and is referred to as the validation set. The papers used for validation are given in table 3.2. The data have been obtained in EFRs and DTRs as noted in the table. Particles were considered to have obtained full devolatilization if a paper showed consistent results for particle yield fractions over time and/or the residence time was long compared to the particle size.[12] Data which describe the char yield for fully devolatilized particles are scarce in literature, and papers[91,92,99,102,104,108,156], which do not provide data on fully devolatilized particles have been omitted from the study. Likewise, papers,[9,128] where the experimental conditions are outside the parameter intervals for the calibration data set, are also omitted from this study. The parameter intervals are given in table 3.1 for woody biomasses. Furthermore, char yield data[106,110] obtained from reactor types (e.g. fluid bed reactors), where

particle and operating conditions are vastly different from suspension firing conditions, may not be comparable and have been disregarded.

As the amount of published data describing char yield for non-wood biomass is limited, the presented model is developed based on wood biomass only. Considerations regarding expansion of the model to include herbaceous biomass char yield is presented in section 3.4.4 and 3.4.5. The parameter spans valid for the herbaceous char yield model are identical to the ones presented in table 3.1, except the potassium content, which has no upper limit for the herbaceous model.

Table 3.1: Parameter span for which the model for wood biomass is made. The full data set containing 37 data points from Trubetskaya et al.[12,13] can be seen in the supplementary material. The herbaceous biomass model use the same parameter spans except for the potassium content, where there is no upper limit; see section 3.4.5.

Parameter	min	max
Size [mm]	0.13	0.93
Final Temperature [K]	873	1673
Heating rate [10^3 K/s]	0.10	10
K content [wt% db]	0.02	0.37

Table 3.2: Data used for model evaluation. Only data for fully devolatilized particles are taken from the cited papers. Data above the dashed line are from wood biomass experiments. Data below the dashed line are from herbaceous material. * Estimated value as described in supplementary material. HR = Heating rate. # = Number of data points. EFR = Entrained flow reactor. DTR = Drop tube reactor. Potassium levels in herbaceous material is accounted for in section 3.4.5. Typical potassium levels in *Cynara Cardunculus* (used by Jiménez et al.[100]) is studied by Solano et al.[157] and the potassium content is taken from the latter.

	Paper	Reactor	Part. size [mm]	Final Temp. [K]	HR [10^3 K/s]	K content [wt%db]	#
A	Chen et al.[158]	DTR	0.35	1073	2.4*	0.05*	1
B	Dall'Ora et al.[101]	EFR	0.30	1273-1573	4.6-11*	0.03-0.1	4
C	Septien et al.[97]	DTR	0.36-0.82	1273-1673	1.2-8.1*	0.08 - 0.09	6
D	Zhang et al.[96]	DTR	0.25	1273	12*	0.03*	1
E	Jiménez et al.[100]	EFR	0.35	1073-1448	10	>0.53*	4

3.3.3 Preprocessing

Preprocessing is performed to develop a robust model. The parameters have been preprocessed individually to ensure linearity between parameters and char yield, as PLS is a linear regression method. The reader is referred to figure 2-4+6 in the paper[12] where the calibration set is originally presented for documentation of the correlations between the four independent parameters and char yield. For **particle size** the correlation seems linear, so no individual preprocessing method is applied here. **Final temperature** and **heating rate** show an exponentially decreasing correlation to char yield. It is, however, possible that it can be approximated by a linear

correlation in the parameter span relevant for suspension firing. Both a logarithmic and no individual preprocessing (linear correlation) are tested as possibilities. The **potassium content** seems to have a linear correlation to char yield until approximate 0.5 wt% db,[12] above which the effect of the potassium levels off. As the latter is only relevant for non-woody biomass, since no woody samples had potassium levels above 0.5 wt% db, no preprocessing of the potassium content parameter has been tested. An overview of the combinations in which the preprocessings have been tested is presented in table 3.3. The data is collected in two matrices; **X** containing values for the independent variables, and **Y** containing the dependent char yield values.

All parameters in the presented model have additionally been scaled to account for unit variance, to ensure that parameters contribute numerically equal regardless of the unit in which they have been measured.

3.3.4 Cross Validation

The cross validation performed in this study is based on the random subset method, because the information, regarding duplicates and chronology of experiments in the papers[12,13] containing the data used for the calibration set, is scarce. The random subset method is described by Dubitzky et al.[159] and ensures that the entire parameter span is used for cross validation. In this paper the cross validation is made with six splits and six iterations, i.e. each subset consists of approximately 17 % of the data set. The cross validation is performed at least ten times for all models described in table 3.3. The explained variances in **Y** and RMSECV values are averages of the performed cross validations. The calibration set contains two different types of woody biomass, pine and beech. A common cross validation approach is to remove one type of biomass to see if the remaining biomass type would give similar results. In this case, however, it could lead to dubious results, due to the differences in char yield values. In other words, as the two biomass types are primarily producing two different ranges of char yield values, using one type to predict the other would require an extrapolation of the model, which is undesirable.

3.3.5 Principal Component Analysis

A PCA reveals systematic behavior in a data set. Ideally the data should be normally distribution, but even when this is not the case PCA can reveal some systematic behavior in a data set. In this case only the first two principal components (PCs) are deemed of interest, so only these are shown in figure 3.1. The loading plots for figure 3.1 can be seen in supplementary material. In the direction of the first PC there is a separation of the data points into biomass type. Within each biomass type there is also a correlation to char yield in the direction of the first PC. In the direction of the second PC the scattering due to differences in char yield is more pronounced. Since the data show systematic behavior with respect to char yield in the PCA, a PLS model is developed.

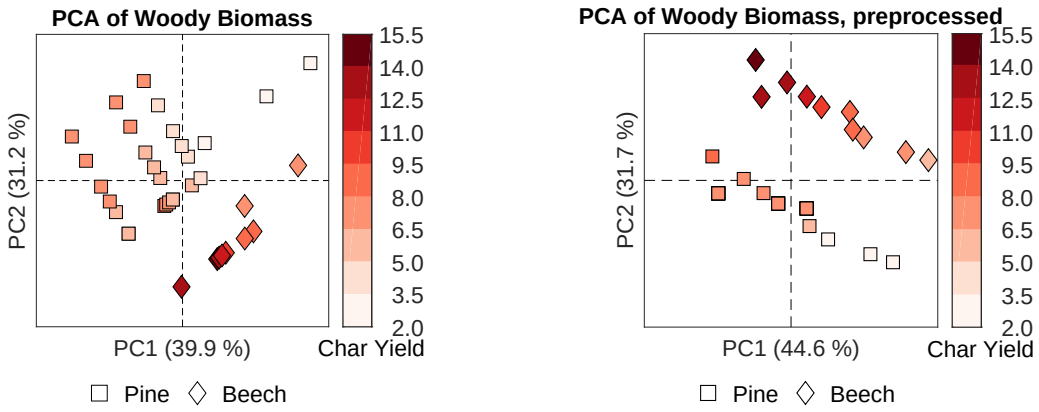

(a) Original variables.

(b) Preprocessed variables corresponding to model 10 presented in table 3.3. Some of the pine samples are located identically, which means not all are visible in this plot.

Figure 3.1: PCA plot for the 37 biomass data points from Trubetskaya et al.[12,13] given in supplementary material colored by char yield [wt%daf]. Explained variances in PC1 and PC2 are given in the parentheses on the axes. Loading plots can be seen in supplementary material.

3.4 Results

Table 3.3: Overview of tested PLS models for wood biomass. All models are made with one PLS component. ExpVarY and RMSECV are average values of at least ten cross validation runs. ExpVarY = Explained variance in **Y**, FT = final temperature, HR = heating rate, KC = potassium content, CY = char yield. x = parameter is included. - = parameter not included directly as input parameter.

Model #	**Size**	**FT**	**HR**	**KC**	**CY**	**ExpVarY** [%]	**RMSECV** [wt%points daf]
1	x	x	x	x	x	72.9	1.6
2	x	x	log(x)	x	x	81.8	1.3
3	x	log(x)	log(x)	x	x	81.7	1.4
4	x	x	log(x)	x	log(x)	81.5	1.1
5	x	log(x)	log(x)	x	log(x)	81.3	1.1
6	-	x	x	x	x	77.6	1.5
7	-	x	log(x)	x	x	88.6	1.1
8	-	x	x	x	log(x)	80.5	1.4
9	-	x	log(x)	x	log(x)	86.5	1.0
10	-	log(x)	log(x)	x	log(x)	86.5	1.0
11	-	log(x)	log(x)	x	x	88.8	1.1

3.4.1 Partial Least Squares Regression Model

The PLS model is developed to be able to predict the char yield of woody biomasses and thereby also the volatile yields. The preprocessing methods described in section 3.3.3 have been tested in different combinations reported in table 3.3.

Based on the RMSECV and explained variance in $\mathbf{Y}$, the most well-performing models are number 7, 9, 10, and 11. As previously noted a logarithmic correlation is likely between the final temperature and the char yield, hence model 10 and 11 are preferred over model 7 and 9. All graphs presented in the paper have been inspected for both model 10 and 11, but as they are qualitatively similar; only one set will be presented. Since the RMSECV (and RMSEP given in section 3.4.3) are lower for model 10 it will be preferred. As stated in table 3.3 the size parameter is not included in model 10, and in general when the size parameter is included the regression models seem to predict the char yield less accurately than when it is omitted. This will be discussed in the subsequent section 3.5. One PLS component is used for prediction in all the PLS models reported here. Various plots were inspected for outlier detection, but none have been found. An example of hotelling T^2 vs Q residuals is presented in the supplementary material.

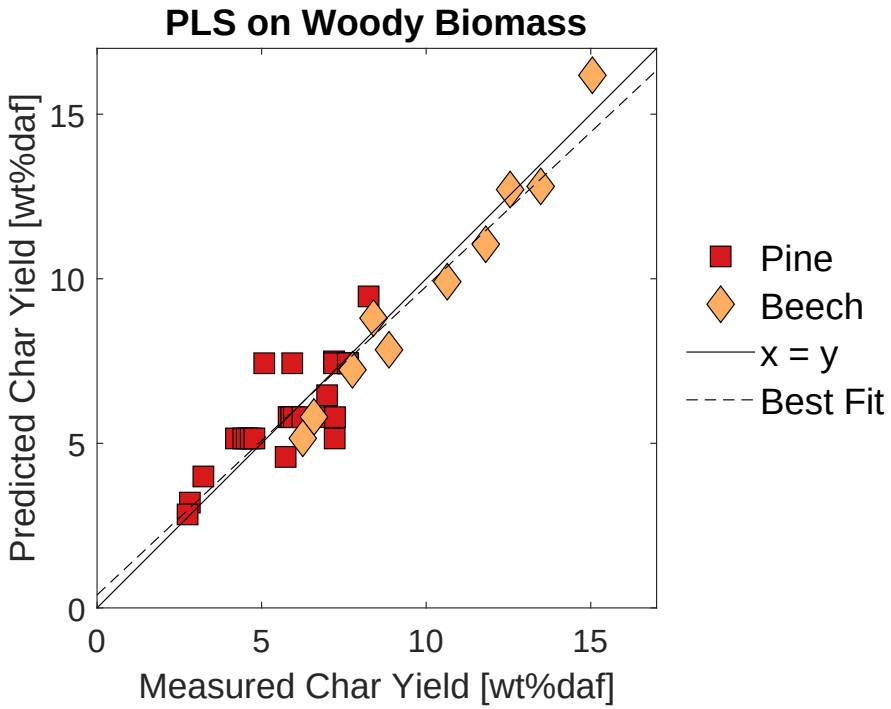

Figure 3.2: PLS plot of model 10 for the wood biomass calibration set.

In figure 3.2 the cross validated predicted char yields have been plotted as a function of the measured char yield for model 10. The figure shows good agreement between the two, and the model has RMSECV = 1.0 wt%point and r^2 = 0.87. The model is condensed to a regression vector, which is given both for the preprocessed data and for the raw data in table 3.4.

Table 3.4: Regression vectors for model 10.

Parameter	**Reg. vec.** (Preprocessed)	**Reg. vec.** (Raw data)
Intercept	0	3.4370
log(FT)	-0.4521	-0.6598
log(HR)	-0.6850	-0.2130
K content	0.5713	0.6852

The char yield can be predicted for new data, by converting the regression vector values back to the values, they would have without the preprocessing. Thus the char yield from wood devolatilization can be predicted for new data from equation (3.1).

$$CY_{wood} = 10^{3.4370+0.6852 \cdot KC - 0.6598 \cdot log(FT) - 0.2130 \cdot log(HR)} \tag{3.1}$$

Here CY_{wood} is the char yield in wt%daf, KC is the potassium content in wt%db, FT is the final temperature in K, and HR is the heating rate in K/s.

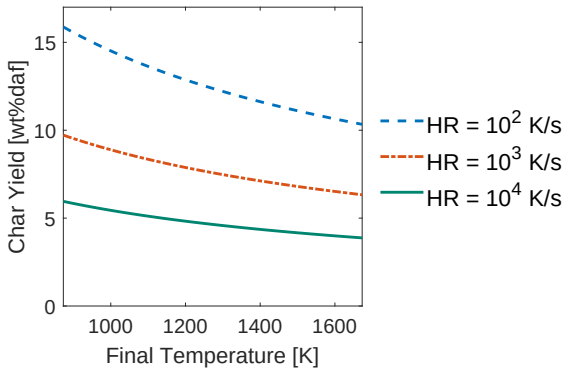

(a) K content = 0.19 wt%db.

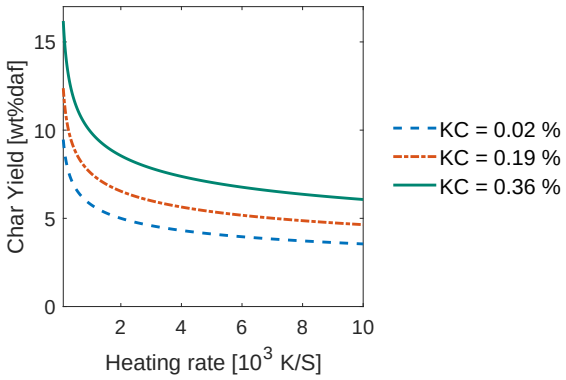

(b) Final Temperature = 1273 K.

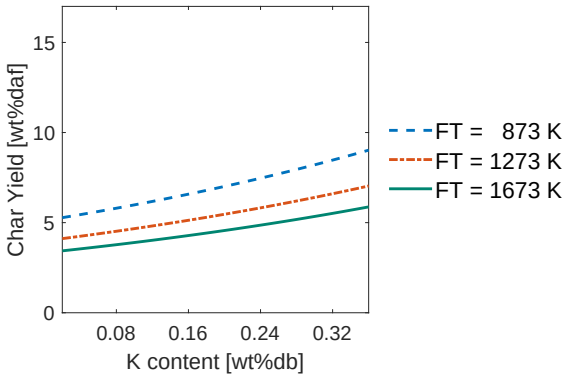

(c) Heating rate = 5000 K/s.

Figure 3.3: Model predictions for different parameters. HR = Heating rate, KC = potassium content in [wt%db], FT = Final temperature.

3.4.2 General Tendencies

The general tendencies predicted by the model can be seen in figure 3.3a through 3.3c. In figure 3.3a it can be seen that the char yield decreases for increasing final temperature. In figure 3.3b it can be seen that the char yield decreases rapidly with increasing heating rate in the lower end of the heating rate range and that the changes are leveling out for higher values of the heating rate. Both figure 3.3a and 3.3b show an exponential correlation between heating rate, final temperature, and char yield. Figure 3.3c shows that the char yield increases as a function of increasing potassium concentrations in the biomass. All these findings are in good agreement with the experimental observations made by Dall'Ora et al.[101], Trubetskaya et al.[12], and Septien et al.[97]

3.4.3 Model Validation with External Data

The model has been validated with data from external experimental studies given in table 3.2. The predicted and measured char yield values for the external data is depicted in figure 3.4.

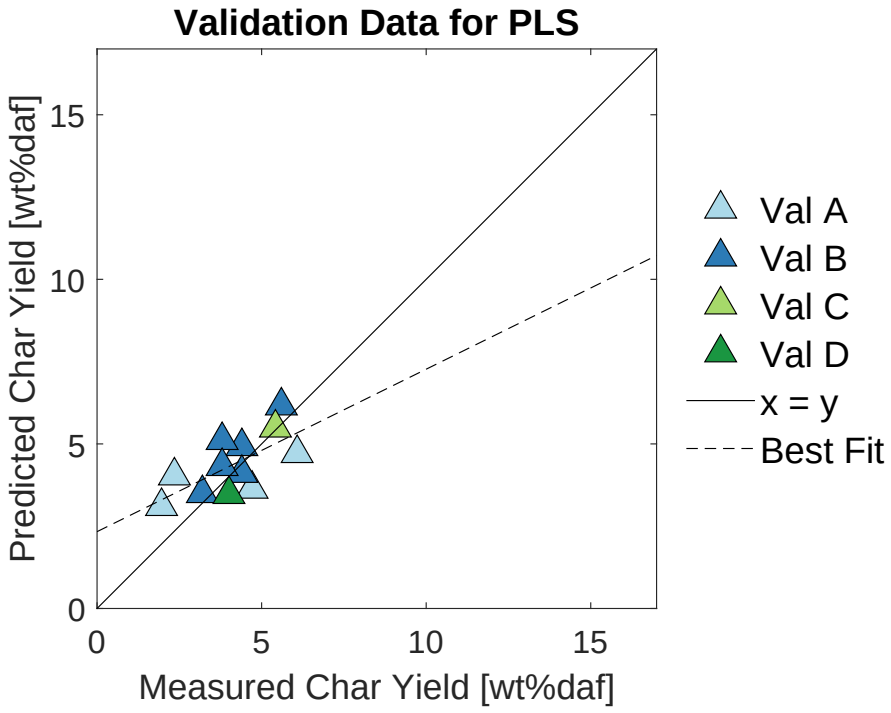

Figure 3.4: PLS plot for model 10 for the validation data given in supplementary material. Best fit line is for the validation data. Val A from Dall'Ora et al.[101], Val B from Septien et al.[97], val C from Chen et al.[158], and Val D from Zhang et al.[96]. The validation data are only in the lower end of the char yield range. The axes values are the same as in figure 3.2 for comparability.

The figure shows predicted vs. measured char yield for the validation data. There are limited data available for external validation, but in general the data are predicted well. More data,

especially in the upper char yield range, would be preferable in order to evaluate this part of the model as well. The root mean squared error of prediction (RMSEP) is 0.9 wt%points for the external data. I.e., the average error for predicted biomass char yield for the completely independent data sets is ± 0.9 wt% points which is low and similar to the RMSECV value of 1.0 wt%points, indicating that the model is robust.

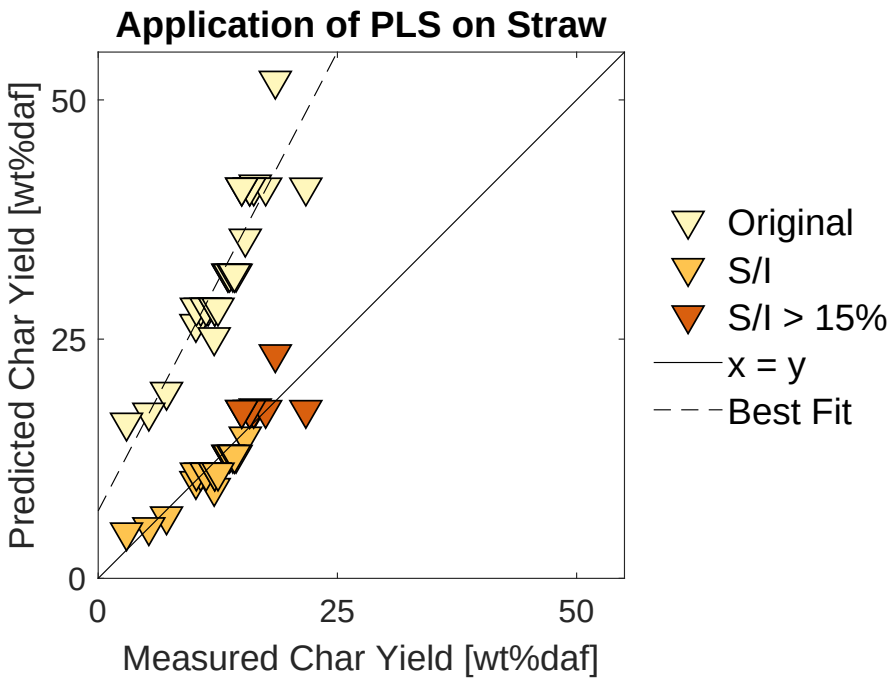

Figure 3.5: Predicted vs. measured char yield for model 10 in [wt%daf] for straw data by Trubetskaya et al.[12,13] both for the original and the slope/intercept corrected model. The measured char yield data above 15 wt% daf are colored a darker orange to indicate which predicted values are found by extrapolation of the model. S/I = slope/intercept corrected model. The dashed best fit line is for the original model. The slope intercept corrected model has been corrected to have the best fit as the y=x line. Straw data is given in the supplementary material.

3.4.4 Predicting Char Yield of Straw

Straw is also a commonly used biomass fuel in suspension fired boilers. Trubetskaya et al.[12,13] have conducted experiments with wheat straw, but no additional wheat straw data obtained under suspension firing conditions applicable as validation data have been found. Consequently, a model for straw char yield has been developed by making a slope/intercept correction to the wood biomass model. An advantage of this approach is that the model is modified to give the best possible fit for the data, so biomass samples which are very similar are predicted well. Another advantage is that the slope/intercept is unbiased in determining the communal importance of the input parameters. A disadvantage of the slope/intercept is that it is not applicable for data which is different from the data used to modify the model. The following model is hence only valid for straw/herbaceous material which have the same characteristics as

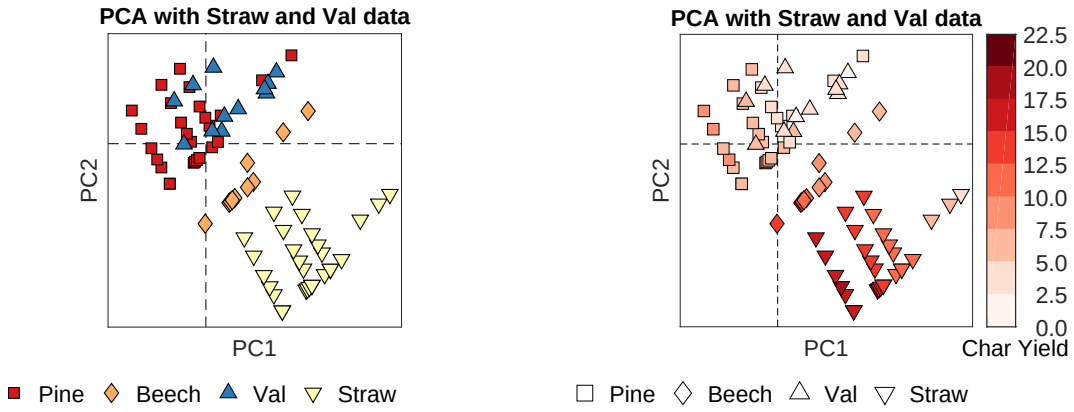

(a) Colored by biomass type.

(b) Colored by char yield. NB. Colorbar is in a different scale than the one presented previously.

Figure 3.6: The validation data and straw data incorporated into the PCA first introduced in figure 3.1a.

the wheat straw given in supplementary material. The predicted vs. measured wheat straw char yield can be seen in figure 3.5. It can be seen that the data are approximately linear, which strengthens the validity of expanding the model by a slope/intercept correction. Slope/intercept corrections are a standard procedure described both in academia[160] and industry[161]. A more generally applicable model is presented in section 3.4.5.

The slope/intercept correction is further supported by the results in figure 3.6a and 3.6b, which show PCA plots for the original calibration set together with validation data and straw data. Since the validation data for wood are occupying the same space in the PCA vector space as the calibration set, it is plausible that the prediction model is applicable also for the validation set, which is in good agreement with the results observed in section 3.4.3. The straw data are located away from the calibration set in the PCA plot, so applying the char yield model for wood directly as presented in equation (3.1) is not likely to yield useful results. The differences in locations in the PCA plots are primarily attributable to the potassium content being higher for straw. However, it is worth noticing that the tendency with respect to char yield in the PCA vector space is the same for straw and woody data, so a slope/intercept corrected model is appropriate.

Since some of the char yields for the straw exceed the maximum char yield in the calibration set, these data points have been excluded before making the slope/intercept correction. They are removed because having to extrapolate a PLS model is generally not advisable. As can be seen in figure 3.5 the removed straw data are approximately located on a straight line with the same slope as the remaining straw data, so the changes obtained by removing them are minor. A comparison of the model statistics with and without char yield data above 15 wt% daf and the original straw data can be seen in table 3.5. The expression for straw char yield can be seen in equation (3.2). The equation has not been validated against an external validation set and should thus be used more cautiously than the model for wood biomass, especially if the potassium content is vastly different in the sample one wants to predict the char yield of.

$$CY_{Straw} = \frac{10^{(3.4370+0.6852\cdot KC-0.6598\cdot log(FT)-0.2130\cdot log(HR))} - 10.6603}{1.4963} \quad (3.2)$$

Here CY_{straw} is the char yield in wt%daf, KC is the potassium content in wt%db, FT is the final temperature in K, and HR is the heating rate in K/s.

Table 3.5: Model statistics for the PLS model for the cross validated calibration set for woody biomass, the validation data for woody biomass, and the straw data. The original straw model (Model 10) has been reported as well as slope/intercept corrected data with and without char yield data above 15 wt%daf. * RMSECV. ** RMSEP.

Included Data	**RMSE** [wt%points daf]	$\mathbf{r^2}$
Woody cross validated calibration Data, Model 10	1.0*	0.87
Woody validation Data, Model 10	0.9**	0.45
Straw, Model 10	19.8**	0.82
Straw, Model 10 (S/I)	1.8**	0.82
Straw, Model 10 (S/I), yield $<$ 15 wt% daf	0.9**	0.93

3.4.5 Predicting Char Yield of Herbaceous Material

Straw is not the only herbaceous material used for suspension firing and a more broadly applicable char yield model would be advantageous. A possible way of modifying the model for wood presented in equation (3.1) in order to include additional biomass species is to determine the potassium concentration at which the catalytic effect of this compound levels off. An advantage of this approach is a more versatile model, but it comes at the cost of lower model accuracy. The cut off level for the effect of potassium is here determined from the wheat straw experimental data by Trubetskaya et al.[12,13], and the cut off level is then tested for other herbaceous material experimental data by Trubetskaya et al.[12,13] and independent data by Jiménez et al.[100].

As previously mentioned, the linear correlation observed in the experimental data between char yield and potassium content levels off around 0.5 wt%db, so the 1.1 wt%db reported for the straw in the experiments used for model generation will likely cause an overshoot in the prediction of the char yield, if the wood model were used. However, if the wood model is used with a correction in potassium content, some of the differences between wood and herbaceous biomass can be highlighted. To determine the concentration, where the effect of potassium levels off, the RMSEP for the straw is used as an optimization parameter; the lower the RMSEP, the better. For the given straw data the potassium content, which yields the lowest squared error (RMSEP) between measured and predicted straw char yield, is 0.53wt%db. So for biomass with a potassium content above 0.53 wt%db the input to the model in equation (3.1) should be fixed at 0.53 wt%db. Figure 3.7 depicts the predicted vs. measured straw char yield, if one uses the wood biomass model with the real straw potassium content and with a potassium content of maximum 0.53 wt%db. This indicates that the major differences in biomass char yield for wood and straw is due to the catalytic effects of potassium in the devolatilization process. This is further strengthened when the cut off value of 0.53 wt%db is used for other herbaceous biomass,

as shown in figure 3.8. Using the same cut off value of 0.53 wt%db on different herbaceous biomass types shows that the change in potassium content accounts for the majority of the difference in char yield between wood and herbaceous material in general, but the potassium content cut off value of 0.53 wt%db is not equally good for all biomass types. RMSEP values and r^2 values for the herbaceous biomass can be seen in table 3.6.

Table 3.6: Model statistics for herbaceous biomass with a cut off value for potassium of 0.53wt%db in model 10. The cut off value for potassium has been determined by determining the minimal possible RMSEP for the straw data, all data points included. Validation data are below dashed line.

Biomass Type	**RMSEP** [wt%points daf]	$\mathbf{r^2}$
Wheat Straw	1.6	0.82
Wheat Straw, yield $<$ 15 wt% daf	1.1	0.93
Leached Wheat Straw	1.4	0.70
Alfalfa	2.2	0.95
Rice husk	2.7	0.86
Thistle (Val E)	2.3	0.01

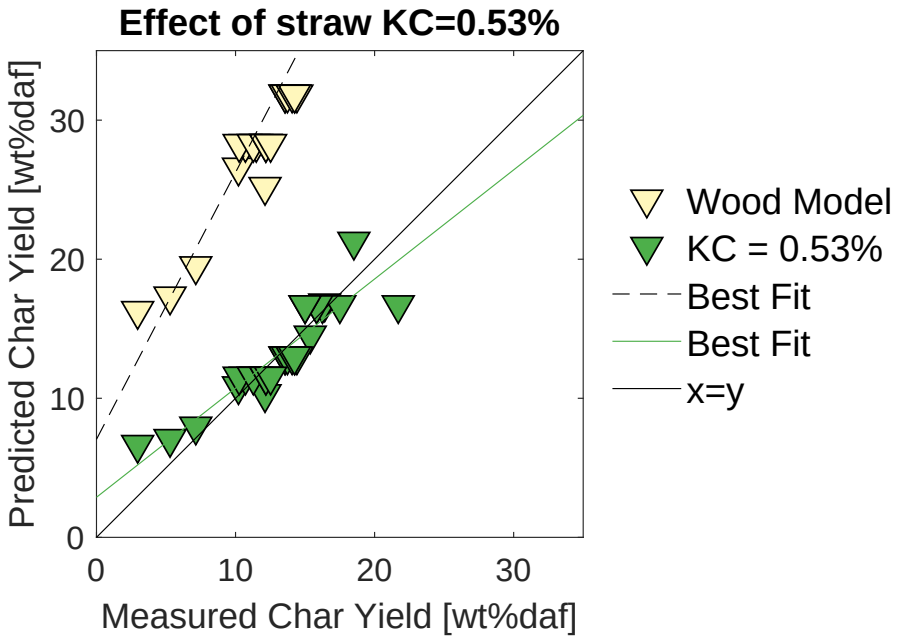

Figure 3.7: Predicted vs. measured char yield for model 10 in [wt%daf] for the original straw data by Trubetskaya et al.[12,13] and for the wood model with a cut off value of KC = 0.53 wt%db. KC = potassium content.

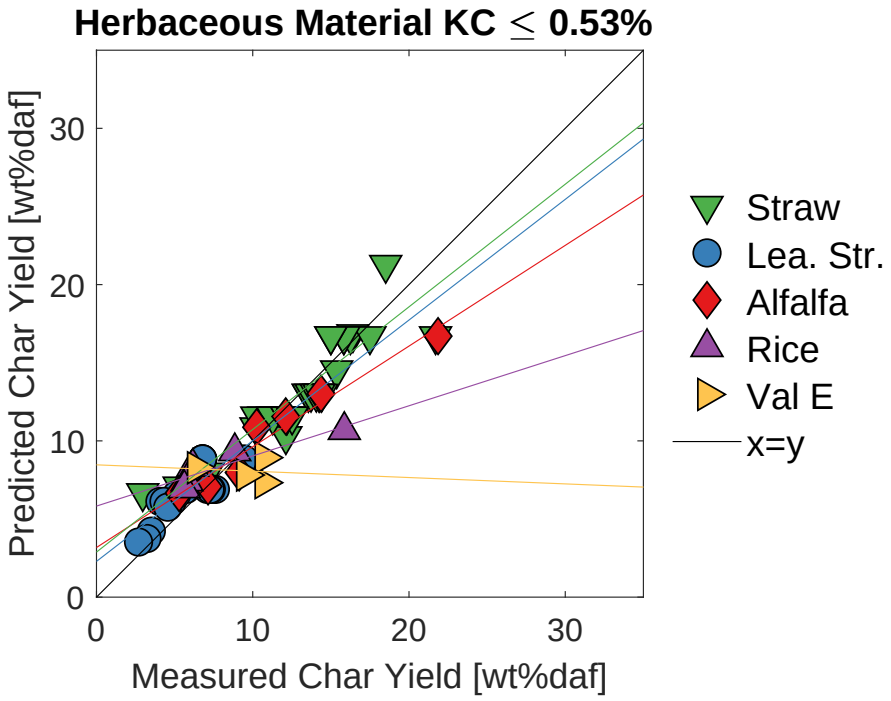

Figure 3.8: Predicted vs. measured char yield for model 10 in [wt%daf] for leached wheat straw, rice husk, alfalfa, and wheat straw. The two latter have a cut off value of KC = 0.53 wt%db. The leached wheat straw has KC = 0.13 wt%db. Rice husk KC = 0.25 wt% db. Val E = validation data from Jiménez et al.[100] from *Cynara Cardunculus* thistle with a cut off value of KC=0.53 wt%db. KC = potassium content. Best fitted lines for all biomass types can be seen in their respective colors.

3.5 Discussion

The model is generally good at predicting char yield from woody biomass from both the calibration data set and from externally sourced data with RMSECV = 1.0 wt%point and RMSEP = 0.9 wt%point, respectively. Model validity is further supported by the PCA, which shows that the char yield is correlated to one or more parameters in the data set. Expansion of the model to include wheat straw, by a slope/intercept correction, also yields good modeled results; RMSEP = 0.9 wt%point for straw with a char yield below 15 wt%daf. The model is further expanded to include different herbaceous biomass of higher potassium contents. For the versatile model, the RMSEP = 1.1 wt%daf for straw with a char yield below 15 wt%daf.

An advantage of developing a model using chemometrics is the prevention of bias in the selection of which parameters should have the most influence in the model, namely false assumptions about how the parameters influence the char yield and which physical phenomena are more important. Parameters are only excluded from the developed model if they do not enhance the prediction accuracy of the desired dependent parameter, specifically the char yield.

In this study, the particle size is excluded as input parameter to the model in the development process, because inclusion decreases the model accuracy. This can be observed by comparing the

model statistics for models 1-5 with the ones for models 6-11 in table 3.3, where the RMSECV and the explained variance in **Y** both increase when the size is excluded. It is possible that the reduction to a simple mean sieve size is too crude an estimate for a biomass particle distribution, as biomass particle sizes are generally difficult to determine.[155] Even when the size parameter is omitted it is still implicit in the model as the size affects the wood particle heating rate.

The heating rate can be difficult to determine accurately. In a WMR, which was used to generate most of the calibration set data,[12] the heating rate can be controlled, but in other reactor types it must be estimated, as seen in the supplementary material. In the present work, a simple model is utilized to estimate particle heating rates, based on the assumption that the calculated heating rate for an isothermal particle is a reasonable approximation of the heating rate in the real particle. The larger the particle, the worse the assumption with respect to isothermicity. The assumption is justifiable, because the model yields consistent results both through the cross and external validation.

The potassium cut off value of 0.53 wt%db for biomass is useful in expanding the model to include more biomass types. It is, however, also an additional parameter, which has been fitted, and which requires validation. The cut off value results in RMSEP = 2.2 wt%daf for alfalfa and RMSEP = 2.3 wt%daf for thistle, which is comparable to the RMSEP values for the herbaceous biomass with lower potassium levels. The accuracy of the model should be considered taking into account that the char yield is usually otherwise determined by proximate analysis, which overestimates the char yield for suspension firing conditions more than is the case for the model presented here.

For all models presented in this paper there is a tendency that the char yield is slightly over-predicted for low char yields and underpredicted for high char yields as indicated by the best fit lines in figures 3.2, 3.4, 3.7, and 3.8. This indicates that the model does not account for extreme values very well and that the PLS models do not account for all variations in the data sets. One possibility of enhancing prediction would be to develop PLS models with a higher number of input parameters, which would also allow for a higher number of PLS components in the model development phase. A disadvantage in using more input parameters is that usefulness of the model diminishes if complicated measurements are necessary to determine the char yield. For the purpose of presenting a simple model for biomass char yield as an input parameter to more complicated devolatilization models/CFD, the current compromise between complexity and accuracy has been deemed sufficient.

The model is limited by the uncertainties related to measurements in the original data, which was reported to have a measurement error of ± 5 wt% within a 90 % confidence interval. For a char yield of 10 wt%daf, this corresponds to a char yield of 10 ± 0.5 wt%daf. This should be compared to an RMSEP = 0.9 wt%points. The average error made by the prediction model is just shy of twice the error reported for the calibration set data, which is considered as being reasonable taking the number of parameters and data points into account. Especially considering the difficulty of determining uncertainties in high heating rate experiments.

It is possible to increase the quality of the model by conducting additional devolatilization experiments in EFRs and WMRs. This should be done primarily to explore the design space

more systematically, but also to increase the amount of experimental data. In the design space covered by the experiments for the calibration set, the input parameters are correlated to the degree seen in the correlation coefficient chart in figure 3.9. The chart gives the correlation (negative or positive) between the input parameter values chosen in the experiments. The higher the absolute value in the coefficient chart, the more the two parameters are correlated in the conducted experiments. It is advantageous not to have a high correlation between parameters in order to be able to determine the effects of the individual parameters. Despite being generally good, the chart still suggests that variations in the particle size have not been tested equally for the two wood types, which would have been optimal. The correlation between heating rate and final temperature might be more difficult to separate as they are physically linked, but more WMR experiments could decouple these two parameters.

	HR	FT	KC	Size	log(HR)	log(FT)
HR		0.46	0.14	-0.04	0.85	0.41
FT	0.46		0.14	-0.03	0.32	0.995
KC	0.14	0.14		-0.38	0.06	0.14
Size	-0.04	-0.03	-0.38		0.10	-0.05
log(HR)	0.85	0.32	0.06	0.10		0.28
log(FT)	0.41	0.995	0.14	-0.05	0.28	

Figure 3.9: Correlation coefficient chart for the parameters used to obtain the calibration set of wood biomass data.

3.6 Conclusion

Often a proximate analysis is used to determine the char yield for a biomass sample, however, for suspension firing combustion conditions with high heating rates and high final temperatures the char yields are lower. The models presented in this paper can be used to more accurate estimations of char yield under suspension firing conditions.

Through PCA and PLS experimental char yield data from woody biomass particles have been used to develop a simple model for predicting the char yield of woody biomass with an RMSECV = 1.0 wt%daf. The input parameters for the model are final temperature, heating rate, and potassium content. Validation of the model has been carried out using experimental data from four different studies, which gave an RMSEP = 0.9 wt%daf. The model has been expanded to include wheat straw by applying a slope/intercept correction, which yielded an RMSEP =

0.9 wt%daf. At a slight cost in model accuracy the model is further expanded to include all herbaceous biomass. This gives RMSEP = 1.1 wt% daf for straw, and slightly higher RMSEP values for other herbaceous biomass. The expansion is conducted by determining the potassium content, where the catalytic effects of potassium on the devolatilization process levels off. The value is determined to be 0.53 wt%db. Thus the char yield of biomass can be determined from equation (3.1) repeated below.

$$CY_{biomass} = 10^{3.4370+0.6852 \cdot KC - 0.6598 \cdot log(FT) - 0.2130 \cdot log(HR)}$$

Here $CY_{biomass}$ is the char yield in wt%daf, FT is the final temperature in K, HR is the heating rate in K/s, KC is the potassium content in wt%db, if $KC > 0.53$ wt%db then $KC = 0.53$ in the above equation. The model is relevant for suspension firing conditions.

3.7 Acknowledgments

The authors gratefully acknowledge the financial and advisory support received from Ørsted A/S, Burmeister and Wain Scandinavian Contractors A/S, and Rambøll A/S. We also thank the Nordic Five Tech (N5T) alliance for financial support.

3.8 Supporting Information

The following files are available free of charge.

- Supplementary Material: Raw data for chemometric analysis, supplementery plots from the analysis and a model for estimating missing parameters in char yield data.

Paper B

This chapter contains the paper "The Influence of Size and Morphology on Devolatilization of Biomass Particles"[87] by Leth-Espensen, A; Li, T.; Glarborg, P.; Løvåa, T.; and Jensen, P.A. It has been submitted for publication in a peer-reviewed journal in April 2019.

4 The Influence of Size and Morphology on Devolatilization of Biomass Particles

4.1 Abstract

This modeling study examines the effect of particle morphology on devolatilization of biomass particles at conditions relevant for suspension firing. A model, which can calculate devolatilization times and particle temperatures for both spherical and cylindrical particles is established, and modeling predictions are compared to experimental data from literature relevant for suspension firing with good consistency. The model predicts devolatilization times, which vary with more than two orders of magnitude in the particle size range (d_p = 0.2-3 mm) used in suspension firing. For the relevant gas temperature (T_g = 1300-1900 K) and density (ρ = 400-1000 kg/m^3) intervals, the devolatilization times vary with approximately a factor of two in both cases. Variations in moisture content primarily influence the time for onset of devolatilization, which may affect flame stability in suspension fired boilers. When modeling cylindrical biomass particles as spheres, the model further shows that it is more accurate to keep the diameter of the cylinder than to adjust the radius to create a sphere with the same volume as the original cylinder. Finally, the present study includes an analysis of the relative effect on devolatilization time of relevant physical parameters for three particle sizes (d_p = 78.8µm, 400 µm, and 1560 µm). The analysis shows that a 30 % decrease in T_g increases devolatilization times by 82 % for small particles, but only by 11 % for larger particles.

4.2 Introduction

Increased interest in climate change has given rise to the use of biomass as a fuel in suspension firing units. Typically, suspension firing is conducted at high temperatures (> 1000 K), high heating rates (> 1000 K/s), and with small particles (d_p < 3 mm). Suspension firing has traditionally been done with coal, but due to the wanted reduction in net CO_2 emission, biomass has been introduced. Biomass particles differ from coal in size, shape, chemical composition and volatile fraction.[70,142,162,163] Models for coal particle combustion have often assumed an isothermal, zero dimensional (0D)[164] or one dimensional (1D) spherical geometry.[165] This approach is not suitable for elongated biomass particles, where the increased size results in internal tem-

perature gradients, which cannot be neglected. Thus, with the transition from coal to biomass particles, modeling is required to include particles of different morphologies.[166–169] Compared to other morphologies, it is recommended by Trubetskaya[73,155] to model biomass particles as cylinders in devolatilization models. Typical aspect ratios ($AR = L/d_p$) for wood[72] are 2-3 and up to approximately 14 for herbaceous material.[73]

Experimental studies have illustrated the importance of representing particle gradients accurately. It is well known that thermal conversion of larger particles involves significant internal gradients. Larfeldt et al.[170] conducted experiments with large cylindrical particles (d_p = 50 mm, L = 300 mm) at moderate temperatures (973 K) in an electrically heated furnace, and Pilar Remacha et al.[171,172] conducted experiments in a flat flame burner for medium sized, spherical particles (d_p = 3-15 mm) at T_g = 1380 K. Both of these experimental studies showed internal temperature gradients for large particles, and it was concluded that an isothermal 0D approach is not sufficient to describe devolatilization in larger particles. However, even for particle sizes relevant for suspension firing, it may be important to account for gradients. Bharadwaj et al.,[111] who conducted experiments in a downfired turbulent flow combustor at T_w = 1523 K, with a particle sieve size of 0.707-0.841 mm and aspect ratio 2-3, showed that both intraparticle heat and mass transfer are necessary to account for biomass particle devolatilization for particle sizes relevant for suspension firing. Based on model work, Johansen et al.[14] came to the same conclusion valid for all particle sizes under conditions relevant for suspension firing.

Bharadwaj et al.[111] further show that the aspect ratio decreases during devolatilization for both wood (red oak) and herbaceous material (alfalfa). The same conclusion was drawn for small softwood particles (sieve size 45-75 μm) by Lewis and Fletcher[92] in a flat flame burner at T_g = 1163-1433 K. Lu et al.[167] have looked at devolatilization of three different particle shapes (d_p = 0.32-16 mm) in an entrained flow reactor and a single particle reactor and conclude that particle morphology influences devolatilization times and conversion rates due to the increase in surface to volume ratio for non-spherical particles. The corresponding model developed by Lu et al. indicates that particle morphology effects are important for particles exceeding 200-300 μm. Another devolatilization model describing both spherical particles and other geometries has been presented by Thunman et al.[173], and further developed by Ström and Thunman.[140] This model was validated against experimental data relevant for fluidized beds (d_p 10-40 mm, $T_g < 1123$ K, HR $\lesssim$ 10 K/s). Gubba et al.[174] presented a model to account for intraparticle heat and mass transfer for co-firing with biomass, which can be implemented into CFD. However, their model was only validated with experimental data for large particles (d_p = 9.5 mm) at intermediate temperatures (T_g = 1050 K), so it is not necessarily applicable for the smaller particles utilized in suspension firing. To the knowledge of the authors, no model exists, which is validated against relevant experimental data and can adequately predict devolatilization times for small particles ($d_p < 3$ mm) at high temperatures and heating rates for different morphologies.

Even though particle devolatilization is described extensively in the literature, work that illustrates the effect of biomass particle morphology on particle ignition and devolatilization time for conditions relevant for suspension firing is scarce. The purpose of this paper is to further develop the model by Thunman, Ström, and coworkers[140,166] to be relevant for suspension firing conditions, i.e. to be able to predict devolatilization behavior in smaller particle sizes at higher

temperatures and heating rates. Firstly, this is done by a modification to the model, so it now include sink and source terms for the energy required to heat water vapor and devolatilization gasses after reactions. Secondly, a new kinetic scheme incorporating both low and high heating rate Arrhenius kinetics is implemented, and submodels accounting for particle specific heat capacity and particle thermal conductivity are chosen according to the physico-chemical condition in a suspension firing unit. Thirdly, the model presented here is compared to experimental data from the literature in both the lower and the upper end of the suspension firing fuel size range. In this way, it is ensured that the improved model can describe all particle sizes in the relevant size range (d_p = 0.1-3 mm). Furthermore, this paper also illustrates the influence of key biomass properties' effect on devolatilization time. The effect of morphology, gas temperature, particle size, density, and moisture content on pyrolysis for three representative particle sizes (d_p = 79 µm, d_p = 0.8 mm, and d_p = 3 mm) has been investigated. The effect of these parameters on ignition time and flame stability in suspension fired units is discussed.

4.3 Method

The model adopted here, is originally by Thunman et al.[173] and Ström and Thunman.[140], and is developed for combusting particles in fluidized and fixed beds, i.e. for larger particles at lower temperatures than what is typically the case for suspension firing. In this paper the model is further developed to be able to describe single particle devolatilization under suspension firing conditions. Section 4.3.1 describes the structure of the model as it is put forward by Thunman, Ström and coworkers.[140,173] Section 4.3.2 describes the new additions to the model, by presenting submodels and the kinetic scheme, chosen here, in order to expand the model to include devolatilization of smaller particles at suspension firing conditions.

4.3.1 Model Description

The model is constructed as a shell model, comparable in structure to an onion. It is a combination of a sharp interface model and a finite reaction zone model.[175] At $t = 0$ the particle primarily consists of moist wood, with infinitesimally thin outer layers of dry wood and char. As time progresses the outer regions of the particle are dried and devolatilized. Consequently, at time t, the particle consists of three concentric shells; an outer char shell, a middle dry shell, an inner moist shell. A sketch of the shell structure can be seen in figure 4.1.

The evaporation of water happens at the interface between the moist and the dry zone. The devolatilization takes place in the dry zone, marked by the light peach colored area in figure 4.1. The heat balance for the outer shell includes external radiation and convection. The heat balances of the model can be seen in equation 4.1 through 4.3, and the mass balances can be seen in equation 4.4 through 4.6. There are some slight modifications to the originally developed equations[140] marked in blue in equation 4.1 and 4.2. Q_{l2} is a source term for the energy required to heat the water released during evaporation and the energy required to heat the wood, from

which the water has been released. The water vapor is heated from the release temperature, T_{b1}, to the temperature where it is transferred to the next shell, T_{b2}. The newly dried wood is heated from the release temperature, T_{b1}, to the temperature of the dry wood layer, T_{l2}. In the same fashion, Q_{l3} is a source term for the energy required to heat the gas released from the devolatilization, the energy required to heat the water released during evaporation (which has been transported trough the dry layer), and the energy to heat the char, in which the devolatilization has taken place. The volatiles and the water vapor are heated from the temperature at the shell boundary, T_{b2}, to the outer shell temperature, T_{b3}. The newly devolatilized wood (now char) is heated from the boundary temperature, T_{b2}, to the char layer temperature, T_{l3}.

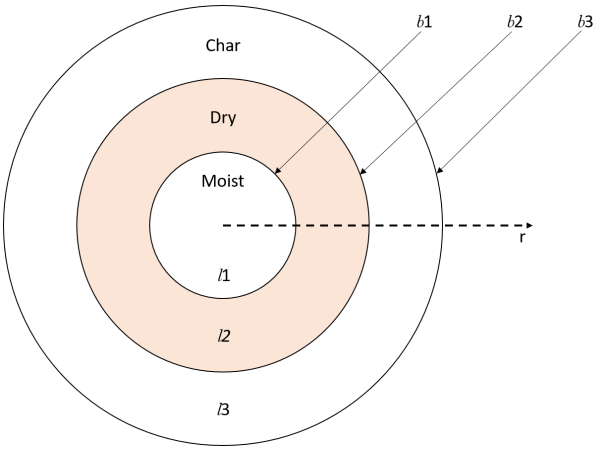

Figure 4.1: Sketch of shell structure. Adapted from Ström and Thunman.[140]

$$\frac{dT_{l3}}{dt} = \frac{\alpha_{l3}}{V_{l3}}\left(A_{b3}\frac{dT}{dr}\Big|_{b3,l3} - A_{b2}\frac{dT}{dr}\Big|_{b2,l3}\right) + \frac{Q_{l3}}{C_p\rho V} \tag{4.1}$$

$$\frac{dT_{l2}}{dt} = \frac{\alpha_{l2}}{V_{l2}}\left(A_{b2}\frac{dT}{dr}\Big|_{b2,l2} - A_{b1}\frac{dT}{dr}\Big|_{b1,l2}\right) + \frac{Q_{l2}}{C_p\rho V} \tag{4.2}$$

$$\frac{dT_{l1}}{dt} = \frac{\alpha_{l1}A_{b1}}{V_{l1}}\frac{dT}{dr}\Big|_{b1,l1} \tag{4.3}$$

$$\frac{dm_{l3}}{dt} = \gamma\omega_{b2} \tag{4.4}$$

$$\frac{dm_{l2}}{dt} = \omega_{b1}/Y_{m,db} - \omega_{b2} \tag{4.5}$$

$$\frac{dm_{l1}}{dt} = -\omega_{b1}/Y_m \tag{4.6}$$

The boundaries (b) and shell layers (l) are numbered from the center outwards, so $l1$ is the wet layer, $b1$ is the boundary between wet and dry layer and so on. T_{li} is the temperature of layer i, α is the thermal diffusivity, V is the layer volume, A is the surface area, m is the layer mass, γ is the char yield, ω_{wb1} is the drying reaction rate, ω_{b2} is the pyrolysis reaction rate, and Y_m is the mass fraction of moisture. Boundary conditions for the heat balances are given in equation

4.7 through 4.9, assuming no heat accumulation at the boundaries.

$$hA_{b3}(T_g - T_{b3}) + \sum \epsilon_1 \sigma A_{b3}(T_w^4 - T_{b3}^4) = k_{p3}A_{b3}\frac{dT}{dr}\Big|_{b3,l3} \tag{4.7}$$

$$k_{l3}A_{b2}\frac{dT}{dr}\Big|_{b2,l3} = k_{l2}A_{b2}\frac{dT}{dr}\Big|_{b2,l2} + Q_{rxn,b2} \tag{4.8}$$

$$k_{l2}A_{b1}\frac{dT}{dr}\Big|_{b1,l2}F_{b1} = Q_{rxn,b1} \tag{4.9}$$

Here h is the heat transfer coefficient, ϵ is the emissivity, σ is the Stefan-Boltzmann constant, k is the thermal conductivity, and Q_{rxn} is a reaction heat flow. F_{b1} is an empirical parameter, which determines the ratio of the heat transferred to the drying front for water evaporation to that used to heat up the wet wood layer.

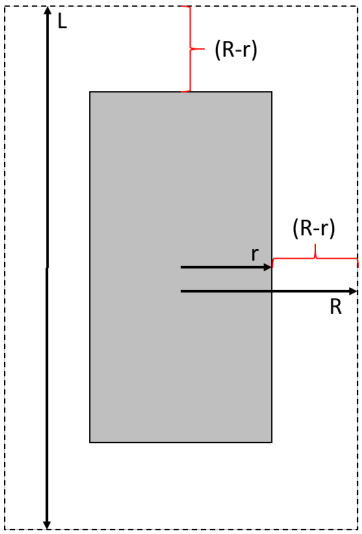

Figure 4.2: Sketch of geometry of cylindrical particle. Dashed line is initial outline of particle layer, solid grey figure is particle at $t > 0$.

The model can describe devolatilization of both spherical and cylindrical particles. The sizes of the particles are characterized by the initial radius R for the sphere, and by both an initial radius, R, and a length, L, for the cylinder. The one-dimensional geometry of the sphere and an assumption of isotropy means that changes in size for the spherical particles can be characterized only by one time-dependent variable, the radius r. The cylindrical particles are two-dimensional, but can also be described using only one variable, r, plus the two constant parameters for the initial dimensions, R and L. The length of the cylindrical particle is defined as a function of r as $l = L - 2(R - r)$. The implementation of the model is only made for cylinders with $L > 2R$. A sketch of the cylindrical particle can be seen in figure 4.2. By assuming that the reduction in diameter of a given shell equals the reduction in length, the number of variables needed to describe a cylinder can be reduced to one, assuming isotropy in the angular direction. This approach is a simplification of the end effects, but it allows for a simpler model. A model with a more detailed description of the end effects would have a devolatilization time higher than that for a sphere, but lower than the one predicted for a cylinder with the model presented here. As will be shown in section 4.5.2, the devolatilization time for a sphere and a cylinder with AR = 1.01 are practically the same, so describing the end effects at a higher computational cost is

not relevant here. The same one variable approach to describe cylinders has been utilized by Porteiro et al.[176]. Yang et al.[20] have, using a two variable approach, described the end effects in more detail by allowing a faster release of volatiles at the cylinder ends. However, this approach typically yields greater computational costs, thus it has not been pursued here.

The model as presented by Thunman, Ström, and co-workers[140,173] has been validated against experimental data with different morphologies (spheres, cylinders, and parallellipipeds), but only for large particles ($d_p > 9.5$ mm) at moderate temperatures ($T_g < 1276$ K). Thus, the original model has a verified capacity to predict biomass devolatilization under these conditions. However, larger particles at moderate temperatures are primarily heat transfer controlled. In contrast, the smaller particles utilized at suspension firing will be kinetically controlled or in the transition region between kinetically controlled and heat transfer limited devolatilization. For the purpose of expanding the model to be able to predict devolatilization under suspension firing conditions, alternative submodels and expression for relevant physico-chemical properties are put forward in the subsequent section.

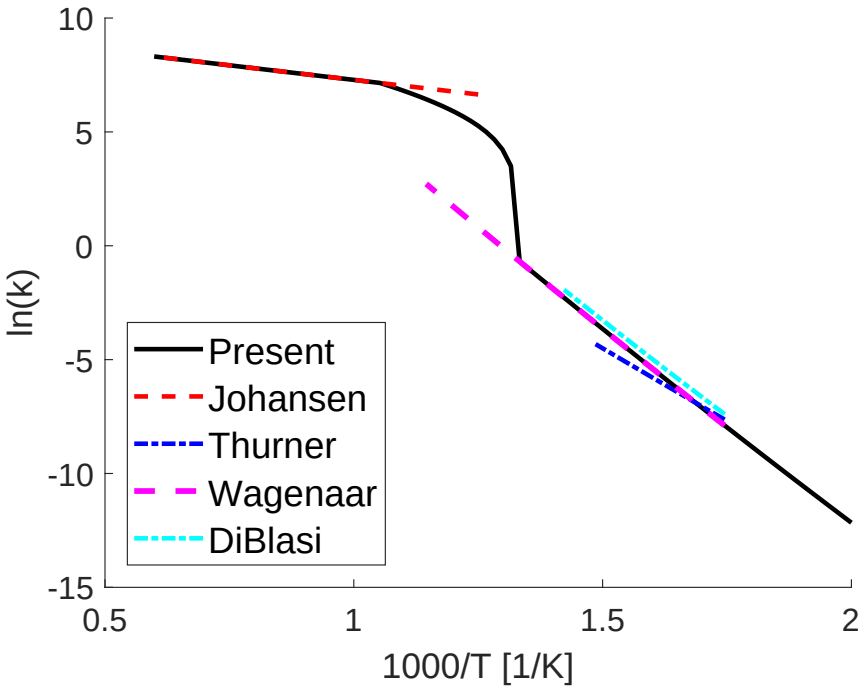

Figure 4.3: Arrhenius plot for kinetic scheme used in this model and literature models for high heating rate kinetics from Johansen et al.[9] and low heating rate kinetics from Wagenaar et al.[177], DiBlasi and Branca[178], and Thurner and Mann.[179]

4.3.2 Model Input Parameters

An overview of the model parameters used in this study can be seen in table 4.1.

Table 4.1: Model input parameters.

Parameter	Value	Ref.
h [J/(s m^2 K)]	Estimated as described by Leth-Espensen et al.	137
ϵ [-]	0.85	180,181
$\mathcal{L}_{H_2O}$ [J/kg]	2256 000	182
ΔH_{desorp} [J/kg]	3610 000	183
ΔH_{devo} [J/kg]	200 000	140,184
A_{L1} [s^{-1}]	$1.11 \cdot 10^{11}$	168,177
$E_{a,L1}$ [J/mol]	$177 \cdot 10^3$	168,177
A_{L2} [s^{-1}]	$9.28 \cdot 10^9$	168,177
$E_{a,L2}$ [J/mol]	$149 \cdot 10^3$	168,177
A_{L3} [s^{-1}]	$3.05 \cdot 10^7$	168,177
$E_{a,L3}$ [J/mol]	$125 \cdot 10^3$	168,177
A_H [s^{-1}]	$18.9 \cdot 10^3$	9
$E_{a,H}$ [J/mol]	$21.305 \cdot 10^3$	9
T_{boil} [K]	373.15	
C_g [J/(kg K)]	$\Big(19.50583 + 19.88705 \cdot \frac{T_g}{1000} - 8.598535 \cdot (\frac{T_g}{1000})^2 + ...$ $...1.369784 \cdot (\frac{T_g}{1000})^3 + 0.527601 \cdot (\frac{1000}{T_g})^2\Big) \cdot \frac{1000}{28}$	185
$C_{p,H2O\,vap}$ [J/(kg K)]	$\Big(30.09200 + 6.832514 \cdot T/1000 + 6.793435 \cdot (T/1000)^2 ...$ $...-2.53448 \cdot (T/1000)^3 + \frac{0.082139}{(T/1000)^2}\Big)\frac{1000}{18}$	186
$C_{p,dry\,w}$ [J/(kg K)]	$z1 = 380/T$ $z2 = 1800/T$ $g1 = z1^2 \cdot exp(z1)/(exp(z1) - 1)^2$ $g2 = z2^2 \cdot exp(z2)/(exp(z2) - 1)^2$ $C_{p,dry\,w} = (g1 + 2 \cdot g2) \cdot 1000 \cdot R \;/\; 7.72$	187,188
$C_{p,wet\,w}$ [J/(kg K)]	$A = 10^3 \cdot ((0.02355T - 1.320y/(1-y) - 6.191)y/(1-y)$ $C_{p,wet} = C_{p,wood}(1-y) + 4190y + A$	189
$C_{p,char}$ [J/(kg K)]	$C_{p,char} = (g1 + 2 \cdot g2) \cdot 1000 \cdot R \;/\; 11.3$	187,188
$k_{wet\,wood}$ [J/(m K s)]	$1.15 \cdot min(0.13 + 0.0003 \cdot (T - 273), 0.3)$	128,190,191
$k_{dry\,wood}$ [J/(m K s)]	$min(0.13 + 0.0003 \cdot (T - 273), 0.3)$	128,190
k_{char} [J/(m K s)]	$max(0.08 - (T - 273) \cdot 10^{-8}, 0.3)$	128,190,191
Shrin. ratio drying [-]	10 % (compared to wet)	173
Shrin. ratio devol. [-]	50 % (compared to dry)	173

The kinetic scheme builds on Arrhenius equations with different kinetic parameters for low and high heating rates, which can be seen in equation 4.10 through 4.12.

$$k_L = k_{L1} + k_{L2} + k_{L3} \tag{4.10}$$

$$k_{Lj} = A_{Lj}\, exp(-E_{a,Lj}/(RT)), \quad j = 1, 2, 3 \tag{4.11}$$

$$k_H = A_H\, exp(-E_{a,H}/(RT)) \tag{4.12}$$

The low heating rate kinetics are described by Wagenaar et al.[177] as three competing reactions and the high heating rate kinetics are described by a single first order reaction (SFOR) by Johansen et al.[9]. In this paper both low and high heating rate kinetics are treated as SFORs.

The low heating rate kinetics are combined to a single rate constant as shown in equation 4.10, in order to ensure that the obtained char yield is not dependent on three competing reactions, relevant only for low temperatures. The transition from the low to the high heating rate should happen around 800 K.[128] It is here chosen to be linear, with the transition temperature interval between 750 and 950 K. An Arrhenius plot of the pyrolysis rates of different studies and the combined function utilized here can be seen in figure 4.3. Compared to the kinetics utilized here, the figure shows that at low temperatures the high heating rate kinetics predicts the reaction rate to be high, and at high temperatures the low heating rate kinetics also predicts the reaction rate to be high. The discrepancies between low and high heating rate kinetics also show that it is necessary to have different kinetic schemes when covering a large temperature span.

The specific heat capacities for wood and char are sensitive to temperature. Relations for C_p should not be extrapolated outside the interval, in which they have been derived without careful consideration. Comparison of some examples of C_p values for both dry wood and char can be seen in figure 4.4. Extrapolation of the linear C_p expressions result in extreme values for the specific heat capacities, especially at high temperatures. The only pair of related C_p values, which do not increase significantly by extrapolation to the relevant temperature interval are behold by Merrick et al.[187], hence they have been chosen in the present work, even though they have originally been derived for coal. An expression for the specific heat capacity for wet wood is derived by TenWolde et al.[189], and is dependent on both moisture content and the C_p of dry wood. This expression is utilized here, using the expression for dry wood C_p developed by Merrick et al.

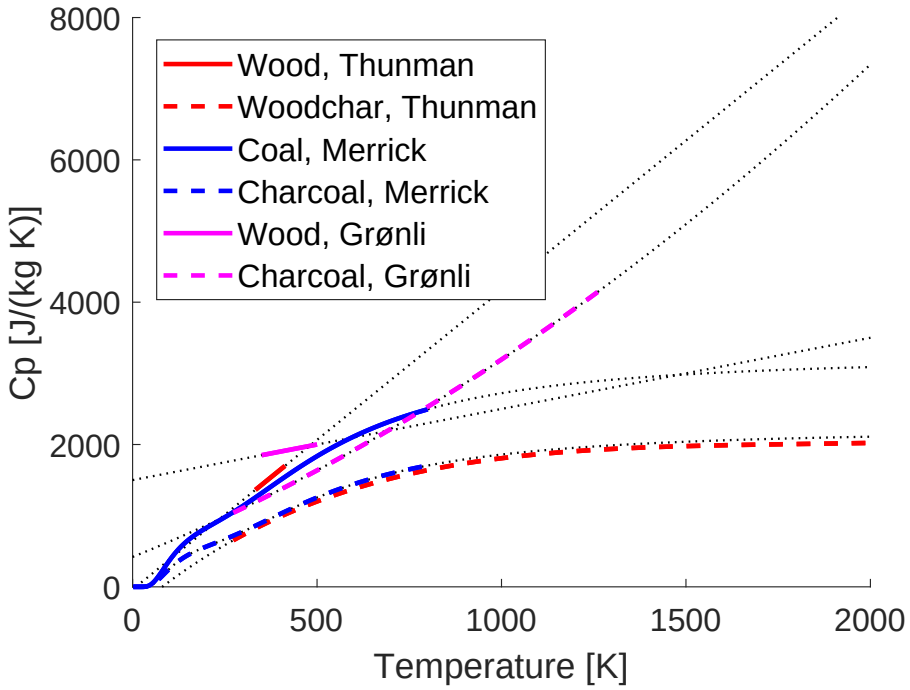

Figure 4.4: Comparison of C_p values from Thunman et al.[173], Merrick[187] and Grønli and Melaaen.[192] Black dotted lines are extrapolation of models.

The change of enthalpy as a result of the desorption of water from a coal particle has been addressed by Callanan et al.[183] for multiple samples, all giving similar results. An average

value of the provided data, 3.61 kJ/g, has been utilized here. The value is connected with some uncertainty as the data are obtained for coal particles, but the water content is low in the experiments investigated here (0-6 wt % wb) and in suspension firing units in general, meaning that the effect of any uncertainties are assumed insignificant. The change in enthalpy as a function of devolatilization reported in literature varies from being highly endothermic at 611 J/g wood[193] to being exothermic at -222 J/g.[194]. There seem to be little consensus in literature on any value for the heat of devolatilization, and most sources provide both exothermic and endothermic values.[140,194] The discrepancy is likely due to differences in biomass, differences in operating conditions, and a different definition on how the devolatilization process is delimited. Most sources do, however, report the process to be slightly endothermic. In this work different heat of devolatilization values have been tested and compared to experimental results, and a value of 200 J/g has been chosen as it represents experimental data well. The influence of changes in heat of devolatilization is tested in section 4.5.1.

The thermal conductivity of virgin wood is normally considered to be considerably higher than that of char,[190] but Brown[195] has shown that the thermal conductivity of char at elevated temperatures is twice that of virgin wood at ambient temperature, consequently both must be determined accurately. The thermal conductivity employed in this work builds on the correlation set forward by Koufopanos et al.[190]. They developed an empirical expression for the devolatilization of wood particles (d_p = 20 mm) under moderate temperatures ($T_g < 873$ K), that has been widely adopted, also for high heating rate experiments.[128,196] No thermal conductivity correlation for wood at higher temperatures has been found in literature. Thermal conductivity for wet wood is approximately 15 % higher than that of dry wood according to table values for multiple wood species from the WoodHandbook[191], thus a 15 % increase in wet wood thermal conductivity has also been applied here.

The heat transfer coefficient, h, is an input parameter, which, regardless of particle shape, is estimated as described by Leth-Espensen et al.[137] h is calculated from the Nusselt number, which is not defined for free falling cylindrical particles in turbulent gas streams, hence a spherical correlation has been employed. Duan et al.[197] propose to relate the heat transfer coefficient to the drag coefficient and determine h in this way in order to avoid the dependence on the Nusselt number. Although possible, a limited number of experiments relating drag and heat transfer for cylindrical particles in free fall are available and therefore, a spherical assumption using the correlation for the Nusselt number is currently employed.

The model predicts both the temperature of each of the three particle boundaries (moist wood, dry wood, and char) as shown in figure 4.5 and the temperature and mass of each of the three particle layers. In figure 4.5a the mass of each of the three layers and the total mass of the particle can be seen. It can be seen that the mass of the moist layer decreases over time, whereas the dry wood layer first increase as water is evaporated, and subsequently decreases as the wood is devolatilized. The char layer steadily increases until it reaches the specified char yield. The total mass of the particle decreases over time until only char is left. Figure 4.5b shows the temperature on the outer surface of each shell. The surface temperature is thus identical to the char boundary temperature, T_{b3}, in this figure. The dry layer temperature is increasing as the particle is heated, but stagnates during devolatilization as the process is endothermic.

The moist boundary temperatures, T_{b1}, is close to the center temperature as the entire moist layer is slowly heated to the boiling temperature, and remains at T_{boil} during water evaporation. The moist layer temperature, T_{l1}, is the average temperature in the moist layer and is plotted in the remainder of this paper as a substitute for the particle center temperature, which is not obtained in this model.

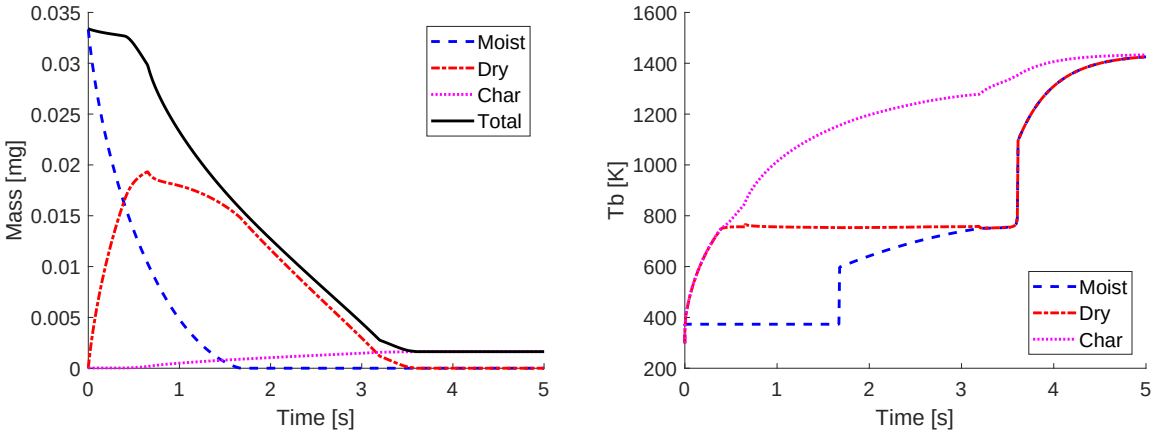

(a) (b)

Figure 4.5: Example of mass and temperature profiles provided by the model. Here for a particle with AR = 2, ρ = 700 kg/m^3, T_g = 1600 K, T_w = 1400 K, moisture content = 4 wt% wb, and r_{ini} = 1560 µm.

4.4 Model Validation

This section covers the validation of the model with experimental data relevant for suspension firing for both spherical and cylindrical particles. The model is validated against data sets involving particles in the diameter range 78.8 µm to 9.5 mm. The degree of devolatilization in the following graphs is release of volatiles excluding the water present in the particle.

4.4.1 Summation of Model Validation

The model is validated for particles in the parameter intervals give in table 4.2. The model is validated in the entire size interval relevant for suspension firing, also the main part of the parameter ranges for moisture content, gas temperature, and density are covered. For the aspect ratio the relevant range for wood particles is covered.

4.4.2 Particles with d_p = 78.8 µm

Experiments with small wood particles have been performed by Johansen et al.[9,10]. The experiments were conducted in a laminar entrained flow reactor with fuel feed rates low enough to

Table 4.2: Parameter intervals in which the model validation has been conducted.

Parameter	Min	Max
d_p	79 µm	9.5 mm
Moisture [wt % wb]	0	6
T_g [K]	1276	1667
ρ [kg/m^3 (dry)]	580	1000
AR [-]	1	4

create single particle conditions. The maximum gas temperatures were 1405-1667 K, the heating rate was in the order 10^5 K/s, and the residence time from 0-100 ms. The applied experimental parameters are given in table 4.3. The char yield is estimated using the method described by Leth-Espensen et al.[137], and the length is estimated based on recommendations from Masche et al.[72]. Figure 4.6 shows the comparison between experimental results for pine wood and model predictions for T_g = 1405 K and T_g = 1667 K. Also experimental data from four other biomass samples devolatilized under the same conditions in the same equipment have been included in the figure. The fuel types (pine, mischanthus, doped pine, leached mischanthus) all behave very similarly, and the major difference is the char yield. The four additional fuel types aid in describing the very rapid heating of particles of this size, where data points are scarce. The devolatilization of the particles happen within the first 20 ms in the reactor.

The figure shows consistency between experimental and model data. The small particles are rapidly devolatilized after an initial, short heating period. The relatively small diameter of the particles entails that these particles mimic isothermal particles. For an isothermal particle a short heating period would also be expected, before a rapid devolatilization commences.

Table 4.3: Applied model input parameters used to simulate the experiments of Johansen et al.[9] *Completely dry particles, but moisture content > 0 for mathematical reasons.**Obernberger et al.[198] ***Masche et al.[72]

Parameter	T_g = 1405 K	T_g = 1667 K
h_{coef} [J/(s m^2 K)]	1881	2076
R [µm]	39.4	39.4
L*** [µm]	157.6	157.6
ρ** [kg/m^3]	591	591
T_{wall} [K] (estimated value)	1205	1467
T_{gas} [K]	1405	1667
char yield [wt% daf]	4.0	6.4
ash yield [wt% db]	0.2	0.2
Moist cont* [wt % wb]	0.0001	0.0001

4.4.3 Particles with d_p = ~3 mm

Experiments with 3 mm particles have been conducted by Lu et al.[199] in a single particle combustor. The particles are fixed on a small wire, located in a hot fluegas above a flame, and the devolatilization time is determined by video registration. The particles have been carved

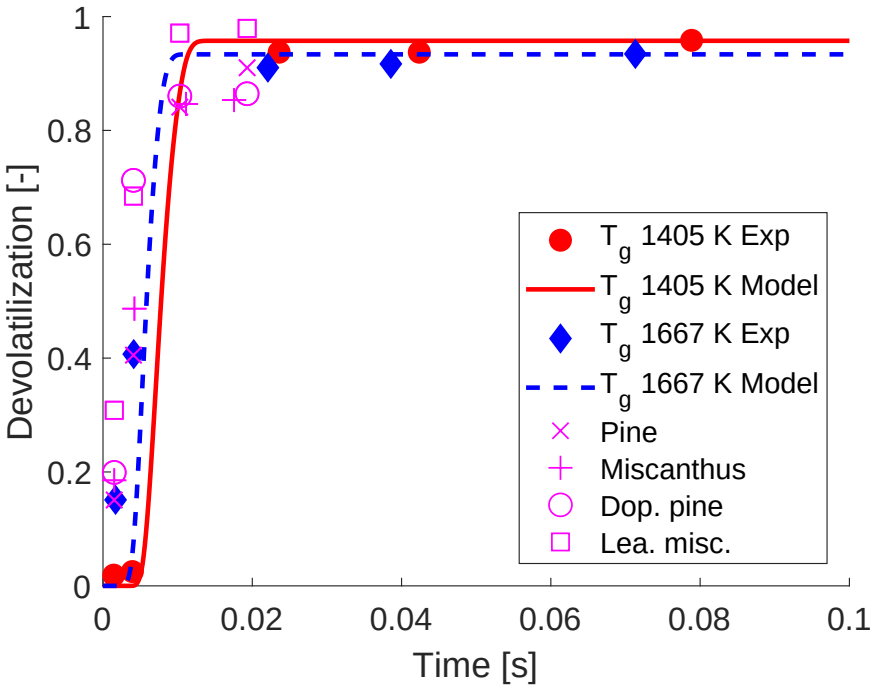

Figure 4.6: Comparison of model predictions to literature data for pine from Johansen et al.[9]. $d_p = 78.8$ µm, AR = 2, $\rho = 591$ kg/m^3, moisture content ≈ 0. Additional input parameters to the model are given in table 4.3. The pink data points are for four biomass types (pine, miscanthus, KCl doped pine, leached miscanthus) devolatilized under identical conditions as reported by Johansen et al.[10]

to near-spherical shapes, and are modeled as such. The temperature in the gas phase is $T_g = 1487$ K, and the initial heating rates are in the order $10^2 - 10^3$ K/s. The experimental data are given in table 4.4. Figure 4.7 shows the comparison of the devolatilization times for 3 mm spherical particles of different density for pine and beech wood. The wood type is indirectly a parameter in the model as the char yield varies depending on the wood sort. The char yield was estimated using the method described by Leth-Espensen et al.[137] The particles also vary slightly in diameter.

The measured pyrolysis time increases with increasing density in the experimental dataset in agreement with the model predictions. The model is particularly accurate for the beech samples, but for both wood species, the trend is captured well. Complete devolatilization of the 3 mm particles was obtained after 3.5 to 6.5 seconds.

4.4.4 Particles with $d_p = 9.5$ mm

Lu[200] has conducted experiments with spherical and cylindrical particles, both 9.5 mm in diameter, and the cylinders have a length of 38 mm. The experiments were conducted in a single particle combustor, and each experiment was repeated three to four times. For the spherical particles the settings were the same in all three repetitions. For the cylindrical particles the settings were the same except that the thermocouple measuring the center temperature was

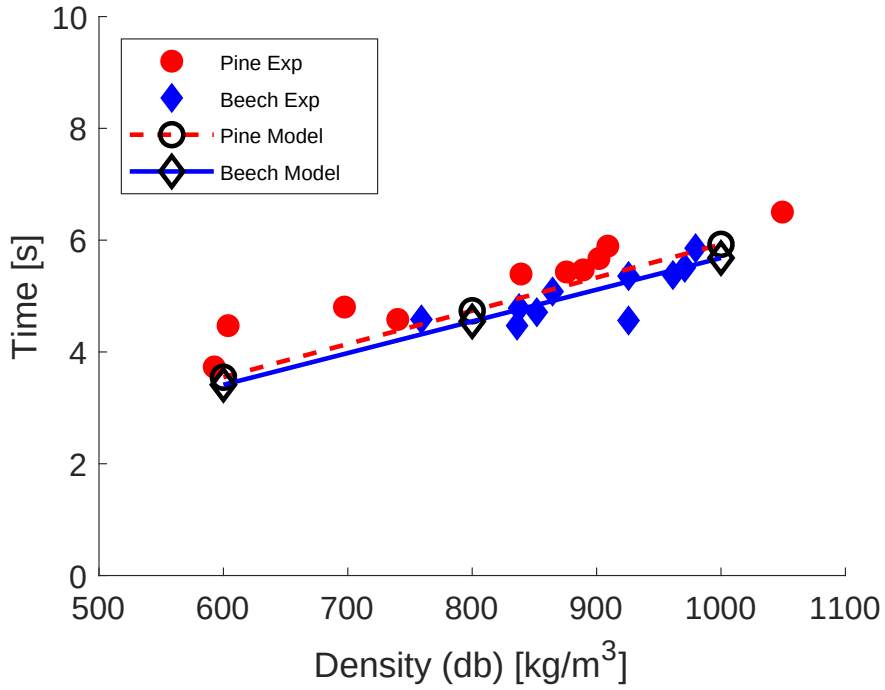

Figure 4.7: Comparison of devolatilization time for 3 mm spherical particles of different density. Experimental data from Lu et al.[199] $T_g = 1487$ K, $T_w = 1187$ K (estimated value), moisture content = 5.5 wt % wb. Additional input parameters to the model are given in table 4.4.

placed radially in experiment 1 and 2, and axially in experiment 3 and 4. The maximum gas temperature in the experiments was 1276 K, and the initial heating rate was in the order of $10^1 - 10^2$ K/s. The experimental data are given in table 4.5.

The temperatures in the devolatilization experiment for the cylindrical particle have previously been compared to the model presented by Ström and Thunman[140], and these results are also included in figure 4.9b. The two models show similar results for the temperatures of these large particles. Ström and Thunman have, however, not reported the degree of devolatilization related to the temperature measurements, and the comparison of experimental data from devolatilization of spherical and cylindrical poplar particles at identical conditions in the same set-up have not been made either. The latter is the reason of interest for this study.

Figure 4.8a and figure 4.8b show the degree of devolatilization and the temperature measurements for the spherical particles. The devolatilization of the spherical 9.5 mm particles take approximately 35 seconds. Figure 4.9a and figure 4.9b show the degree of devolatilization and the temperature measurements for the cylindrical particles. For the 9.5 mm cylindrical particle the devolatilization time is approximately 50 s. For both the spherical and the cylindrical particles, the thermocouple influences the devolatilization. The conducting material of a thermocouple may cause measurement errors of up to 300 K for millimeter-sized particles in high temperatures ($T_g = 1653$ K).[171] It is especially critical for the center temperatures, which are thus likely measured above the temperature in an unaffected particle.

Table 4.4: Applied model input parameters used to simulate the experiments of Lu et al.[199] *Estimated from empirical correlation from Leth-Espensen et al.,[137] determined for ρ = 600, 800, and 1000 kg/m^3.

Parameter	Pine	Beech
h_{coef} [J/(s m^2 K)]	112.0	114.2
R [mm]	1.56	1.515
T_{wall} [K] (estimated value)	1187	1187
T_{gas} [K]	1487	1487
char yield* [wt% daf]	7.6/8.1/8.5	12.8/13.6/14.2
Moist cont [wt % wb]	5.5	5.5

The devolatilization is predicted well by the model both for the spherical and cylindrical particles, albeit the model prediction is slightly faster than the experimental results. The surface temperature is also predicted well. The center temperature is predicted reasonably by the model. The particle center temperatures measured experimentally are likely an overestimate as they have been measured with a thermocouple, which entails the shortcomings described above. The particle center temperatures predicted by the model are likely an underestimate, as e.g., the moist layer temperature is defined as equal to T_{boil} until all water is evaporated. However, the stepwise temperature profile for drying is also observed by Pilar Remacha et al.[172] during drying of alumina particles in a flat flame burner at 1573 K, so the assumption is expected to be reasonable. The combination of overprediction of experimental temperatures and underprediction of model temperatures is the reason for the small discrepancies seen in figure 4.8b and 4.9b. The results of the quardruplicate experiments also show that the experimental variation is considerable.

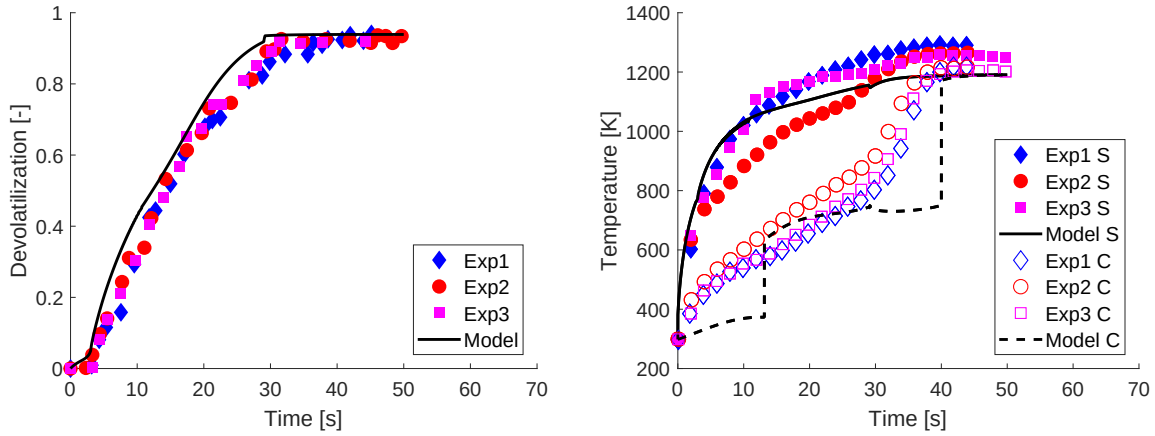

(a) **(b)**

Figure 4.8: Comparison of model to experimental data of spherical particles from Lu et al.[200] d_p = 9.5mm, ρ = 580 kg/m^3, T_g = 1276 K, T_w = 1176 K (estimated value), moisture content = 6 wt% wb. Additional input parameters to the model are given in table 4.5. The small fluctuation in the graphs around t = 30 s is due to the change in kinetic scheme. S = surface temperature, C = Center temperature.

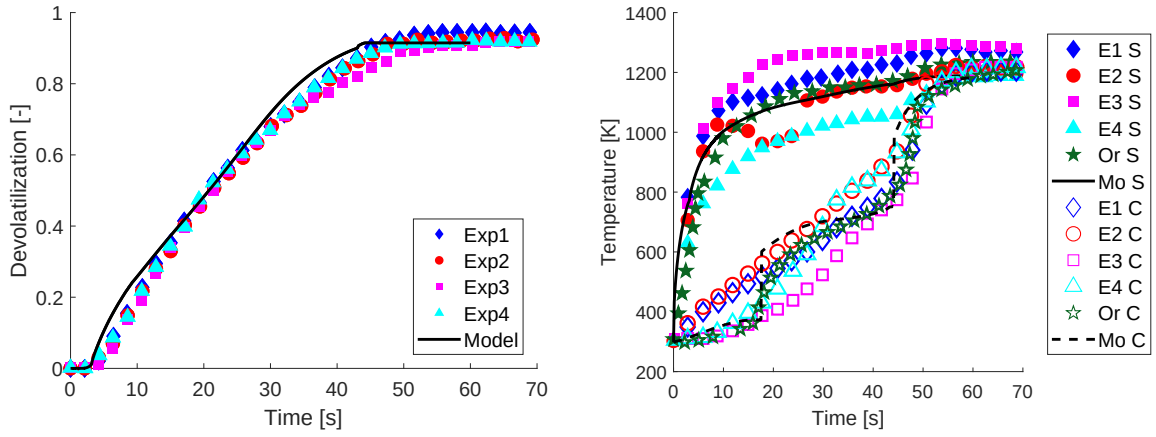

(a) **(b)**

Figure 4.9: Cylindrical particles modeled with current model (Mo) compared to model results from Ström and Thunman (Or) and experimental data from Lu et al.[200] $d_p = 9.5$ mm, AR = 4, $\rho = 580$ kg/m^3, $T_g = 1276$ K, $T_w = 1176$ K, moisture content = 6 wt% wb. Input parameters to the model are given in table 4.5. S = surface temperature, C = Center temperature.

Table 4.5: Applied model input parameters used to simulate the experiments of Lu.[200]

Parameter	Cylinder	Sphere
h_{coef} [J/(s m^2 K)]	54.43	54.43
R [mm]	4.75	4.75
L [mm]	38	-
ρ [kg/m^3]	580	580
T_{wall} [K] (estimated value)	1176	1176
T_{gas} [K]	1276	1276
char yield [wt% daf]	8.4	6.4
Moist cont [wt % wb]	6	6

4.5 Model predictions

4.5.1 Sensitivity Analysis

To investigate the influence of the material value properties and some particle and boundary conditions a sensitivity analysis with respect to devolatilization time has been conducted. The influence of particle properties and devolatilization conditions is tested for three different particle sizes (d_p = 79 µm, 800 µm, and 3.12 mm), since the influence of the model parameters varies depending on size. The other applied particle parameters can be seen in table 4.6.

The smaller particles are kinetically controlled, whereas the devolatilization process for the larger particles is limited by heat transfer mechanisms. In table 4.7 the effect of decreasing and increasing a number of parameters by 30 % can be seen. It can be concluded that radius, density, and gas temperature are important parameters, when determining the devolatilization time. For the first two the impact is highest for the smaller particles, whereas the impact of

Table 4.6: Parameters for sensitivity analysis.

Parameter	Value
AR [-]	2
T_g [K]	1600
ρ [kg/m^3]	700
char [wt % daf]	5
moist [wt% wb]	4
ΔH_{devo} [j/kg]	200 000
ΔH_{desorp} [j/kg]	3 610 000

T_g is most pronounced for the larger particles. The influence of particle heat conductivity, k_p, is considerable for larger particles, whereas the effect for smaller particles seems to be less pronounced in good agreement with the larger particles being heat transfer controlled. To check the effect of the kinetic scheme, the Arrhenius reaction rates, k_L and k_H, have both simultaneously been increased and decreased by 30 %. The choice of rate constants mainly influences the smaller particles' devolatilization times, as they are primarily controlled by the kinetics of the devolatilization.

Table 4.7: Sensitivity Analysis. Each parameter is decreased and increased by 30 %. The change in devolatilization time is marked for each particle size as a percentage of the devolatilizatoin time for the particle with no change in input parameter. t_{devo} for each of the three baseline particles are also included in the table.

Parameter	**-30 %**	**+30 %**	**-30 %**	**+30 %**	**-30 %**	**+30 %**
R [μm]	**39.4**		**400**		**1560**	
t_{devo} [s]	**0.0133**		**0.426**		**3.61**	
k_p [J/(m K s)]	+5	-3	+12	-6	+29	-15
C_p [J/(kg K)]	-15	+14	-14	+13	-11	+11
h_{coef} [J/(s m^2 K)]	+23	-14	+15	-10	+4	-3
R [μm]	-35	+38	-37	+40	-41	+47
L (R constant) [μm]	-6	+3	-7	+4	-10	+6
ρ [kg/m^3]	-23	+20	-27	+26	-30	+30
T_{gas} [K]	+82	-31	+40	-21	+11	-8
k_L, k_H	+10	-7	+4	-3	+1	0
char yield [wt% daf]	-2	0	-1	0	0	0
Moist cont [wt % wb]	-2	+2	-4	+4	-4	+4
ΔH_{devo} [J/kg]	-5	+3	-2	+2	-2	+2
ΔH_{desorp} [J/kg]	-2	+2	-3	+3	-3	+3

4.5.2 Parameter Analysis

A parameter analysis was performed to study the effect of particle properties and local conditions on the devolatilization time and further illustrate the influence on the devolatilization process. The analysis is done for a cylindrical particle (d_p = 1.51 mm, AR = 5) as baseline particle. Its characteristics are given in table 4.8. For each input parameter a low, an average and a high

value is chosen to cover the parameter span relevant for suspension firing. The effect of changes in aspect ratio (for particles with the same radius), aspect ratio (for particles with the same volume), radius (for particles with the same aspect ratio), density, moisture content, and gas temperature is shown in figure 4.10.

Table 4.8: Overview over input parameters for particle simulation. The following values are used when nothing else is mentioned.

Parameter	**Value**
AR [-]	5
T_g [K]	1600
R [mm]	0.755
ρ [kg/m^3]	700
moist [wt% wb]	4

The influence of aspect ratio on devolatilization time is shown both for particles with the same radius and for particles with the same volume in figure 4.10a and figure 4.10b, respectively. Comparing the figures shows that in the case of identical radii, the effects on devolatilization times are minor, especially for AR $>$ 5, whereas for particles with the same volume the effects of AR on devolatilization times are greater. Thus from a modeling perspective, even if it is chosen to model biomass particles as spherical, using the true diameter as an input parameter yields a better result with respect to estimating the devolatilization time. However, this approach might lead to other complications, e.g. in CFD, where a true representation of the entire mass of particles is necessary, and where the drag effect would also need to be accounted for.[201]

Comparing the effect of changes in radius in figure 4.10c to the model parameters in the remaining subfigures show that the particle size is an important input parameter to specify as accurately as possible. The devolatilization time varies with approximately two magnitudes within the particle size interval relevant for suspension firing. The particle size influences both the starting time for devolatilization, the amount of volatiles released and the total devolatilization time.

Another parameter, which has a considerable influence, especially on the onset of devolatilization, is the gas temperature as seen in figure 4.10d. The lower the gas temperature, the longer it takes to dry out the particle and heat it to a temperature where the devolatilization is initiated. The high, local temperature near the burner quarl ensures a fast onset of devolatilization, which improves ignition and flame stability.

The influence of the particle density can be seen in figure 4.10e. The density for the particles varies both dependent on biomass type and pelletilization procedure. The changes in density affects both the onset time for the devolatilization and the duration of it.

Compared to the other parameters, the moisture content seen in figure 4.10f has a smaller effect on total devolatilization time, but it has a strong influence on the onset of volatile release, and may consequently influence flame ignition. The moisture content in suspension fired units rarely exceed 10 wt% wb as the pelletilization and milling processes result in partly dried particles.

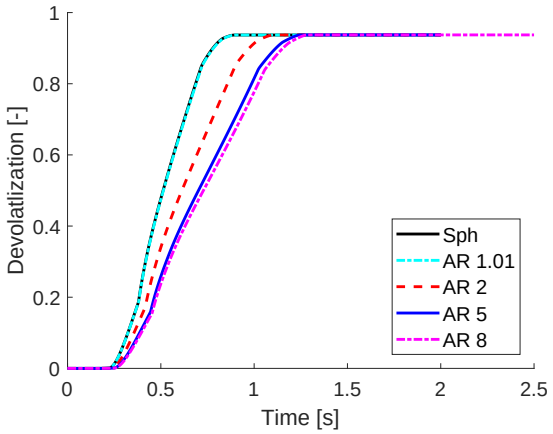

(a) Particles have identical radii.

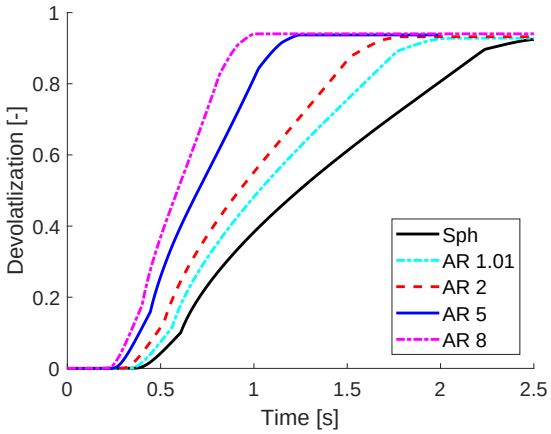

(b) Particles have identical volumes.

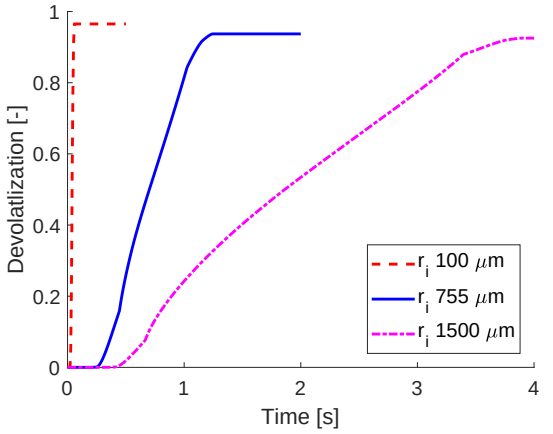

(c) Particles have identical AR.

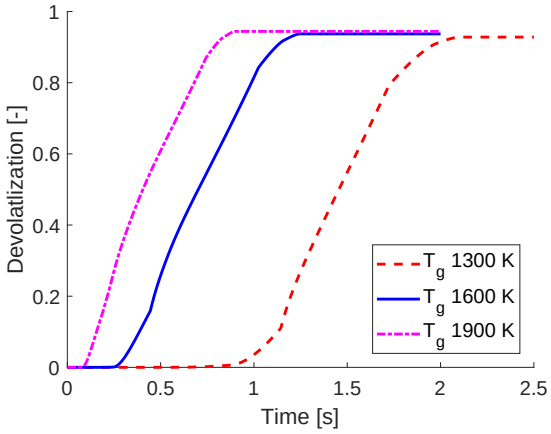

(d)

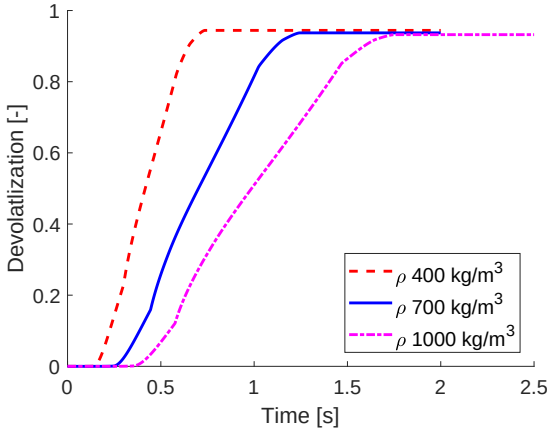

(e)

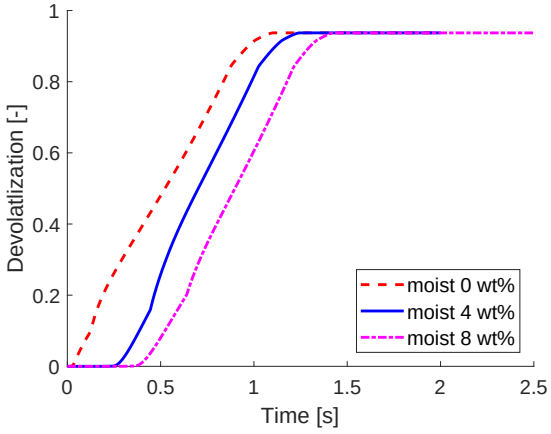

(f)

Figure 4.10: Parameter analysis for relevant particle properties and boundary conditions. Baseline simulation properties include AR = 5, T_g = 1600 K, R = 0.755 mm, ρ = 700 kg/m^3, moisture content = 4 wt % wb, represented by the blue solid lines.

4.6 Conclusion

The presented wood particle devolatilization model can describe biomass particles as both spherical and cylindrical and include end effects. The model fits experimental data from the literature well for particle sizes (d_p = 79 µm to 9.5 mm) and in the temperature range (1276-1667 K), which is relevant for suspension firing.

The model results show that if a cylindrical particle should be approximated by the geometrically simpler sphere, the diameter of the cylinder is a better approximation for a particle size than the same volume approach, where the diameter is determined as the diameter of a sphere with the same volume as the cylinder.

The model further predicts devolatilization times to vary approximately two magnitudes for the particle sizes (d_p = 0.2-3 mm) utilized in suspension fired boilers, affecting both burnout and flame stability. Other parameters of importance for devolatilization time are particle density, and local gas temperature. Of minor importance for the final devolatilization time is moisture content, within the span relevant for pelletilized biomass. The moisture content, however, influences the onset of volatile release substantially.

A sensitivity analysis performed for three different particle sizes (d_p = 79 µm, 800 µm, and 3.12 mm) shows that the importance of determining the input parameters to the model correctly varies greatly with particle size. The most significant parameters are radius, density, and T_g. E.g. for T_g the devolatilization time increases with 82 % for particles with diameter 79 µm, whereas it only increases with 11 % for particles with radius 3.12 mm, when T_g is decreased by 30 %.

4.7 Acknowledgements

The authors thank Ørsted A/S, Rambøll A/S and Burmeister & Wain Scandinavian Contractors A/S for financial and advisory support. The Nordic 5 Tech Alliance (N5T) is also thanked for financial support. The authors also thank Henrik Ström from Chalmers University of Technology for assisting with the model development.

Paper C

This chapter contains a manuscript in preparation with the working title "Determination of Zero Dimensional, Apparent Devolatilization Kinetics for Elongated Biomass Particles at High Heating Rates". The paper is expected to be submitted to a peer-reviewed journal in 2019.

5 Determination of Zero Dimensional, Apparent Devolatilization Kinetics for Elongated Biomass Particles at High Heating Rates

5.1 Abstract

Modeling biomass particle devolatilization at suspension firing conditions is often a compromise between keeping the computational costs at a minimum and including the necessary intraparticle temperature and mass gradients. Here, a simple model for devolatilization at conditions relevant for suspension firing of biomass is presented. It employs Arrhenius parameters in a single first order devolatilization reaction, where the effects of kinetics and heat transfer limitations are lumped together. By lumping the rate limiting effects in the apparent Arrhenius parameters, a biomass particle can be modeled as a zero dimensional, isothermal particle, which is often done in computational fluid dynamics, due to limitations in computational power. This model includes the effects of particle aspect ratio, maximum gas temperature, and particle radius and is validated against both experimental data and a more rigorous 2D devolatilization model. It is developed using the multivariate data analysis tool, partial least squares regression.

5.2 Introduction

With the aim of obtaining a CO_2 neutral heat and energy production, the interest in retrofitting suspension firing units to combust biomass instead of coal has increased over the past decades. Suspension firing of biomass is typically done with small particle sizes (d_p = 0.1-3 mm),[11,72] at high temperatures ($T > 1000$ K),[15] and at high heating rates ($> 10^3$ K/s).[202]

Modeling a suspension firing unit often involves CFD simulations.[15] To avoid too high computational costs, subprocesses in the particle combustion modeling in CFD require simplifications. Coal particles have historically been modeled as isothermal in CFD combustion simulations, and this approach has sometimes been extended to also include modeling of biomass pyrolysis.[100,203,204] However, model work validated against experimental data[14,111] shows that biomass particles at sizes and temperatures relevant for suspension firing cannot be regarded as thermally thin, i.e. isothermal. More complicated models, which include temperature gradients, on the

other hand, are not feasible in CFD for industrial modeling purposes, due to high computational costs.[205]

Advances have been made to account for the complicated process of biomass devolatilization in a simple lumped model, where apparent devolatilization kinetics have compensated for a lack of heat transfer limitations in a simple isothermal model.[14,205,206] These models use an apparent kinetic scheme for the lumped effects of pyrolysis and internal heat and mass transfer limitations in the particle, but none of them take the effect of biomass density, gas temperature, or particle morphology into account.

To compromise between the need for a simple devolatilization model and describing the complicated phenomenon of biomass particle pyrolysis, this paper introduces lumped Arrhenius kinetic parameters for a single first order global pyrolysis model. The parameters of a zero dimensional, isothermal model are found by fitting to predictions of a two dimensional model[87] that is validated against experimental data. The comparison is done for different gas temperatures, particle sizes, particle aspect ratios, and densities. The combined effect of these experimental properties on the Arrhenius parameters is quantified using the multivariate data analysis method, partial least squares regression (PLS).

5.3 Model Description

5.3.1 The Two Dimensional Model

The two dimensional model is described in detail elsewhere[87,140,173], and only a short recap will be given here. The two dimensional model is a shell model, where the particle is divided into three concentric shells. The innermost layer is a moist layer, the middle layer is a dry biomass layer, and the outer layer is char. The shells move inwards during the devolatilization, transforming the model particle from consisting of practically only a moist shell in the beginning to be all char after full devolatilization. The model was first presented by Thunman et al.[173], and subsequently developed by Ström and Thunman[140] and adapted to account for biomass devolatilized under suspension firing conditions by Leth-Espensen et al.[87] The model accounts for intraparticle heat and mass transfer and both cylindrical and spherical particles can be modeled. In the latter case the model is one dimensional. The cylinder is the preferred simple geometry to model biomass particles,[73] whereas coal particles tend to be almost spherical in nature due to their brittleness and lack of fibrosity.

5.3.2 The Zero Dimensional Model

The 0D model is based on the following assumptions:

- The particle is isothermal.

- The particle is spherical.
- The particle diameter is defined as the diameter of the cylinder, which best approximates the biomass particle.
- Devolatilization enthalpy is assumed to be 0.
- The kinetics can be described by a single first order reaction model.

The devolatilization process in the isothermal particle is modeled as a global reaction, using the single first order reaction (SFOR) model, described in equation 5.1.[207]

$$\frac{d\Upsilon}{dt} = k(\Upsilon^* - \Upsilon) \tag{5.1}$$

Here t is the time, Υ is the fraction of volatiles released, Υ^* is the fraction of volatiles present in the particle at $t = 0$, and k is an Arrhenius reaction rate constant given in equation 5.2.

$$k = A \cdot exp\Big(\frac{-E_a}{R_g T}\Big) \tag{5.2}$$

R_g is the gas constant, T is the particle temperature, and A and E_a are the Arrhenius pre-exponential factor and activation energy, respectively. The temperature in the particle is uniform and determined by the radiation and convective heat transfer and is given in equation 5.3.

$$\frac{dT}{dt} = \frac{1}{\rho C_p}\frac{3}{R}\Big(\sigma\epsilon(T_w^4 - T^4) + h(T_g - T)\Big) \tag{5.3}$$

Here ρ is the density, C_p is the specific heat capacity of the fuel, R is the particle radius, σ is the Stefan-Boltzmann constant, ϵ is the emissivity, T_w is the radiation temperature (reactor wall temperature), and h is the heat transfer coefficient. Expressions for the model input parameters are given in table 5.1. The two coupled differential equations are solved using the `ode45` solver in Matlab®.

Table 5.1: Input parameters to 0D model.

Parameter	Value	Ref.
h [J/(s m^2 K)]	Estimated as described by Leth-Espensen et al.	137
Υ^* [J/(s m^2 K)]	Estimated as described by Leth-Espensen et al.	137
ϵ [-]	0.85	180,181
C_g [J/(kg K)]	$\Big(19.50583 + 19.88705 \cdot \frac{T_g}{1000} - 8.598535 \cdot (\frac{T_g}{1000})^2 + ...$ $...1.369784 \cdot (\frac{T_g}{1000})^3 + 0.527601 \cdot (\frac{1000}{T_g})^2\Big) \cdot \frac{1000}{28}$	185
$C_{p,dry\,wood}$ [J/(kg K)]	$z1 = 380/T$ $z2 = 1800/T$ $g1 = z1^2 \cdot exp(z1)/(exp(z1) - 1)^2$ $g2 = z2^2 \cdot exp(z2)/(exp(z2) - 1)^2$ $C_{p,dry\,wood} = (g1 + 2 \cdot g2) \cdot 1000 \cdot R \ / \ 7.72$	187,188

5.3.3 Fitting the Arrhenius Parameters

In order to approximate the 2D model with a 0D model the Arrhenius equation must account both for the rate of the kinetics and for any heat transfer limitations in a given particle. The apparent kinetic scheme is obtained by fitting the Arrhenius equation. The pre-exponential factor, A, and the activation energy, E_a, in the Arrhenius equation are coupled, though, so the procedure suggested by Rawlings and Ekerdt[208] is used here. In order to minimize the correlation between the fitted parameters, a modified Arrhenius equation as seen in equation 5.4 has been used.

$$k(T) = k(T_{ref}) \cdot exp\left(\frac{-E_a}{R_g}\left(\frac{1}{T} - \frac{1}{T_{ref}}\right)\right) \tag{5.4}$$

$k(T_{ref})$ is the rate constant at a reference temperature, here 1600 K, the midpoint in the temperature interval. $k(T_{ref})$ and E_a are fitted to the result from the 2D devolatilization model using the `lsqcurvefit` command in Matlab®, which works by minimizing the residual sum of squares between the model results from the 2D model and the 0D model. The residual sum of squares is given in equation 5.5. The value of A can be calculated from $k(T_{ref})$ and E_a.

$$RSS = \sum_{t=0}^{t_{end}} (y_{2D} - y_{0D})^2 \tag{5.5}$$

An example of a fitted curve and the 2D cylindrical model output can be seen in figure 5.1.

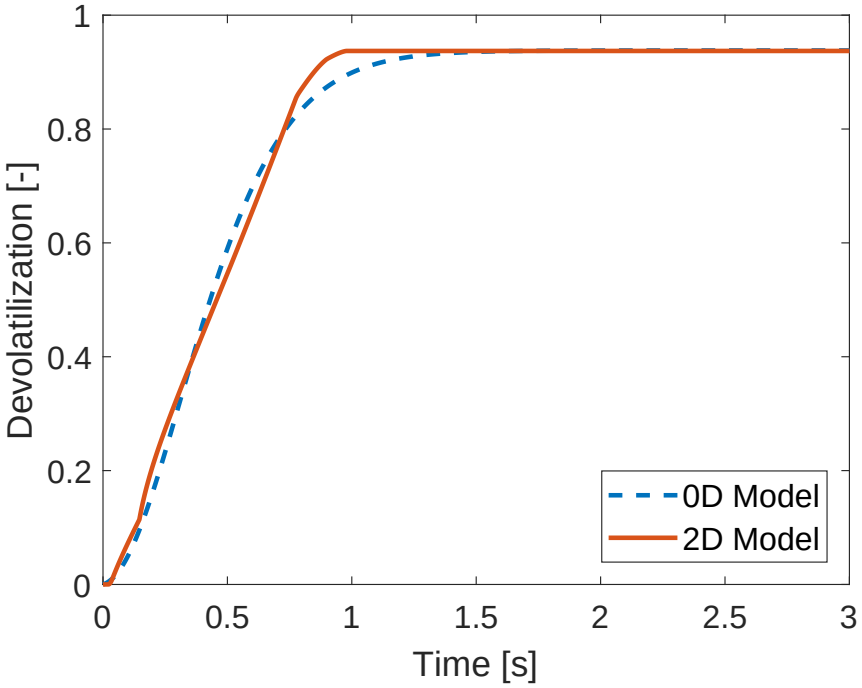

Figure 5.1: Example of fitting the 0D model to the 2D cylindrical model, here for a particle of d_p = 1510 µm, AR = 2, ρ = 700 kg/m^3, and T_g = 1600 K.

Table 5.2: Input parameter span.

Parameter	Symbol	Unit	Min	Max
Radius	R	µm	39.4	1560
Density	ρ	kg/m^3	700	1300
Gas temperature	T_g	K	1300	1900
Aspect ratio	AR	-	1.01	8

5.3.4 Chemometrics

Chemometrics is a statistical approach to extract data from chemical or biological data sets. A common method within chemometrics is partial least squares regression (PLS).[151,152] An in depth description of PLS is beyond the scope of this manuscript, but can be found elsewhere.[151,152,154,209] The PLS models presented here are calculated in PLS Toolbox version 8.1.1 and Matlab version 9.3.0 (R2017b).

Parameters Definition

The input parameters tested for the model are particle radius, particle density, gas temperature, and particle aspect ratio. The parameter spans for each variable can be seen in table 5.2. They cover the gas temperature, density, aspect ratio, and particle size intervals relevant for suspension firing conditions. 35 simulations with the 2D model have been made to span the parameter space. The parameter values for each cimulation can be seen in the supplementary material in Appendix C. To show the correlation (negative or positive) between input parameters, the correlation coefficient chart is made. It is shown in figure 5.2. The higher the absolute value in the correlation coefficient matrix, the higher degree of correlation between two input parameters. When the degree of correlation is high the effect of each input parameter cannot be separated due to confounding. Here the degree of correlation is numerically low (≤ 0.23), which means the influences on the model results can largely be ascribed to each individual input parameter.

Preprocessing

In PLS a correlation between a matrix of input variables ($\mathbf{X}$) and a matrix of output variables ($\mathbf{Y}$) is determined. PLS is a linear regression method, and ideally there should be linearity between input and output parameters. Often in chemical and biological systems linearity is not the case, though, and individual preprocessing of some input variables is then necessary to increase the linearity. To remedy the problem with linearity between input parameters and the Arrhenius parameters individual preprocessing is applied. The different individual preprocessing methods tested can be seen in table 5.3. When studying, e.g., the effect of the particle radius on the Arrhenius parameters it is clear that the correlation is nonlinear as seen in figure 5.3. Thus, both R, $log(R)$, $R^{1/2}$, and $R^{1/3}$ have been tested as preprocessing methods, and the quality of the preprocessing is then determined based on the Explained variance for the input matrix

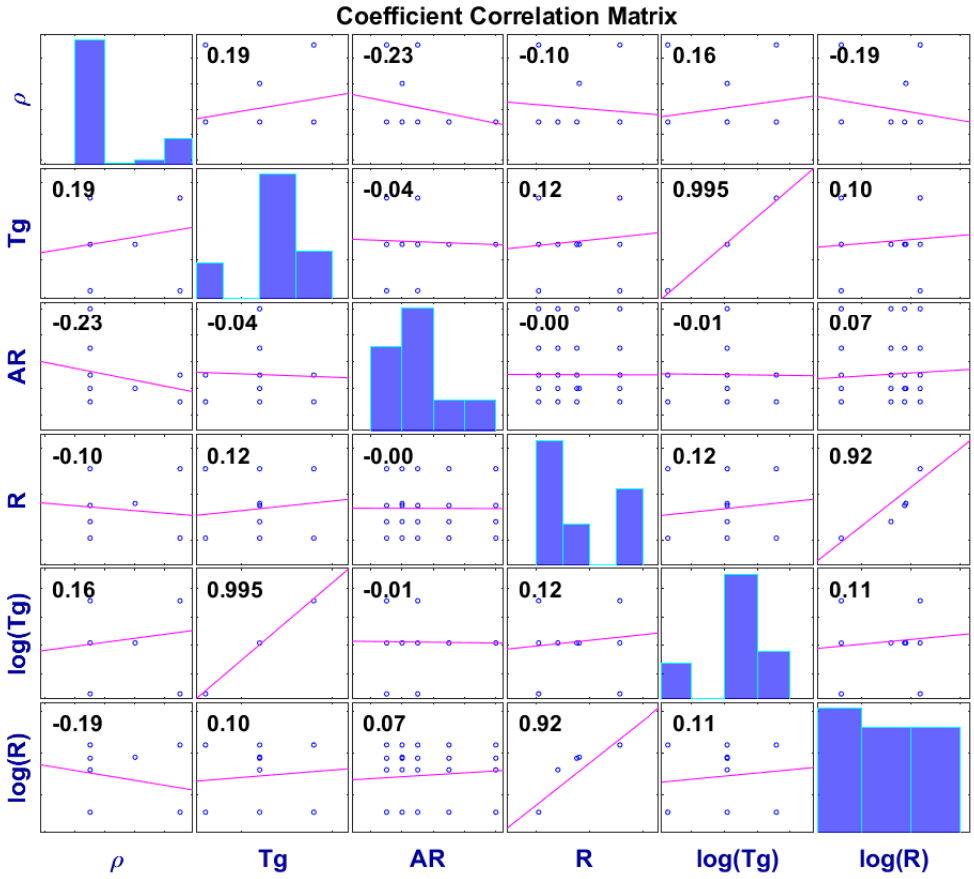

Figure 5.2: Correlation coefficient chart.

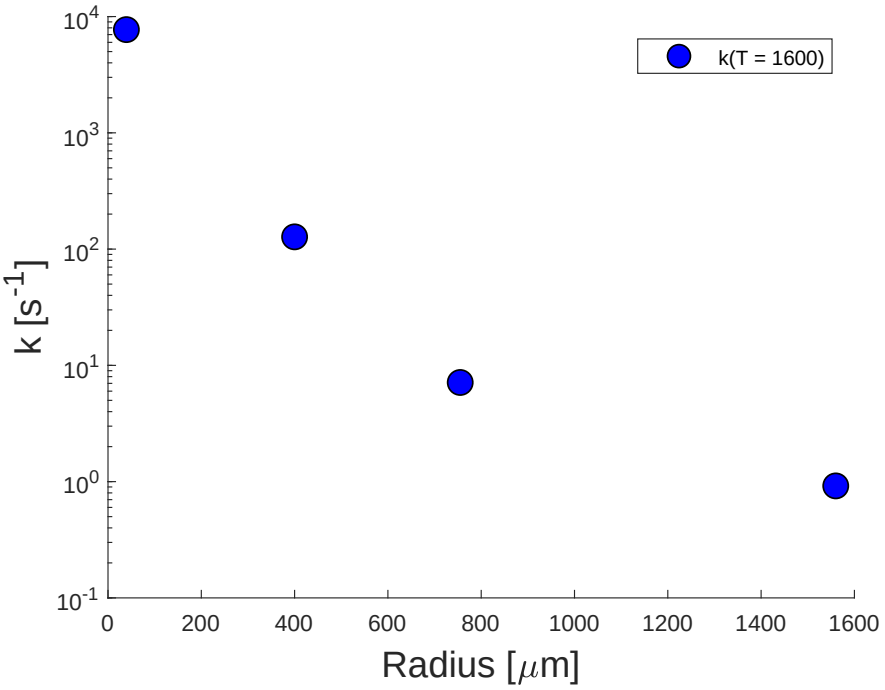

Figure 5.3: Reaction rate as a function of initial particle radius for particles simulated with the 2D code with $\rho = 700$ kg/m^3, $AR = 2$.

(EV($\mathbf{X}$)), the output matrix (EV($\mathbf{Y}$)), and the Root mean squared error of cross validation (RCV) for both A and E_a.

Furthermore the input variables here are not on the same scale, which would, due to numerical reasons, mean that the importance of the variables would be dependent on the unit in which they were measured and the absolute variation in parameter span for each individual parameter. To account for the differences in scale and variation all input parameters have also been scaled to account for unit variance.

Cross Validation

The cross validation is made to ensure that the presented model is robust. It is a way of testing if a subset of the data can be predicted from the remaining data. Cross validation can be done in many ways. Here the random subset method[159] cross validation with 6 splits and 20 iterations is applied, thus on average 17 % of the data set is removed in each iteration.

When choosing the most optimal preprocessing for the input variables in a PLS model, and consequently the best model, it is dependent on the cross validation. RCV values should preferably be low, and EV values preferably high. The values in table 5.3 is the basis for choosing the relevant preprocessings for a model. Due to the slightly lower RCV(A) and RCV(E_a) and higher EV($\mathbf{X}$) and EV($\mathbf{Y}$) values model 14 has been chosen in the following.

Table 5.3: Table of tested PLS models. EV = Explained variance, RCV = Root means squared error of cross validation. x = parameter included, - = parameter not included.

No.	ρ	T_g	AR	r	A	E_a	EV(X)	EV(Y)	RCV(A)	RCV(E_a)
1	x	x	x	x	log(x)	x	47.9	84.6	1.3	2.0· 10^4
2	x	x	x	log(x)	log(x)	x	56.8	96.0	0.65	1.1· 10^4
3	x	x	x	$x^{1/2}$	log(x)	x	52.5	92.9	0.83	1.4· 10^4
4	x	x	x	$x^{1/3}$	log(x)	x	54.6	94.7	0.73	1.3· 10^4
5	x	x	log(x)	log(x)	log(x)	x	56.3	96.0	0.64	1.1· 10^4
6	x	log(x)	x	log(x)	log(x)	x	55.9	96.2	0.62	1.0· 10^4
7	x	$x^{1/4}$	x	log(x)	log(x)	x	56.0	96.1	0.64	1.0· 10^4
8	x	$x^{1/3}$	x	log(x)	log(x)	x	56.1	96.1	0.64	1.0· 10^4
9	x	1/x	x	log(x)	log(x)	x	55.6	96.3	0.64	1.0· 10^4
10	log(x)	log(x)	x	log(x)	log(x)	x	55.7	96.2	0.63	1.0· 10^4
11	log(x)	log(x)	log(x)	log(x)	log(x)	x	55.2	96.2	0.63	1.0· 10^4
12	x	log(x)	log(x)	log(x)	log(x)	x	55.4	96.2	0.63	1.0· 10^4
13	x	log(x)	-	log(x)	log(x)	x	63.7	96.3	0.60	1.0· 10^4
14	-	log(x)	x	log(x)	log(x)	x	66.2	96.3	0.56	1.0· 10^4
15	-	log(x)	log(x)	log(x)	log(x)	x	66.2	96.3	0.57	1.0· 10^4

5.4 Results

5.4.1 PLS Model

The PLS model presented here is developed to be able to predict the Arrhenius parameters in a lumped SFOR kinetic scheme accounting both for the reaction rate and the heat transfer limitations. Two graphs showing the 0D model predictions of $log(A)$ and E_a as a function of the $log(A)$ and E_a values given by fitting the 0D model to the 2D model can be seen in figure 5.4. The figure shows that there is good agreement between the values for $log(A)$ and E_a predicted by the simple 0D model and by fitting to the 2D model. The Arrhenius parameters for the 0D model can be found through the regression vector. The regression vectors both for the preprocessed input parameters and for the raw input parameters can be seen in table 5.4. The regression vectors for the preprocessed input parameters show that both for $log(A)$ and E_a an increase in AR, $log(T_g)$ or $log(r)$ would result in a decrease of $log(A)$ and E_a. The raw regression vector can be used for predictive purposes. In equation 5.6 and 5.7 the values for $log(A)$ and E_a can be estimated for pyrolysis situations similar to the ones used for model development.

Table 5.4: Regression vectors for model 14.

Parameter	reg. A preprocessed	reg. E_a preprocessed	reg. A raw data	reg. E_a raw data
Intercept	0	0	58.9436	908212
AR	-0.0251062	-0.0503960	-0.0356625	-976.190
log(T_g)	-0.236492	-0.278340	-14.1090	-226445
log(r)	-0.929798	-0.900167	-4.13324	-54567.3

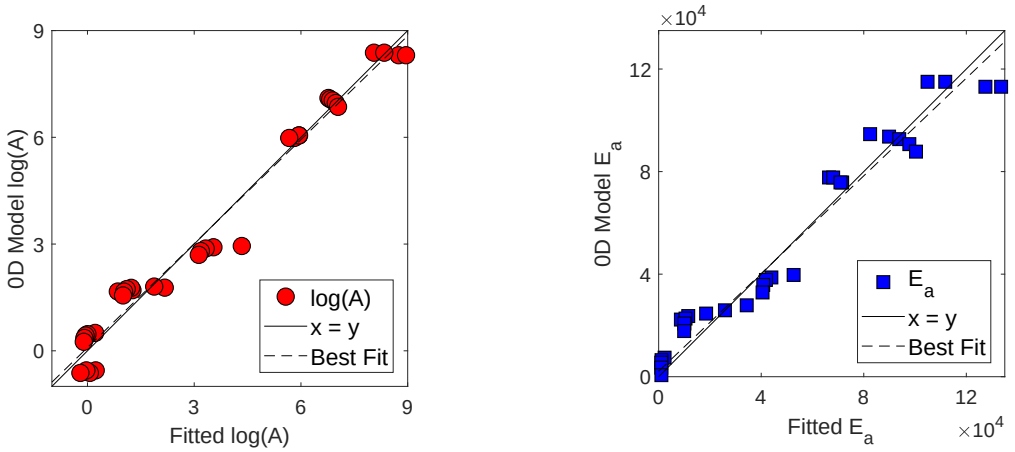

Figure 5.4: Comparison of $log(A)$ and E_a determined from a fit to the 2D model and as predicted by the 0D lumped kinetics model 14. $r^2 = 0.97$ and $r^2 = 0.95$ for the $log(A)$ and E_A graphs respectively.

$$log(A) = 58.9436 - 0.0356625 \cdot AR - 14.1090 \cdot log(T_g) - 4.13324 \cdot log(r) \tag{5.6}$$

$$E_a = 908212 - 976.190 \cdot AR - 226445 \cdot log(T_g) - 54567.3 \cdot log(r) \tag{5.7}$$

5.4.2 Arrhenius Plots

The Arrhenius parameters produced for four different particle sizes (d_p = 78.8 µm, d_p = 800 µm, d_p = 1.51 mm, and d_p = 3.12 mm) for different aspect ratios have been used to generate the four Arrhenius plots in figure 5.5. In all four figures it can be seen that the aspect ratio only has a minor influence on the Arrhenius parameters, and that the effect of aspect ratio levels off for higher values of AR. The effect of aspect ratio on the apparent rate constant is most pronounced for the smaller particles. Furthermore, the apparent reactivity is smaller for the large particles. This is probably due to the larger heat transfer limitations in the large particles.

5.4.3 Validation

Validation of the 0D model (equation 5.1 to 5.3 and equation 5.6 and 5.7) is here done by comparison both to the result from the 2D model presented by Leth-Espensen et al.[87] and to experimental data not related to the model development. Lewis and Fletcher[92] have conducted experiments in a flat flame burner with dry sawdust particles (45-75 µm) at a maximum temperature of 1433 K. In figure 5.6a the devolatilization as a function of time can be seen. Both the experimental data from Lewis and Fletcher, predictions by the 2D model and the 0D model with the apparent kinetics presented in equation 5.6 and 5.7 are shown. The two models show good agreement. The experimental data is also matched well, but unfortunately only full conversion

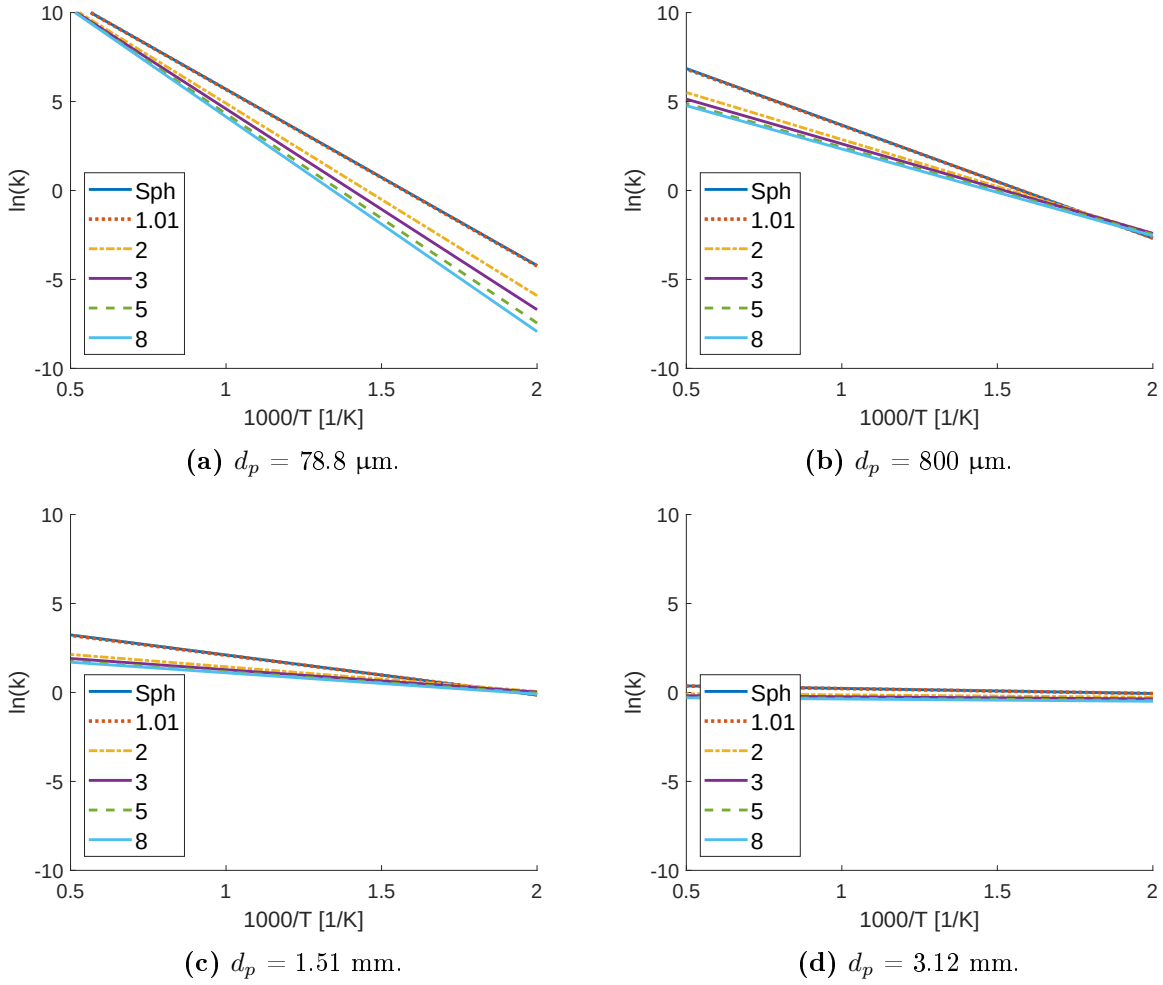

(a) $d_p = 78.8$ µm. **(b)** $d_p = 800$ µm.

(c) $d_p = 1.51$ mm. **(d)** $d_p = 3.12$ mm.

Figure 5.5: Arrhenius plots for the lumped values for A and E_a for different aspect ratios for four particle sizes.

data is available, which is not ideal for model validation. To the knowledge of the authors, no data is publicly available, which describes the devolatilization of not fully converted biomass particles under suspension firing, which has not been used in the development of the 2D model.[87] Examples for comparison between the 2D and the 0D model for other particle sizes can also be seen in figure 5.6. The 0D model shows god agreement with the more complicated 2D model and predicts devolatilization times well. The model predictions are best for smaller particles as they are heated up rapidly, and thus closer to being isothermal. An overall comparison of the devolatilization time predicted by the 2D model and the 0D model can be seen in figure 5.7. Devolatilization time is defined as the time, where 99 % of full conversion is reached. The 0D model predicts most devolatilization times adequately, and shows limitations only for particles, which simultaneously have extremely high radius, gas temperature, and density. In extreme cases the 0D model may predict negative activation energies, as can be deduced from equation 5.7, see examples in the table in supplementary material in appendix C. As negative E_a values are non-physical, the model cannot be trusted in these instances and such values have been disregarded in figure 5.7. From figure 5.7 it can be seen that the 0D model tends to overpredict the devolatilization time with approximately 0.2 s, however, the prediction capability is overall good, and the trend is captured well by the model.

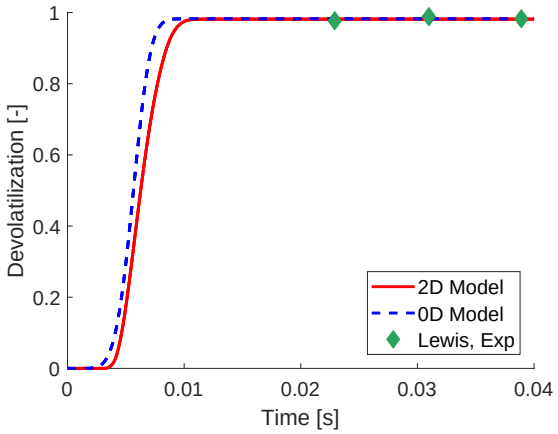

(a) $d_p = 60$ µm. $AR = 2$. Experimental data from Lewis and Fletcher[92].

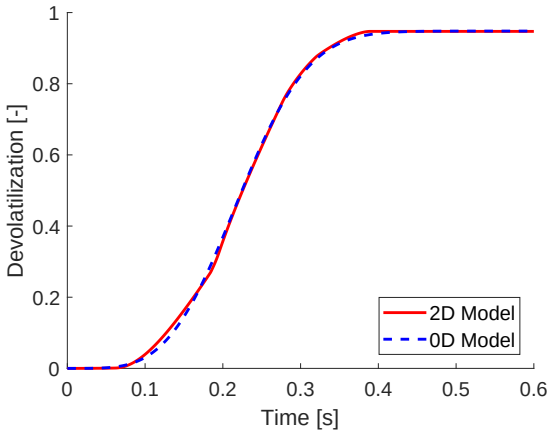

(b) $d_p = 800$ µm, $AR = 2$.

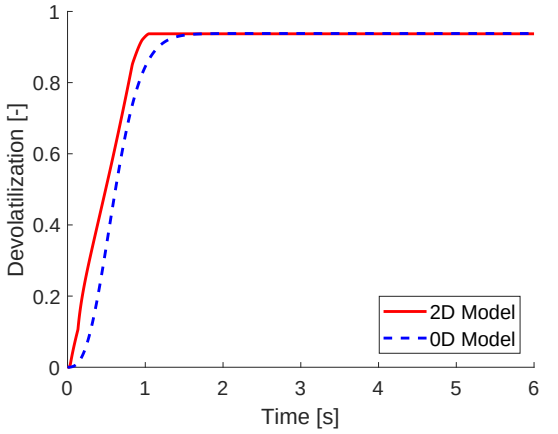

(c) $d_p = 1.51$ mm, $AR = 3$.

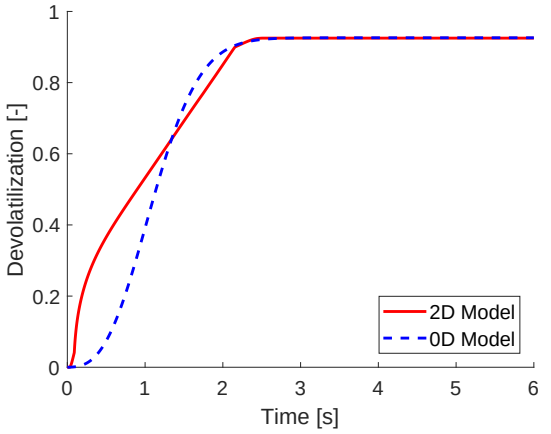

(d) $d_p = 3.12$ mm, $AR = 1.01$.

Figure 5.6: 0D model with the apparent kinetics modeled by the PLS model given in equation 5.6 and 5.7 compared to a 2D devolatilization model.[87] $\rho = 700$ kg/m^3, $T_g = 1600$ K.

5.5 Conclusion

The developed 0D model describes devolatilization of cylindrical biomass particles using a lumped single first order Arrhenius equation to account for both kinetics and heat transfer limitations in the particle. The model includes aspect ratio, gas temperature and particle radius. The model further shows that of aspect ratio, particle radius, and gas temperature, especially the latter two are critical for the particle devolatilization. The model is compared to experimental data and a more complicated 2D model and shows good agreement, especially for the smaller particles, where the heat transfer limitation are less severe. The devolatilization model presented is simple and can be implemented into CFD without adding substantially to the computational costs.

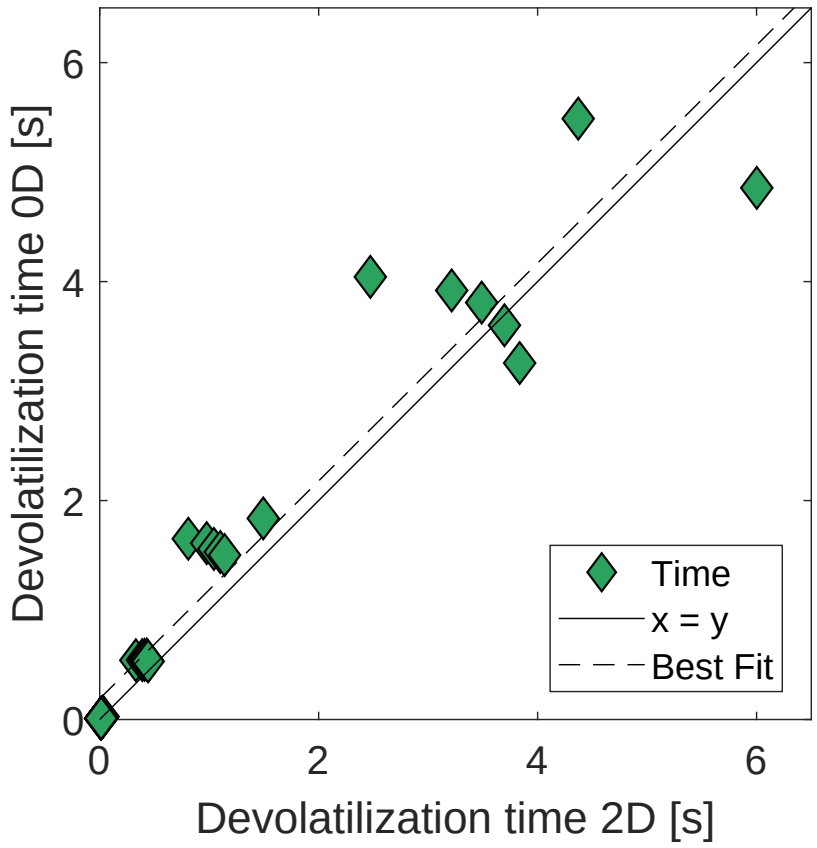

Figure 5.7: Comparison of the time predicted by the 2D model and the 0D model, $r^2 = 0.92$.

5.6 Acknowledgment

The authors gratefully acknowledge the financial and advisory support received from Ørsted A/S, Burmeister and Wain Scandinavian Contractors A/S, and Rambøll A/S. We also thank the Nordic Five Tech (N5T) alliance for financial support.

6 Conclusion and Further Work

This thesis aims to add to the understanding of suspension firing of biomass through modeling of particle devolatilization. To have an adequate understanding of biomass devolatilization is crucial for predicting flame stability and burnout in a suspension firing unit, as a large fraction of the volatiles and thereby the energy is released during the devolatilization process, when combusting biomass particles. The overall intention has been to contribute to the knowledge bank in order to aid in the development of the next generation of bio-dust burners. Two of the models presented in this thesis can be implemented into CFD, and thereby assist in commercial development of new bio-dust boilers, and the last model aids in elucidating the influence of particle morphology.

6.1 Conclusion

A literature review presenting the fundamentals of suspension firing and biomass particle devolatilization has been conducted, where the subprocesses of heating, drying, devolatilization, volatile, and char oxidation has been covered. The focus has been on devolatilization as this is the main topic in this thesis and an important process in suspension firing of biomass particles, because the volatiles released during suspension firing ensures flame ignition and stability.

A simple model to estimate the char yield from biomass devolatilization at high heating rates is developed. Determining the correct split into volatiles and char during devolatilization is important as the time frame and heat release are vastly different when comparing oxidation of volatiles and char. Thus any subsequent models describing these two phenomena are only relevant if the split is estimated adequately. The model presented to obtain the char yield is concerning high heating rate devolatilization, i.e. conditions relevant for suspension firing. The model includes the effect of gas temperature (873-1673 K), heating rate ($0.1 \cdot 10^3$ - $12 \cdot 10^3$ K/s), and potassium content (0.02 - 0.37 wt% db) in the biomass. It is developed using the method of PLS and predicts the char yield from independent, experimental data from literature well with an RMSEP = 0.9 wt% char daf.

Additionally, a second model is presented, which describes the course of the devolatilization for different particle morphologies. The model includes both spheres (one dimensional) and cylinders (two dimensional). Coal particles can often be described as spherical, but biomass particles are typically elongated due to their fibrous nature, and modeling them as spheres is not accurate.

The model accounts for devolatilization of non-isothermal particles at suspension firing conditions. The model is validated against experimental data and they are in good agreement. The influence of operating conditions and biomass parameters are tested for three different particle sizes and shows that small particles (79 μm) are primarily kinetically controlled, whereas large particles (3.1 mm) tend to be heat transfer limited. The model further shows that if a cylindrical biomass particle needs to be approximated as a sphere due to restrictions in computational power, a sphere with the same initial diameter as the cylinder is better than a sphere with the same initial volume as the cylinder when estimating devolatilization times.

If one wants to model the devolatilization using a zero dimensional, isothermal particle, a kinetic scheme is also presented, where the effects of the temperature gradients in the particle and the kinetics are lumped into the expression for the reaction rate. The kinetic scheme presented is an SFOR Arrhenius expression, where the pre-exponential factor and the activation energy are estimated based on particle aspect ratio, particle diameter, and gas temperature. The results from the isothermal particle model corresponds well to the 2D cylindrical particle model also presented in the thesis and to experimental data.

Overall, the models presented in this thesis can be implemented into CFD or used separately for modeling devolatilization. The models are simple yet accurate and are all validated against experimental data. It is the hope that they add to the current modeling of devolatilization by elucidating the effects of operating conditions on char yield and particle morphology, and further that this thesis will act as a stepping stone for future studies on pulverized fuel combustion.

6.2 Further Work

The topic of suspension firing is vast and many interesting new studies could be proposed in order to expand the knowledge within this field and hopefully thereby aid in understanding and optimization of energy production. This section is dedicated primarily to proposals of experimental and modeling studies, which are linked to the work covered in this thesis, but many more investigations could be done.

6.2.1 Experimental Studies

This thesis is constituted of a literature study and three manuscripts, which all deal with modeling different aspects of devolatilization under suspension firing conditions. The aim has been to elucidate the effect of biomass particle properties and experimental conditions on char yield and devolatilization times and kinetics. The models presented here are empirical or have empirical input parameters and are consequently dependent on quality experimental data obtained under condition relevant for suspension firing. The data already available in literature is gratefully acknowledged. To the knowledge of the author, however, no data is available for devolatilization of biomass particle sizes in the range 125 μm - 3 mm at PF conditions, and no data is available for fully devolatilized particles in the size range 1-3 mm. Typically particles for suspension firing

are in the range 0.1-3 mm, and the majority of the mass and consequently the energy originates from particles in the upper half of the size range. Thus the models presented in this thesis are validated against data in the lower part of the size range (0.050-1 mm) for the char yield model, and for extreme values, both low and high, for the devolatilization models ($d_p < 125$ µm or $d_p > 3$ mm). A considerable addition to the knowledge on suspension firing could thus be obtained from quality experimental data in the size range in between these extreme values. This would add value both in itself and through the possibility of validating models against data for all relevant particle sizes.

Another topic which would advance from more experimental data is the determination of Nusselt numbers for biomass particles (or inert cylinders) in free fall. obtaining such numbers experimentally would present a multitude of challenges, which will not be dealt with here. However, the approach suggested by Duan et al.[197] where the Nusselt number is determined on the basis of drag coefficient is interesting and investigating this further may be a feasible way of estimating the Nusselt number for cylinders in a free fall more accurately.

6.2.2 Modeling Work

The investigations of the Nusselt numbers for particles in free fall would also require some modeling work. A CFD study might aid in determining a more correct Nusselt number in combination with the experimental study proposed above. Other CFD studies, which would be of interest, and which are more directly linked to the work here, are implementations of both the char yield model and the lumped Arrhenius kinetics for elongated particles into a full scale CFD simulation of a suspension firing unit. This would hopefully lead to more accurate CFD simulations and would validate the proposed PLS models further.

It may also be feasible to implement the 2D devolatilization model into CFD in pilot scale in order to see if the model can be validated against already conducted experiments and to investigate the effect of particle morphology further. Implementing the model into full scale would probably lead to increases in computational costs higher than what is currently feasible, but might be interesting in the future.

6.2.3 Overall Outlook

In addition to the experiments and simulations proposed above the postdevolatilization processes should not be forgotten. The entire combustion process in a full scale suspension firing boiler, from heating of the particle to combustion of the char and volatiles, consists of subprocesses, which are all interlinked. Thus describing the phenomena in detail requires that all aspects of the combustion process are considered. Pulverized fuel combustion should be optimized both on the modeling and the experimental side, and preferably with already obtained knowledge in mind. Ultimately, the combustion of small particles at high heating rates and temperatures in a swirling jet flame should be described by experimental and modeling work in such detail that

existing facilities can be operated in an optimal way with respect to fuel efficiency, and emission limitations. Furthermore the knowledge of suspension firing should ideally, ultimately, also be so comprehensive that newly designed facilities would have severely lower levels of emission and a higher fuel efficiency. The work presented here should be considered as a modest stepping stone towards this utopian scenario.

Bibliography

[1] The United Nations. Sustainable development goals. `url: https://www.un.org/sustainabledevelopment/`, 2019. Visited 29th of March 2019.

[2] The European Comission. 2020 climate & energy package. `url: https://ec.europa.eu/clima/policies/strategies/2020\_en`, 2019. Visited 29th of March 2019.

[3] The Danish government. Danmark som foregangsland på energi og klima - status på den grønne omstilling. Technical report, Danish Ministry of Energy, Utilities and Climate, Copenhagen, Denmark, 4 2018.

[4] Ritzau. Stort forlig: Bred politisk aftale giver billigere el og flere havmøller. Politiken (Danish National Newspaper), 2018. Published 29th of June.

[5] Det Etiske Råd (The Danish Council on Ethics). Redegørelse om bioenergi, fødevarer, og etik i en globaliseret verden. Technical report, The Danish Council on Ethics, Copenhagen, Denmark, 2012. p. 39-42.

[6] Ørsted A/S (former DONG Energy A/S). Dong energy stoppper al brug af kul i 2023. `url: https://orsted.com/da/Media/Newsroom/News/2017/02/DONG-Energy-to-stop-all-use-of-coal-by-2023`, 2017. Visited 29th of March 2019.

[7] State of Green. From sustainable biomass to competitive energy. Technical report, Confederation of Danish Industry; Danish Energy Association; Danish Agriculture & Food Council; Danish Wind Industry Association; Ministry of Business and growth Denmark; Danish ministry of Energy, Utilities and Climate; Ministry of Environment and Food, Copenhagen, Denmark, 2015.

[8] DTU Chemical and Biochemical Engineering. GREEN. `url: http://www.kt.dtu.dk/forskning/chec/afsluttede-projekter/green`, 2018. Visited 29th of March 2019.

[9] J. M. Johansen, R. Gadsbøll, J. Thomsen, P. A. Jensen, P. Glarborg, P. Ek, N. De Martini, M. Mancini, R. Weber, and R. E. Mitchell. Devolatilization kinetics of woody biomass at short residence times and high heating rates and peak temperatures. *Appl. Energ.*, 162:245–256, 2016.

[10] J. M. Johansen, P. A. Jensen, P. Glarborg, N. De Martini, P. Ek, and R. E. Mitchell. High Heating Rate Devolatilization Kinetics of Pulverized Biomass Fuels. *Energy and Fuels*, 32(12):12955–12961, 2018.

[11] J. S. Johansen, S. Clausen, A. Fateev, K. L. Nielsen, J. Wadenbäck, M. Tonell, P. A. Jensen, and P. Glarborg. Analysis of a 30MW$_{th}$ Bio-Dust Fired Swirl Burner, Part I: Detailed Experimental Measurements. Manuscript in preparation, 2019.

[12] A. Trubetskaya, P. A. Jensen, A. D. Jensen, M. Steibel, H. Spliethoff, and P. Glarborg. Influence of fast pyrolysis conditions on yield and structural transformation of biomass chars. *Fuel Process. Technol.*, 140:205–214, 2015.

[13] A. Trubetskaya, P. A. Jensen, A. D. Jensen, A. D. Garcia Llamas, K. Umeki, and P. Glarborg. Effect of fast pyrolysis conditions on biomass solid residues at high temperatures. *Fuel Process. Technol.*, 143:118–129, 2016.

[14] J. M. Johansen, P. A. Jensen, P. Glarborg, M. Mancini, R. Weber, and R. E. Mitchell. Extension of apparent devolatilization kinetics from thermally thin to thermally thick particles in zero dimensions for woody biomass. *Energy*, 95:279–290, 2016.

[15] J. S. Johansen, L. Myllerup, J. Eriksson, S. Clausen, A. Fateev, K. L. Nielsen, J. Wadenbäck, M. Tonell, P. A. Jensen, and P. Glarborg. Analysis of a 30MW$_{th}$ Bio-Dust Fired Swirl Burner, Part II:Comparison of Experimental Measurements and CFD Simulations. Manuscript in preparation, 2019.

[16] J.M. Beér, J. Chomiak, and L.D. Smoot. Fluid dynamics of coal combustion : A review. *Prog. Energy Combust. Sci.*, 10:177–208, 1984.

[17] A. D. Jensen and P. Glarborg. Combustion and high temperature processes. Compendium, Technical University of Denmark, 2009.

[18] R.A. Chaplin. *Thermal Power Plants - Volume II*. EOLSS Publications, 2009. Chapter 1.

[19] J.A. Kent. *Kent and Riegel's Handbook of Industrial Chemistry and Biotechnology*. Springer US, 2010. p.862.

[20] Y. B. Yang, V. N. Sharifi, J. Swithenbank, L. Ma, L. I. Darvell, J. M. Jones, M. Pourkashanian, and A. Williams. Combustion of a Single Particle of Biomass. *Energ. Fuels*, 22(8):306–316, 2008.

[21] A. V. Bridgwater. Review of fast pyrolysis of biomass and product upgrading. *Biomass Bioenerg.*, 38:68–94, 2012.

[22] J.H. Clark and F. Deswarte. *Introduction to Chemicals from Biomass*. Wiley Series in Renewable Resource. Wiley, 2014. table 3.5.

[23] J. M. Johansen. Amagerværket unit 1: Near burner investigation (full scale). Technical report, Technical University of Denmark, 2012. Also available as chapter 10 in the PhD thesis by Johansen.

[24] Energy research center of the Netherlands. Database for biomass and waste. `url`: https://www.ecn.nl/phyllis2, 2019. Visited: 27th of March 2019.

[25] P. Stępień, J. Pulka, M. Serowik, and A. Białowiec. Thermogravimetric and Calorimetric Characteristics of Alternative Fuel in Terms of Its Use in Low-Temperature Pyrolysis. *Waste Biomass Valori.*, 0(0):1–9, 2018.

[26] L. Zhang, C. Xu, and P. Champagne. Overview of recent advances in thermo-chemical conversion of biomass. *Energ. Convers. and Manage.*, 51:969–982, 2010.

[27] A. Demirbas. Combustion characteristics of different biomass fuels. *Prog. Energ. Combust.*, 30(2):219–230, 2004.

[28] V. Eijsink. New development in enzyme research. Presentation, Bio4Fuels Days 2017, 2017.

[29] J.M. Berg, J. L. Tymoczko, and L. Stryer. *Biochemistry*. W.H. Freeman, 7 edition, 2010. p. 338-339.

[30] H. V. Scheller and P. Ulvskov. Hemicelluloses. *Annu. Rev. Plant Biol.*, 61(1):263–289, 2010.

[31] H. Bohlmann. Chapter two - introductory chapter on the basic biology of cyst nematodes. In C. Escobar and C. Fenoll, editors, *Plant Nematode Interactions*, volume 73 of *Advances in Botanical Research*, pages 33 – 59. Academic Press, 2015.

[32] H. Pereira. Chapter 3 - the chemical composition of cork. In H. Pereira, editor, *Cork*, pages 55 – 99. Elsevier Science B.V., Amsterdam, 2007.

[33] F. Lu and J. Ralph. Chapter 6 - lignin. In R.-C. Sun, editor, *Cereal Straw as a Resource for Sustainable Biomaterials and Biofuels*, pages 169 – 207. Elsevier, Amsterdam, 2010.

[34] C. Di Blasi. Modeling chemical and physical processes of wood and biomass pyrolysis. *Prog. Energ. Combust. Sci.*, 34(1):47–90, 2008.

[35] H. Chen. *Chemical Composition and Structure of Natural Lignocellulose*, pages 25–71. Springer Netherlands, Dordrecht, 2014. p. 62-63.

[36] L. A. Hansen, H. P. Nielsen, F. J. Frandsen, K. Dam-Johansen, S. Hørlyck, and A. Karlsson. Influence of deposit formation on corrosion at a straw-fired boiler. *Fuel Process. Technol.*, 64(1):189–209, 2000.

[37] B. M. Jenkins, L. L. Baxter, T. R. Miles Jr., and T. R. Miles. Combustion properties of biomass. *Fuel Processing Technology*, 54:17–46, 1998.

[38] M. Müller-Hagedorn, H. Bockhorn, L. Krebs, and U. Müller. A comparative kinetic study on the pyrolysis of three different wood species. *J. Anal. Appl. Pyrolysis*, 68-69:231–249, 2003.

[39] M. Barrio, B. Gøbel, H. Rimes, U. Henriksen, J. E. Hustad, and L. H. Sørensen. *Steam Gasification of Wood Char and the Effect of Hydrogen Inhibition on the Chemical Kinetics*, chapter 2, pages 32–46. John Wiley & Sons, 1 edition, 2008.

[40] C. Wilén, A. Moilanen, and E. Kurkela. Biomass feedstock analyses. Technical Report 282, Technical Research Centre of Finland, 1996.

[41] P. J. Kramer and T. T. Kozlowski. *Physiology of Woody Plants*. Academic Press, 1979. chapter 2.

[42] J. D. Ovington and H. A. I. Madgwick. The sodium, potassium and phosphorus contents of tree species grown in close stands. *New Phytol.*, 57(3):273–284, 1958.

[43] S. Meier. Elemental Analysis of Wood Fuels. Technical Report June, New York State Energy Research and Development Authority, 2013.

[44] H. M. Eriksson and C. Jonsson. Four tree species and the calcium, magnesium, and potassium budgets of a swedish forest site. *New Zeal. J. For. Sci.*, 24(2-3):415–426, 1994.

[45] J.-C. Liu and P. Trüby. Bodenanalytische Diagnose von K- und Mg-Mangel in Fichtenbeständen (*Picea abies* Karst.). *Z. Pflanz. Bodenkunde*, 152(3):307–311, 1989.

[46] J. Bodig and B.A. Jayne. *Mechanics of wood and wood composites.* Van Nostrand Reinhold, 1982. p.5.

[47] F. F. P. Kollmann. *Mechanics and Rheology of Wood*, page 57. Springer-Verlag New York Inc., 01 1968.

[48] G. Tsoumis. *Chemical composition and ultrastructure of wood*, pages 34–56. Verlag Kessel, Thessaloniki, Greece, 1991. p. 35.

[49] M. S. Bashir, P. Jensen, F. J. Frandsen, S. Wedel, K. Dam-Johansen, J. Wadenbäck, and S. T. Pedersen. Suspension-firing of biomass. part 1: Full-scale measurements of ash deposit build-up. *Energ. Fuels*, 26:2317–2330, 2012.

[50] B. M. Jenkins, R. R. Bakker, and J. B. Wei. On the properties of washed straw. *Biomass and Bioenergy*, 10(4):177–200, 1996.

[51] K. Kubica, M. Jewiarz, R. Kubica, and A. Szlęk. Straw Combustion: Pilot and Laboratory Studies on a Straw-Fired Grate Boiler. *Energ. Fuels*, 30(6):4405–4410, 2016.

[52] C. Bang, A. Vitina, J. S. Gregg, and H. H. Lindboe. Analysis of biomass prices. Future Danish prices for straw, wood chips and wood pellets. Technical report, Ea Energy Analyses, 2013.

[53] J. M. O. Scurlock. Miscanthus: A Review of European Experience with a Novel Energy Crop. *U.S. Department of Energy, Environmental Sciences Division, Publication No. 4845*, pages 1–18, 1999.

[54] U.S. Department of Energy Office of Fossil Energy. `url: https://fossil.energy.gov/education/energylessons/coal/coal\_history.html`, 2017. Visited: 2017.

[55] O. Williams, G. Newbolt, C. Eastwick, S. Kingman, D. Giddings, S. Lormor, and E. Lester. Influence of mill type on densified biomass comminution. *Appl. Energ.*, 182:219–231, 2016.

[56] J. R. Pels, D. S. de Nie, and J. H. A. Kiel. Utilization of ashes from biomass combustion and gasificatoin, 2005. 14th European Biomass Conference & Exhibition.

[57] H. Li, Q. Chen, X. Zhang, K. N. Finney, V.N. Sharifi, and J. Swithenbank. Evaluation of a biomass drying process using waste heat from process industries: A case study. *Appl. Therm. Eng.*, 35:71–80, 2012.

[58] G. Thek and I. Obernberger. *The Pellet Handbook: The Production and Thermal Utilization of Biomass Pellets.* Taylor & Francis, 2012. chap 4.1.

[59] J. Bodig and B.A. Jayne. *Mechanics of wood and wood composites.* Van Nostrand Reinhold, 1982. p.42.

[60] P. H. Mitchell. Calculating the equilibrium moisture content for wood based on humidity measurements. *Bioresources*, 13(1):171–175, 2018.

[61] H. Spliethoff and K.R.G. Hein. Effect of co-combustion of biomass on emissions in pulverized fuel furnaces. *Fuel Process. Technol.*, 54:189–205, 1998.

[62] G. Thek and I. Obernberger. *The Pellet Handbook: The Production and Thermal Utilization of Biomass Pellets.* Taylor & Francis, 2012. chap. 3.2.4.

[63] W. Stelte. Steam explosion for biomass pre-treatment. Technical report, Danish Technological Institute, 2013.

[64] E. Alakangas. New European Pellets Standard - EN 14961-1. Technical report, EUBIONET III, 2009.

[65] E. Alakangas and P. Paju. Wood pellets in Finland - technology, economy, and market. *OPET Report 5*, page 85, 2002.

[66] M. Masche, M. Puig-Arnavat, P. A. Jensen, J. K. Holm, S. Clausen, J. Ahrenfeldt, and U. B. Henriksen. From wood chips to pellets to milled pellets: The mechanical processing pathway of Austrian pine and European beech. *Powder Technol.*, 2019.

[67] S. H. Larsson, M. Thyrel, P. Geladi, and T. A. Lestander. High quality biofuel pellet production from pre-compacted low density raw materials. *Bioresource Technol.*, 99(15):7176–7182, 2008.

[68] T. Lin, L. F. Rodríguez, S. Davis, M. Khanna, Y. Shastri, T. Grift, S. Long, and K. C. Ting. Biomass feedstock preprocessing and long-distance transportation logistics. *GCB Bioenergy*, 8(1):160–170, 2016.

[69] M. W. McElroy, R. C. Carr, D. S. Ensor, and G. R. Markowski. Size distribution of fine particles from coal combustion. *Science*, 215(4528):13–19, 1982.

[70] M. Mandø, L. Rosendahl, C. Yin, and H. Sørensen. Pulverized straw combustion in a low-NOx multifuel burner: Modeling the transition from coal to straw. *Fuel*, 89(10):3051–3062, 2010.

[71] C. Yin. Chapter five - biomass co-firing. In L. Rosendahl, editor, *Biomass Combustion Science, Technology and Engineering*, Woodhead Publishing Series in Energy. Elsevier Science, 2013. p.90-91.

[72] M. Masche, M. Puig-Arnavat, J. Wadenbäck, S. Clausen, P. A. Jensen, J. Ahrenfeldt, and U. B. Henriksen. Wood pellet milling tests in a suspension-fired power plant. *Fuel Process. Technol.*, 173:89–102, 2018.

[73] A. Trubetskaya, G. Beckmann, J. Wadenbäck, J. K. Holm, S. P. Velaga, and R. Weber. One way of representing the size and shape of biomass particles in combustion modeling. *Fuel*, 206:675–683, 2017.

[74] A. Trubetskaya, Y. Poyraz, R. Weber, and J. Wadenbäck. Secondary comminution of wood pellets in power plant and laboratory-scale mills. *Fuel Process. Technol.*, 160:216–227, 2017.

[75] M. Temmerman and P. D. Jensen. Von Rittinger theory adapted to wood chip and pellet milling, in a laboratory scale hammermill. *Biomass Bioenerg.*, 56:70–81, 2013.

[76] S. Mani, L. G. Tabil, and S. Sokhansanj. Grinding performance and physical properties of wheat and barley straws, corn stover and switchgrass. *Biomass Bioenerg.*, 27:339–352, 2004.

[77] M. Momeni. *Fundamental Study of Single Biomass Particle Combustion.* PhD thesis, Technical University of Denmark, 2013.

[78] J. Ballester, J. Barroso, L.M. Cerecedo, and R. Ichaso. Comparative study of semi-industrial-scale flames of pulverized coals and biomass. *Combust. Flame*, 141:204–215, 2005.

[79] N. Syred and J. M. Beér. Combustion in Swirling Flows: A Review. *Combust. Flame*, 201(2):143–201, 1974.

[80] A. M. Godridge. Pulverized coal furnaces. `url: http://www.thermopedia.com/content/1066/`, 2011. Visited 4th of April 2019.

[81] R. Weber and J. Dugué. Combustion accelerated swirling flows in high confinements. *Prog. Energ. Combust. Sci.*, 18(4):349–367, 1992.

[82] J.P. Smart and R. Weber. NOx Reduction and Burnout Optimisation using an Aerodynamically Air Staged Burner and an Air Staged Precombustor Burner. *J. I. Energy*, pages 237–245, 1989.

[83] B. Damstedt, J. M. Pederson, D. Hansen, T. Knighton, J. Jones, C. Christensen, L. Baxter, and D. Tree. Biomass cofiring impacts on flame structure and emissions. *P. Combust. Inst.*, 31:2813–2820, 2007.

[84] C. Yin, L. Rosendahl, and S. K. Kær. Towards a better understanding of biomass suspension co-firing impacts via investigating a coal flame and a biomass flame in a swirl-stabilized burner flow reactor under same conditions. *Fuel Process. Technol.*, 98:65–73, 2012.

[85] T. Nussbaumer. Overview on technologies for biomass combustion and emission levels of particulate matter. Technical Report June, Swiss Federal Office for the Environment (FOEN), 2010.

[86] M. A. Stanish, G. S. Schajer, and Ferhan Kayihan. A mathematical model of drying for hygroscopic porous media. *AIChE Journal*, 32(8):1301–1311, 1986.

[87] A. Leth-Espensen, T. Li, P. Glarborg, T. Løvås, and P. A. Jensen. The influence of size and morfology on devolatilization of biomass particles. submitted article, 2019.

[88] A. L. Brown, D. C. Dayton, M. R. Nimlos, and J. W. Daily. Design and characterization of an entrained flow reactor for the study of biomass pyrolysis chemistry at high heating rates. *Energ. Fuels*, 15(5):1276–1285, 2001.

[89] A. Demirbas and G. Arin. An Overview of Biomass Pyrolysis. *Energ. Source.*, 24(5):471–482, 2002.

[90] Z. Zhang, S. Yani, M. Zhu, J. Li, and D. Zhang. Effect of Temperature and Heating Rate in Pyrolysis on the Yield , Structure and Oxidation Reactivity of Pine Sawdust Biochar. In *Proceedings of Chemeca 2013: Challenging Tomorrow*, pages 863–869, 2013.

[91] K. Umeki, K. Kirtania, L. Chen, and S. Bhattacharya. Fuel Particle Conversion of Pulverized Biomass during Pyrolysis in an Entrained Flow Reactor. *Ind. Eng. Chem. Res.*, 51:13973–13979, 2012.

[92] A. D. Lewis and T. H. Fletcher. Prediction of Sawdust Pyrolysis Yields from a Flat-Flame Burner Using the CPD Model. *Energ. Fuels*, 27:942–953, 2013.

[93] A. Trubetskaya, G. Surup, A. Shapiro, and R. B. Bates. Modeling the influence of potassium content and heating rate on biomass pyrolysis. *Appl. Energ.*, 194:199–211, 2017.

[94] A. Williams, M. Pourkashanian, and J.M. Jones. The combustion of coal and some other solid fuels. *Proc. Combust. Inst.*, 28(2):2141–2162, 2000.

[95] F. F. Costa and M. Costa. Evaluation of particle fragmentation of raw and torrified biomass in a drop tube furnace, 2014. V Conferencia Nacional de Mecanica dos Fluidos, Termodinamica e Energia, Poto, Portugal.

[96] Y. Zhang, S. Kajitani, M. Ashizawa, and K. Miura. Peculiarities of Rapid Pyrolysis of Biomass Covering Medium- and High-Temperature Ranges. *Energ. Fuels*, 20(8):2705–2712, 2006.

[97] S. Septien, S. Valin, C. Dupont, M. Peyrot, and S. Salvador. Effect of particle size and temperature on woody biomass fast pyrolysis at high temperature (1000 - 1400°C). *Fuel*, 97:202–210, 2012.

[98] M. Simone, E. Biagini, C. Galletti, and L. Tognotti. Evaluation of global biomass devolatilization kinetics in a drop tube reactor with CFD aided experiments. *Fuel*, 88(10):1818–1827, 2009.

[99] N. P. Niemelä, H. Tolvanen, T. Saarinen, A. Leppänen, and T. Joronen. CFD based reactivity parameter determination for biomass particles of multiple size ranges in high heating rate devolatilization. *Energy*, 128:676–687, 2017.

[100] S. Jiménez, P. Remacha, J. C. Ballesteros, A. Giménez, and J. Ballester. Kinetics of devolatilization and oxidation of a pulverized biomass in an entrained flow reactor under realistic combustion conditions. *Combust. Flame*, 152:588–603, 2008.

[101] M. Dall'Ora, P. A. Jensen, and A. D. Jensen. Suspension Combustion of Wood: Influence of Pyrolysis Conditions on Char Yield, Morphology, and Reactivity. *Energ. Fuels*, 22(8):2955–2962, 2008.

[102] C. Dupont, J.-M. Commandré, P. Gauthier, G. Boissonnet, S. Salvador, and D. Schweich. Biomass pyrolysis experiments in an analytical entrained flow reactor between 1073 K and 1273 K. *Fuel*, 87:1155–1164, 2008.

[103] M. W. Jarvis, T. J. Haas, B. S. Donohoe, J. W. Daily, K. R. Gaston, W. J. Frederick, and M. R. Nimlos. Elucidation of Biomass Pyrolysis Products Using a Laminar Entrained Flow Reactor and Char Particle Imaging. *Energ. Fuels*, 25(4):324–336, 2011.

[104] R. Zanzi, K. Sjöström, and E. Björnbom. Rapid pyrolysis of agricultural residues at high temperature. *Biomass Bioenerg.*, 23:357–366, 2002.

[105] H. Lu, W. Robert, G. Peirce, B. Ripa, and L. L. Baxter. Comprehensive study of biomass particle combustion. *Energ. Fuels*, 22(4):2826–2839, 2008.

[106] K. Anastasakis, I. Kitsiou, and W. De Jong. Fast devolatilization characteristics of 'low cost' biomass fuels, wood and reed. Potential feedstock for gasification. *Fuel Process. Technol.*, 142:157–166, 2016.

[107] A. V. Sepman and L. P. H. de Goey. Plate reactor as an analysis tool for rapid pyrolysis of biomass. *Biomass Bioenerg.*, 35(7):2903–2909, 2011.

[108] T. Nunn, J. B. Howard, J. P. Longwell, and W. A. Peters. Product compositions and kinetics in the rapid pyrolysis of sweet gum hardwood. *Ind. Eng. Chem. Proc. D. D.*, 24:836–844, 1985.

[109] E. Hoekstra, W. P. M. Van Swaaij, S. R. A. Kersten, and K. J. A. Hogendoorn. Fast pyrolysis in a novel wire-mesh reactor: Decomposition of pine wood and model compounds. *Chem. Eng. J.*, 187:172–184, 2012.

[110] M. Asadullah, S. Zhang, and C.-Z. Li. Evaluation of structural features of chars from pyrolysis of biomass of different particle sizes. *Fuel Process. Technol.*, 91(8):877–881, 2010.

[111] A. Bharadwaj, L. L. Baxter, and A. L. Robinson. Effects of Intraparticle Heat and Mass Transfer on Biomass Devolatilization: Experimental Results and Model Predictions. *Energ. Fuels*, 18(4):1021–1031, 2004.

[112] O. Senneca. Characterization of Biomass as Non Conventional Fuels by Thermal Techniques. In Dr. Shahid Shaukat, editor, *Pretreatment Techniques for Biofuels and Biorefineries*, chapter 16, page 320. InTech, 2011.

[113] J. F. Stubington and S. Aiman. Pyrolysis Kinetics of Bagasse at High Heating Rates. *Energ. Fuels*, 8(1):194–203, 1994.

[114] P. McNamee, L. I. Darvell, J. M. Jones, and A. Williams. Biomass and Bioenergy The combustion characteristics of high-heating-rate chars from untreated and torrefied biomass fuels. *Biomass Bioenerg.*, 82:63–72, 2015.

[115] M. R. Hajaligol, J. B. Howard, J. P. Longwell, and W. A. Peters. Product compositions and kinetics for rapid pyrolysis of cellulose. *Ind. Eng. Chem. Proc. D. D.*, 21(3):457–465, 1982.

[116] J. Li, G. Bonvicini, L. Tognotti, W. Yang, and W. Blasiak. High-temperature rapid devolatilization of biomasses with varying degrees of torrefaction. *Fuel*, 122:261 – 269, 2014.

[117] G. Di Nola, W. de Jong, and H. Spliethoff. The fate of main gaseous and nitrogen species during fast heating rate devolatilization of coal and secondary fuels using a heated wire mesh reactor. *Fuel Process. Technol.*, 90(3):388 – 395, 2009.

[118] M. Antal Jr. and G. Várhegyi. Cellulose pyrolysis kinetics: The current state of knowledge. *Ind. Eng. Chem. Res.*, 37:1267–1277, 1998.

[119] A. Anca-Couce. Reaction mechanisms and multi-scale modelling of lignocellulosic biomass pyrolysis. *Prog. Energ. Combust.*, 53:41–79, 2016.

[120] C. Di Blasi. Comparison of semi-global mechanisms for primary pyrolysis of lignocellulosic fuels. *J. Anal. Appl. Pyrol.*, 47:43 – 64, 1998.

[121] J. E. White, W. J. Catallo, and B. L. Legendre. Biomass pyrolysis kinetics: A comparative critical review with relevant agricultural residue case studies. *J. Anal. Appl. Pyrol.*, 91:1 – 33, 2011.

[122] M. Nik-Azar, M. R. Hajaligol, M. Sohrabi, and B. Dabir. Effects of heating rate and particle size on the products yields from rapid pyrolysis of beech-wood. *Fuel Sci. Techn. Int.*, 14(4):479–502, 1996.

[123] P.C. Lewellen, W.A. Peters, and J.B. Howard. Cellulose pyrolysis kinetics and char formation mechanism. *Symp. Int. Combust.*, 16(1):1471 – 1480, 1977.

[124] T. R. Nunn, J. B. Howard, J. P. Longwell, and W. A. Peters. Product compositions and kinetics in the rapid pyrolysis of milled wood lignin. *Ind. Eng. Chem. Proc. D.D.*, 24(3):844–852, 1985.

[125] D. Radlein, J. Piskorz, and D. S. Scott. Fast pyrolysis of natural polysaccharides as a potential industrial process. *J. Anal. Appl. Pyrol.*, 19:41–63, 1991.

[126] J. Riaza, R. Khatami, Y. A. Levendis, L. Álvarez, M. V. Gil, C. Pevida, F. Rubiera, and J. J. Pis. Combustion of single biomass particles in air and in oxy-fuel conditions. *Biomass Bioenerg.*, 64:162–174, 2014.

[127] L. Shan, M. Kong, T. D. Bennet, A. C. Sarroza, C. Eastwick, D. Sun, G. Lu, Y. Yan, and H. Liu. Studies on combustion behaviours of single biomass particles using a visualization method. *Biomass Bioenerg.*, 109:54–60, 2018.

[128] J. M. Johansen. *Power Plant Burners for Bio-Dust Combustion*. PhD thesis, DTU, 2015.

[129] N. S. Trivedi, S. A. Mandavgane, and A. Chaurasia. Characterization and valorization of biomass char: a comparison with biomass ash. *Environ. Sci.Pollut. Res.*, 25(4):3458–3467, 2018.

[130] T. H. Fletcher. Chapter six - gasification fundamentals. In T. Wang and G. Stiegel, editors, *Integrated Gasification Combined Cycle (IGCC) Technologies*, pages 223 – 256. Woodhead Publishing, 2017.

[131] D. A. Tillman, A. J. Rossi, and W. D. Kitto. *Wood Combustion, Principles, processes, and economics*, chapter 4. Elsevier, 1 edition, 1981.

[132] N. M. Laurendeau. Heterogeneous kinetics of coal char gasification and combustion. *Prog.Energ. Combust. Sci.*, 4(4):221–270, 1978.

[133] I.W. Smith. The combustion rates of coal chars: A review. *Symp. Int. Combust.*, 19(1):1045 – 1065, 1982.

[134] M. B. Tilghman and R. E. Mitchell. Coal and biomass char reactivities in gasification and combustion environments. *Combust. Flame*, 162(9):3220 – 3235, 2015.

[135] P. A. Campbell, R. E. Mitchell, and L. Ma. Characterization of coal char and biomass char reactivities to oxygen. *Proceedings of the Combustion Institute*, 29(1):519 – 526, 2002. P. Combust. Inst.

[136] J. M. Johansen, P. A. Jensen, S. Clausen, A. Fateev, K. L. Nielsen, J. Thomsen, R. Ø. Gadsbøll, R. Mitchell, R. Weber, M. Mancini, M. Tonell, J. Andersen, L. Myllerup, and P. Glarborg. A scientific basis for the development of the next generation of biodust burners. Poster session presented at 35th International Symposium on Combustion , San Francisco, United States, 2015.

[137] A. Leth-Espensen, P. Glarborg, and P. A. Jensen. Predicting Biomass Char Yield from High Heating Rate Devolatilization Using Chemometrics. *Energ. Fuels*, 32(9):9572–9580, 2018.

[138] Z. Lu, J. Jian, P. A. Jensen, H. Wu, and P. Glarborg. Influence of Torrefaction on Single Particle Combustion of Wood. *Energ. Fuels*, 30(7):5772–5778, 2016.

[139] Z. Lu, J. Jian, P. A. Jensen, H. Wu, and P. Glarborg. Impact of KCl impregnation on single particle combustion of wood and torrefied wood. *Fuel*, 206:684–689, 2017.

[140] H. Ström and H. Thunman. CFD simulations of biofuel bed conversion: A submodel for the drying and devolatilization of thermally thick wood particles. *Combust. Flame*, 160(2):417–431, 2013.

[141] Ansys Fluent. ANSYS Fluent 17.2 Theory Guide. `https://www.sharcnet.ca/Software/Ansys/17.2/en-us/help/flu_th/flu_th_sec_disp_law4.html`, 2016. Accessed: 2018-02-21.

[142] D. E. Priyanto, S. Ueno, K. Hashida, and H. Kasai. Energy-efficient milling method for woody biomass. *Adv. Powder Technol.*, 28(7):1660–1667, jul 2017.

[143] M. Nik-Azar, M.R. Hajaligol, M. Sohrabi, and B. Dabir. Mineral matter effects in rapid pyrolysis of beech wood. *Fuel Process. Technol.*, 51:7–17, 1997.

[144] G. E. Acquah, B. K. Via, O. O. Fasina, S. Adhikari, N. Billor, and L. G. Eckhardt. Chemometric modeling of thermogravimetric data for the compositional analysis of forest biomass. *PLOS ONE*, 12:1–15, 2017.

[145] K. Kim, N. Labbé, J. M. Warren, T. Elder, and T. G. Rials. Chemical and anatomical changes in *Liquidambar styraciflua* l. xylem after long term exposure to elevated CO_2. *Environ. Pollut.*, 198:179 – 185, 2015.

[146] G. Toscano, Å. Rinnan, A. Pizzi, and M. Mancini. The Use of Near-Infrared (NIR) Spectroscopy and Principal Component Analysis (PCA) to Discriminate Bark and Wood of the Most Common Species of the Pellet Sector. *Energ. Fuels*, 31(3):2814–2821, 2017.

[147] M. Mancini, Rinnan Å, A. Pizzi, C. Mengarelli, G. Rossini, D. Duca, and G. Toscano. Near infrared spectroscopy for the discrimination between different residues of the wood processing industry in the pellet sector. *Fuel*, 217:650–655, 2018.

[148] D. Neves, H. Thunman, A. Matos, L. Tarelho, and A. Gómez-Barea. Characterization and prediction of biomass pyrolysis products. *Prog. Energ. Combust. Sci.*, 37(5):611–630, 2011.

[149] S. Wold, K. Esbensen, and P. Geladi. Principal Component Analysis. *Chemometr. Intell. Lab.*, 2:37–52, 1987.

[150] J. E. Jackson. *A user's guide to principal components*. John Wiley & Sons, Inc., 1991.

[151] L. Eriksson, E. Johansson, N. Kettaneh-Wold, and S. Wold. *Multi- and Megavariate Data Analysis. Principles and Applications, page 71*, volume 1. Umetrics Academy, 2003.

[152] K. Kjeldahl and R. Bro. Some common misunderstandings in chemometrics. *J. Chemometr.*, 24:558–564, 2010.

[153] R. Bro and A. K. Smilde. Principal component analysis. *Anal. Methods*, 6:2812–2831, 2014.

[154] C. B. Zachariassen. *Process Analytical Chemistry and Technology in Pectin Production*. PhD thesis, University of Copenhagen, 2007.

[155] A. Trubetskaya. *Fast pyrolysis of biomass at high temperatures*. PhD thesis, Department og Chemical amd Biochemical Engineering, DTU, 2016.

[156] E. Zanzi, R. and Sjöström, K. and Björnbom. Rapid high-temperature pyrolysis of biomass in a free-fall reactor. *Fuel*, 75(5):545–550, 1996.

[157] M. L. Solano, E. Manzanedo, R. Concheso, M. D. Curt, M. Sanz, and J. Fernández. Potassium fertilisation and the thermal behaviour of *Cynara cardunculus* L . *Biomass Bioenerg.*, 34, 2010.

[158] L. Chen, C. Dupont, S. Salvador, M. Grateau, G. Boissonnet, and D. Schweich. Experimental study on fast pyrolysis of free-falling millimetric biomass particles between 800° C and 1000° C. *Fuel*, 106:61–66, 2013.

[159] W. Dubitzky, M. Granzow, and D. P. Berrar. *Fundamentals of Data Mining in Genomics and Proteomics, page 178*. Springer US, 2007.

[160] C. E. Eskildsen, P. W. Hansen, T. Skov, F. Marini, and L. Nørgaard. Evaluation of multivariate calibration models transferred between spectroscopic instruments: Applied to near infrared measurements of flour samples. *J. Near Infrared Spec.*, 24(2):151–156, 2016.

[161] H. Winning. Standardization of FT-IR instruments. *White Paper from Foss A/S*, 1:1–7, 2014.

[162] M. A. Saeed, G. E. Andrews, H. N. Phylaktou, and B. M. Gibbs. Global kinetics of the rate of volatile release from biomasses in comparison to coal. *Fuel*, 181:347–357, 2016.

[163] D. Gera, M. P. Mathur, M. C. Freeman, and A. Robinson. Effect of large aspect ratio of biomass particles on carbon burnout in a utility boiler. *Energ. Fuels*, 16(6):1523–1532, 2002.

[164] H. Jüntgen and K. H. van Heek. An Update of German Non-isothermal Coal Pyrolysis Work. *Fuel Process. Technol.*, 2:261–293, 1979.

[165] P. K. Agarwal, W. E. Genetti, and Y. Y. Lee. Model for devolatilization of coal particles in fluidized beds. *Fuel*, 63(8):1157–1165, 1984.

[166] H. Thunman, F. Niklasson, F. Johnsson, and B. Leckner. Composition of volatile gases and thermochemical properties of wood for modeling of fixed or fluidized beds. *Energ. Fuels*, 15(6):1488–1497, 2001.

[167] H. Lu, E. Ip, J. Scott, P. Foster, M. Vickers, and L. L. Baxter. Effects of particle shape and size on devolatilization of biomass particle. *Fuel*, 89(5):1156–1168, 2010.

[168] N. Sousa and J. L. T. Azevedo. Model simplifications on biomass particle combustion. *Fuel*, 184:948–956, 2016.

[169] J. J. Saastamoinen. Simplified model for calculation of devolatilization in fluidized beds. *Fuel*, 85(17-18):2388–2395, 2006.

[170] J. Larfeldt, B. Leckner, and M. C. Melaaen. Modelling and measurements of the pyrolysis of large wood particles. *Fuel*, 79:1637–1643, 2000.

[171] M. P. Remacha, S. Jiménez, and J. Ballester. Devolatilization of millimeter-sized biomass particles at high temperatures and heating rates. Part 1: Experimental methods and results. *Fuel*, 234:757–769, 2018.

[172] M. P. Remacha, S. Jiménez, and J. Ballester. Devolatilization of millimeter-sized biomass particles at high temperatures and heating rates. Part 2: Modeling and validation for thermally-thin and -thick regimes. *Fuel*, 234:707–722, 2018.

[173] H. Thunman, B. Leckner, F. Niklasson, and F. Johnsson. Combustion of wood particles - A particle model for Eulerian calculations. *Combust. Flame*, 129(1-2):30–46, 2002.

[174] S. R. Gubba, L. Ma, M. Pourkashanian, and A. Williams. Influence of particle shape and internal thermal gradients of biomass particles on pulverised coal/biomass co-fired flames. *Fuel Process. Technol.*, 92(11):2185–2195, 2011.

[175] A. Gómez-Barea, B. Leckner, A. L. Villanueva Perales, and M. Campoy. Analytical solutions of sharp interface models with nth order kinetics. Application to char conversion. *Chem. Eng. J.*, 183:408–421, 2012.

[176] J. Porteiro, J. L. Míguez, E. Granada, and J. C. Moran. Mathematical modelling of the combustion of a single wood particle. *Fuel Process. Technol.*, 87(2):169–175, 2006.

[177] B. M. Wagenaar, W. Prins, and W. P. M. van Swaaij. Flash Pyrolysis Kinetics of Pine Wood. *Fuel Process. Technol.*, 36:291–298, 1993.

[178] C. Di Blasi and C. Branca. Kinetics of Primary Product Formation from Wood Pyrolysis. *Ind. Eng. Chem. Res.*, 40(23):5547–5556, 2001.

[179] F. Thurner and U. Mann. Kinetic Investigation of Wood Pyrolysis. *Ind. Eng. Chem. Process D. D.*, 20(3):482–488, 1981.

[180] K. Ražnjević. *Handbook of Thermodynamic tables and charts.* Hemisphere Publishing Corporation, 1976.

[181] M.G. Grønli. *A theoretical and experimental study of the thermal degredation of biomass.* PhD thesis, NTNU, 1996.

[182] Engineering Toolbox. Latent heat of vaporization of fluids - alcohol, ether, nitrogen, water and more. `https://www.engineeringtoolbox.com/fluids-evaporation-latent-heat-d_147.html`, 2003. Accessed: 2019-03-06.

[183] J. E. Callanan, B. J. Filla, K. M. McDermott, and S. A. Sullivan. Enthalpies of desorption of water from coal surfaces. Proceedings of ACS Symposium, Devision of Fuel Chemistry, Denver, CO, 1987. 185-192.

[184] J. A. Havens, J. R. Welker, and C. M. Sliepcevich. Pyrolysis of Wood: A thermoanalytical Study. *J. Fire Flammability*, 2:321–333, 1971.

[185] M.W. Chase Jr. *"Thermophysical Properties of Fluid Systems" in NIST Chemistry WebBook, NIST Standard Reference Database Number 69.* National Institute of Standards and Technology, Gaithersburg MD, 20899, 1998.

[186] M.W. Chase Jr. *"Water" in NIST Chemistry WebBook, NIST Standard Reference Database Number 69, NIST-JANAF Thermochemical Tables, Fourth Edition, J. Phys. Chem. Ref. Data, Monograph 9.* National Institute of Standards and Technology, Gaithersburg MD, 20899, 1998.

[187] D. Merrick. Mathematical models of the thermal decomposition of coal. 2. Specific heats and heats of reaction. *Fuel*, 62(5):540–546, 1983.

[188] D.W. Green and R.H. Perry. *Perry's Chemical Engineers' Handbook, Eighth Edition.* McGraw Hill professional. McGraw-Hill Education, 2007.

[189] A. Tenwolde, J. D. McNatt, and L. Krahn. Thermal Properties of Wood and Wood Panel Products for Use in Buildings. *USDA Forest Products Laboratory Report for Oak Ridge National Laboratory, Oak Ridge, TN. U.S. Department of Energy, Report ORNLISub/87- 21697/1, September.*, page 43, 1988.

[190] C. A. Koufopanos, N. Papayannakos, G. Maschio, and A. Lucchesi. Modelling of the pyrolysis of biomass particles. Studies on kinetics, thermal and heat transfer effects. *Can. J. Chem. Eng.*, 69(4):907–915, 1991.

[191] United States Departmet of Agriculture Forest Service Forest Products Laboratory. Wood handbook - wood as an engineering material. General Technical Report FPL-GTR-190, 2010.

[192] M. G. Grønli and M. C. Melaaen. Mathematical model for wood pyrolysis - Comparison of experimental measurements with model predictions. *Energ. Fuels*, 14(4):791–800, 2000.

[193] C. K. Lee, R. F. Chaiken, and J. M. Singer. Charring pyrolysis of wood in fires by laser simulation. *Symp. Int. Combust.*, 16(1):1459 –1470, 1977.

[194] J. Rath, M. G. Wolfinger, G. Steiner, G. Krammer, F. Barontini, and V. Cozzani. Heat of wood pyrolysis. *Fuel*, 82(1):81–91, 2003.

[195] L.E. Brown. *An Experimental and Analytical Study of Wood Pyrolysis*. PhD thesis, University of Oklahoma, 1972.

[196] B.V. Babu and A.S. Chaurasia. Pyrolysis of biomass: improved models for simultaneous kinetics and transport of heat, mass and momentum. *Energ. Convers. Manage.*, 45(9):1297 – 1327, 2004.

[197] Z. Duan, B. He, and Y. Duan. Sphere Drag and Heat Transfer. *Scientific Reports*, 5(1):12304, 2015.

[198] I. Obernberger and G. Thek. Physical characterisation and chemical composition of densified biomass fuels with regard to their combustion behaviour. *Biomass Bioenerg.*, 27(6):653–669, 2004.

[199] H. Luo, Z. Lu, H. Wu, P.A. Jensen, and P. Glarborg. Devolatilization of single wood particles - impact of particle density and moisture content. (unpublished results), 2018.

[200] H. Lu. *Experimental and Modeling Investigations of Biomass Particle Combustion*. PhD Thesis, Bringham Young University, 2006.

[201] N. Guo, T. Li, L. Zhao, and T. Løvås. Eulerian-lagrangian simulation of pulverized biomass jet using spheroidal particle approximation. *Fuel*, 239:636–651, 2019.

[202] M. Dall'Ora. *Reactivity and burnout of wood fuels*. PhD thesis, Technical University of Denmark, Department of Chemical Engineering, 2011.

[203] R.I. Backreedy, L.M. Fletcher, J.M. Jones, L. Ma, M. Pourkashanian, and A. Williams. Co-firing pulverised coal and biomass: a modeling approach. *P. Combust. Inst.*, 30(2):2955 – 2964, 2005.

[204] L. Ma, J.M. Jones, M. Pourkashanian, and A. Williams. Modelling the combustion of pulverized biomass in an industrial combustion test furnace. *Fuel*, 86(12):1959 – 1965, 2007.

[205] J. Blondeau and H. Jeanmart. Biomass pyrolysis in pulverized-fuel boilers: Derivation of apparent kinetic parameters for inclusion in CFD codes. *P. Combust. Inst.*, 33(2):1787 – 1794, 2011.

[206] H. Luo, H. Wu, W. Lin, and K. Dam-Johansen. Heat transfer corrected isothermal model for devolatilization of thermally-thick biomass particles, 11 2017. Paper presented at Nordic Flame Days, Stockholm, Sweden.

[207] S. Badzioch and P. G. W. Hawksley. Kinetics of thermal decomposition of pulverized coal particles. *Ind. Eng. Chem. Proc. D.D.*, 9(4):521–530, 1970.

[208] J.B. Rawlings and J.G. Ekerdt. *Chemical Reactor Analysis and Design Fundamentals*. Nob Hill Publishing, 2 edition, 2002. p. 515-520.

[209] S. Wiklund, D. Nilsson, L. Eriksson, M. Sjøstrøm, S. Wold, and N. Faber. A randomization test for PLS component selection. *J. Chemometr.*, 21:427 – 439, 10 2007.

Appendix A Paper in Dansk Kemi

This chapter in the appendix is a paper in press in Danish for the popular science Danish chemistry journal, "Dansk Kemi". The title is "Bestemmelse af koksindholdet i biomasse", which translates to "Determination of char yield in biomass". The paper is due to be published in the Summer 2019.

Bestemmelse af koksindholdet i biomasse

Ved at benytte multivariat dataanalyse kan koksindholdet i biomasse forbrændt ved høje opvarmningsrater kvantificeres. Det er essentielt for arbejdet med at opnå en bedre forståelse for udbrændingen af biomasse i kraftvarmeværker.

Af Anna Leth-Espensen, Peter Glarborg, Peter Arendt Jensen, DTU Kemiteknik

Abstrakt

Klimaforandringer har øget interessen for produktion af strøm og varme med mere miljøvenlige metoder. De genanvendelige energikilder udgjorde ca. 3.6 % af den samlede energimængde brugt i verden i 2017, og tendensen er stigende [1]. Mange steder omlægges energi- og varmeproduktion til mere klimavenlige metoder, fx hos Ørsted, hvor kul ikke længere vil blive brugt i kraftværker fra 2023. For at sikre en stabil varme- og energiforsyning må andre mere klimavenlige løsninger anvendes, og til denne gruppe regnes forbrænding af biomasse. Biomasseforbrænding kan foregå ved forskellige processer. I Danmark produceres en stor del af strøm- og varmeforsyningen i pulverfyrede kedler.

Forbrænding af biomassepartiklerne sker ved en afgasning efterfulgt af oxidation af den dannede koksrest. Ved biomasseforbrænding sker en stor del af energifrigivelsen ved forbrænding af de flygtige afgassede produkter. Det er i modsætning til kulafbrænding, hvor koksforbrændingen giver det langt største bidrag.

Fraktionen af biomasse, der omdannes til koks, er blevet undersøgt ved en række eksperimenter, og det har vist sig, at den kan variere en del afhængigt af driftsforholdene. Ved modellering af fyrrumsprocesserne og for at opnå en forbedret forståelse af udbrændingen er det væsentligt at have kendskab til den dannede koksmængde. Koksindholdet varierer som funktion af bl.a. opvarmningshastighed, omgivelsernes temperatur og indholdet af kalium[2]. På basis af resultater fra tidligere udførte forsøg er det ved hjælp af multivariat dataanalyse muligt at præsentere en formel [2], der kan bestemme koksindholdet i biomasse under betingelser, der svarer til suspensionsfyring. Den dækker både træ og andre bioenergiafgrøder. Formlen er testet med uafhængigt data fra litteraturen og bestemmer koksindholdet med en RMSEP (Root mean squared error of prediction) på 0.9 vægt% (tør, askefri basis) for træ og 1.1-2.7 vægt% (tør, askefri basis) for andre bioenergiafgrøder.

Betingelser i suspensionsfyrede kedler

Suspensionsfyring foregår i kedler, hvor biomassestøv blæses ind i swirl-stabiliserede flammer og brænder ved høje temperaturer. Biomassestøvet består af partikler med en omtrentlig størrelse på 100 µm - 2 mm. Temperaturen i fyrrummet ligger typisk i

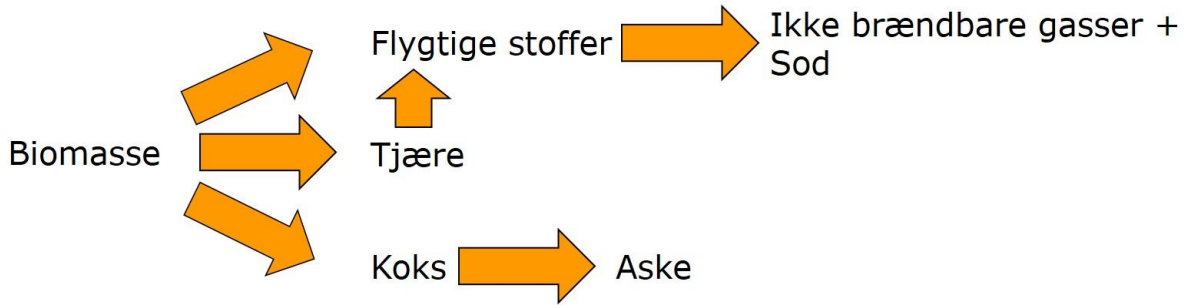

Figur 1: Skematisk oversigt over forbrænding af biomassepartikler.

intervallet 1000-1900 K. Denne kombination gør at opvarmningsraten for partiklerne i nogle tilfælde kan overstige 10^5 K/s[3].

Forskellen på kul og biomasse

Suspensionsfyring foregår ofte i anlæg, der oprindeligt er designet til fyring med kul. Kul- og biomasseforbrænding adskiller sig på en række punkter. Pga. fibrene i biomasse er det mere energikrævende at findele disse, og kulpartikler i suspensionsfyrede anlæg vil derfor typisk være mindre. Desuden er indholdet af flygtige gasser højere og brændværdien mindre for biomasse [4]. De uorganiske forbindelser i biomasse vil også ofte være mere problematiske for driften pga. risiko for belægning og korrosion.

Forbrænding af en biomassepartikel

Når biomassepartikler brænder under suspensionsfyring foregår flere processer samtidigt. Groft sagt kan biomassefyring beskrives af de følgende processer: Opvarmning, frigivelse af vand, frigivelse af flygtige gasser og tjære, omdannelse af tjære til gas, forbrænding af flygtige gasser og forbrænding af koks. En simplificeret oversigt over denne proces kan ses i figur 1. Processen, hvor der frigives gasser og tjære under iltfattige betingelser, kaldes pyrolyse. De gasser, der frigives gennem pyrolyse, forbrænder langt hurtigere end koksen. For at modellere biomassepartikelforbrænding korrekt er det derfor vigtigt at bestemme, hvilken fraktion koksen udgør.

Multivariat dataanalyse

Multivariat dataanalyse, også kendt som kemometri, kan bruges til at beskrive kemiske og biologiske datasæt, således at sammenhænge kan belyses kvantitativt. Kemometriske metoder er beskrevet grundigt andetsteds [5]. I dette studie er benyttet PCA (pricipal component analysis) og PLS (partial least squares regression). Formålet er at bestemme sammenhængen mellem fysisk-kemiske karakteristika ved biomassen og koksudbyttet. For at bestemme koksindholdet er der samlet data fra litteraturen, der beskriver koksmængden fra biomassepyrolyseforsøg, hvor betingelserne ligner dem, der ses i suspensionsfyrede anlæg. Forsøgene, der ligger til grund for denne model, dækker intervallerne givet i tabel 1. Det er også i disse parameterspand, modellen er gyldig.

Tabel 1: Data, der ligger til grund for modellen stammer fra Trubetskaya et al.[6,7].

Parameter	Min.	Max.
Partikelstørrelse [mm]	0,13	0,93
Max. temperature [K]	873	1673
Opvarmningshast. [10^3 K/s]	0,10	12
Kaliumindhold [vægt% tør]	0.02	0.37

Resultater

Analysen, beskrevet nærmere i [2], viser, at biomasse med et højere kaliumindhold har et højere koksudbytte, og at biomasse, der udsættes for højere maximale temperaturer og/eller opvarmningshastigheder, får et lavere koksudbytte. Desuden viser analysen, at partikelstørrelsen for biomassestøvpartiklerne ikke influerer direkte på koksudbyttet. Partikelstørrelsen har dog en indirekte indflydelse, da den påvirker opvarmningshastigheden. For træ pyrolyseret under betingelser relevante for suspensionsfyring (bl.a. beskrevet i tabel 1) er koksudbyttet bestemt vha. ligning (1).

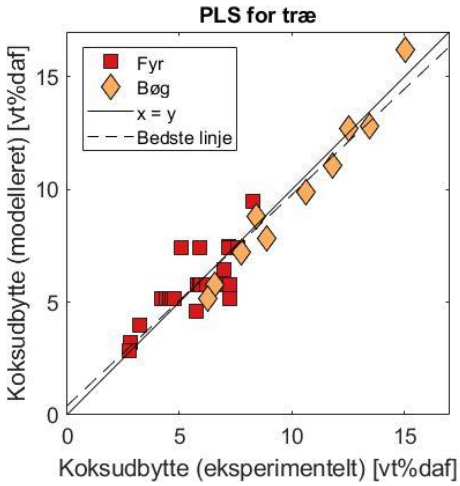

Figur 2: Modelleret og eksperimentelt bestemt koksudbytte for forsøg foretaget ved betingelser relevante for suspensionsfyring. Modellen er udviklet på baggrund af de målte data. Sammenligning med uafhængige datasæt findes i [2]. Figur modificeret fra [2].

Her er C koksudbyttet i vægt% tør askefri basis, K er kaliumindholdet i biomassen i vægt% tør basis, T er den maksimale temperatur i K og H er opvarmningshastigheden i K/s.

$$C = 10^{3,4370+0,6852\cdot K-0,6598\cdot \log(T)-0,2130\cdot \log(H)} \quad (1)$$

Både den målte og det fra modellen bestemte koksudbytte for data fra Trubetskaya et al.[6,7] kan ses i figur 2.

For biomassetyper med højere kaliumindhold er ligning (1) for koksudbyttet også brugt, hvor der er korrigeret for det højere kaliumindhold. Højere kaliumindhold er typisk for fåårige planter, som fx strå eller elefantgræs, der ofte bruges som bioenergiafgrøder. Den katalytiske effekt af kalium, der medfører et højere koksudbytte under biomassepyrolyse, aftager ved kaliumindhold omkring 0,53 vægt% tør basis. Ønskes det at udregne koksudbyttet for pyrolyse af biomasse med kaliumindhold højere end 0,53 vægt% tør basis er K sat til 0,53 i ligning (1). Både det målte og det med modellen estimerede koksudbytte for en række bioenergiafgrøder kan ses i figur 3.

Perspektivering

Modelleringen af koksudbyttet i suspensionsfyrede anlæg præsenteret her er en del af arbejdet på DTU Kemiteknik med at beskrive forbrænding af biomasse. Igangværende arbejde inkluderer både modellering og eksperimentelle forsøgsserier. Fx arbejdes der i øjeblikket på en pyrolysemodel, der kan tage højde for biomassepartiklers morfologi, og CFD (computational fluid dynamics)-simuleringer af partikelforbrænding.

Samarbejde og tak

Ørsted A/S, Burmeister and Wain Scandinavian Contractors A/S og Rambøll A/S takkes for støtte og godt samarbejde. Desuden tak til Nordic 5 Tech (N5T) alliancen og Ørsted A/S for finansiel støtte.

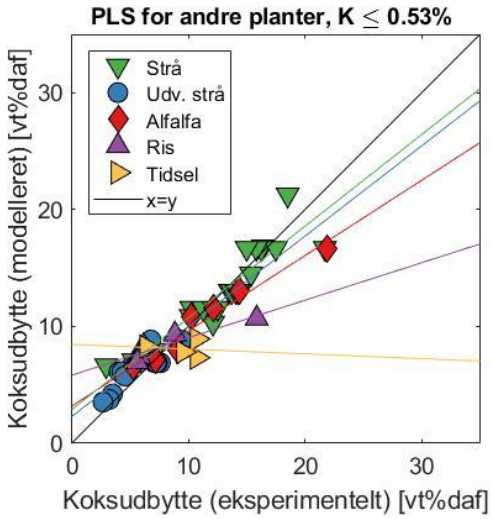

Figur 3: Modelleret og eksperimentalt bestemt koksudbytte for fåårige planter. Alfalfa, hvedestrå og kardontidsel har kaliumindhold højere end 0,53 vægt% tør basis, så K er i disse tilfælde sat til 0,53. Udv. = udvasket. Alle eksperimentelle data stammer fra Trubetskaya et al.[6,7], undtagen dem for kardontidsel, der kommer fra Jiménez et al.[8]. Figur modificeret fra [2].

E-mail:
Anna Leth-Espensen, annlete@kt.dtu.dk
Peter Arendt Jensen, paj@kt.dtu.dk

Kilder

[1] BP Statistical Review of World Energy, 67th Edition, June 2018
[2] A. Leth-Espensen, P. Glarborg, P.A. Jensen, Energy Fuels, 2018, 32, 9572-9580
[3] J.M. Johansen, PhD Thesis, DTU Kemiteknik, 2015
[4] Phyllis2, database for biomass and waste, https://www.ecn.nl/phyllis2, Energy research Centre of the Netherlands
[5] L. Eriksson, E. Johansson, N. Kettaneh-Wold, S. Wold, Multi- and Megavariate Data Analysis Principles and applications, Umetrics AB, 2001
[6] A. Trubetskaya, P.A. Jensen, , A. D. Jensen, M. Steibel, H. Spliethoff, P. Glarborg, Fuel Process. Technol., 2015, 140, 205-214
[7] A. Trubetskaya, P.A. Jensen, A.D. Jensen, A. D. G. Llamas, K. Umeki, P. Glarborg, Fuel Process. Technol., 2016, 143, 118-129
[8] S. Jiménez, P. Remacha, J.C. Ballesteros, A. Giménez, J. Ballester, Combust. Flame, 2008, 152, 588-603

Appendix B Paper A

This chapter in the appendix is the paper "Predicting Biomass Char Yield from High Heating Rate Devolatilization Using Chemometrics"[137] by Leth-Espensen, A; Glarborg, P.; and Jensen, P.A. in the original formatting as printed in Energy & Fuels 2018, 32, 9572-9580. This appendix also include the supplementary material available online.

energy&fuels

Article

Cite This: Energy Fuels 2018, 32, 9572−9580

pubs.acs.org/EF

Predicting Biomass Char Yield from High Heating Rate Devolatilization Using Chemometrics

Anna Leth-Espensen, Peter Glarborg, and Peter Arendt Jensen*

Department of Chemical and Biochemical Engineering, Technical University of Denmark, Søltofts Plads 229, 2800 Kgs. Lyngby, Denmark

Supporting Information

ABSTRACT: This study provides a simple model for biomass char yield obtained under conditions relevant for suspension firing. Using the multivariate data analysis methods, principal component analysis (PCA) and partial least-squares regression (PLS regression), an equation is presented, which predicts the char yield for wood and herbaceous biomass. The model parameters are heating rate (0.1−12 $\cdot 10^3$ K/s), average particle size (0.13−0.93 mm), maximum temperature (873−1673 K), potassium content (from 0.02 wt %db and upward), and char yield (1−15 wt %daf). The model is developed based on wood biomass data and subsequently expanded to include straw and other herbaceous biomass. It is validated against experimental data from the literature, and in general, it exhibits the same characteristics. Independent data sets of wood are predicted with an average error (RMSEP) of 0.9 wt %point daf and straw with an RMSEP = 0.9 wt %daf for the model, when a slope/intercept correction is applied or RMSEP = 1.1 wt %daf otherwise. To include herbaceous biomass, the model introduces a potassium cut off level at 0.53 wt %db, because the catalytic effect of potassium on the devolatilization process levels off above this concentration. The model consists of one equation, making implementation into CFD and devolatilization models possible without adding to the computational costs.

1. INTRODUCTION

The increased awareness of climate change has resulted in a demand for a more sustainable power and heat production. One possible option is suspension firing of biomass, which is often economically advantageous, because biomass particles can be utilized in existing boilers originally constructed for coal combustion. Combustion of single particles, regardless of whether they are coal or biomass, in suspension fired boilers includes devolatilization followed by volatile and char combustion. The combustion of the released volatiles happens relatively fast within the visual flame, while the char combustion is a more time-consuming process.[1,2] Consequently, it is important to know the fractions of volatiles and char for prediction of the burnout of the fuel. The volatile and char fractions are also often used as input parameters in combustion models.[3−5] Differences between coal and biomass particles include, e.g., particle size, chemical composition, and volatile fraction,[6] all of which influence the obtainable char yield. Since so many parameters influence the process, char yield fractions are often determined experimentally for each individual fuel batch, but this is time-consuming and laborious under suspension firing conditions.

Several experimental studies[7−12] have investigated how typical suspension fired conditions influence the char yield of different types of biomass. Typical conditions for suspension firing include high heating rates (>1000 K/s), high final temperatures (>1000 K), and small particles (<3 mm). For fully devolatilized wood particles, char yields in the range of 1−15 wt % dry ash free basis (daf) have been observed.[7,8] Experimental results obtained under suspension firing conditions have shown that particle size,[7−9] final temperature,[7,8,10,11] heating rate,[8] and alkali content[7,8,12] influence the obtained char yield. Higher values for both particle size and potassium content result in a higher char yield for suspension firing conditions. For an increase in particle size, the tendency is weak,[8] whereas the potassium content shows a strong correlation to char yield up to approximately 0.5 wt %db of the biomass.[8] Values above 0.5 wt %db seem not to change the char yield further. An increase in final temperature and/or heating rate yields an exponentially decreasing correlation with char yield.[8]

In this study, the influence of different experimental and material parameters on biomass char yield has been examined through multivariate data analysis. The use of multivariate data analysis to determine biomass thermal conversion properties is limited, but a few examples have been found in literature. Acquah et al.[13] have made a chemometric analysis for predicting the results of thermogravimetric analysis (TGA) experiments, Kim et al.[14] used principal component analysis (PCA) to study biomass properties after exposure to CO_2, and wood pellet properties have been studied using PCA by both Toscano et al.[15] and Mancini et al.[16] To the knowledge of the authors, no papers predicting the char yield of high heating rate experiments with the help of multivariate data analysis have been published. Neves et al.[17] made an empirical model for char yield obtained from devolatilization at final temperatures up to 1273 K and heating rates in the order of 1−100 K/s. Trubetskaya et al.[18] made a one-dimensional kinetic model of the char yield, fitting a set of differential equations.

Received: June 14, 2018
Revised: August 8, 2018
Published: August 9, 2018

DOI: 10.1021/acs.energyfuels.8b02073
Energy Fuels 2018, 32, 9572−9580

Table 1. Data Used for Model Evaluation[a]

	paper	reactor	part. size	final temp.	HR	K content	#
		[mm]	[K]	[10^3 K/s]	[wt %db]		
A	Chen et al.[39]	DTR	0.35	1073	2.4*	0.05*	1
B	Dall'Ora et al.[7]	EFR	0.30	1273−1573	4.6−11*	0.03−0.1	4
C	Septien et al.[9]	DTR	0.36−0.82	1273−1673	1.2−8.1*	0.08−0.09	6
D	Zhang et al.[11]	DTR	0.25	1273	12*	0.03*	1
E	Jiménez et al.[37]	EFR	0.35	1073−1448	10	>0.53*	4

[a]Only data for fully devolatilized particles are taken from the cited papers. Data above the dashed line are from wood biomass experiments. Data below the dashed line are from herbaceous material. *Estimated value as described in supplementary material. HR = Heating rate. # = Number of data points. EFR = Entrained flow reactor. DTR = Drop tube reactor. Potassium levels in herbaceous material are accounted for in section 3.6. Typical potassium levels in *Cynara Cardunculus* (used by Jiménez et al.[37]) is studied by Solano et al.,[38] and the potassium content is taken from the latter.

This paper has two main purposes. First, it presents an exploratory investigation into data from devolatilization of biomass under suspension firing conditions using the key input parameters: particle size, final temperature, heating rate, and potassium content. This investigation is conducted through a principal component analysis (PCA). Subsequently, a model using aforementioned data to predict char yield is presented. The prediction model is calculated using partial least-squares regression (PLS). The model is interpreted, evaluating the importance of the input parameters in a quantifiable way. The prediction model is simple, so it can be implemented into more complicated models and CFD simulations without adding substantial computational time.

2. METHOD

Chemometrics is the subject of extracting information from chemical measurements with a statistical approach. Commonly used methods within chemometrics are PCA and PLS.[19−21] In-depth descriptions of PCA and PLS is beyond the scope of this paper but can be found in the literature.[19−24] The PCA and PLS models presented here are made in PLS Toolbox version 8.1.1 and Matlab version 9.3.0 (R2017b). The data have been extracted from the relevant papers using WebPlotDigitizer version 4.1.

2.1. Definitions of Parameters Used for Model Development. The input parameters to the models are particle size, final temperature, heating rate, and potassium content, as they affect char yield from high heating rate biomass devolatilization.[8,17] In the scope of this paper, **particle size** is defined as the average between the upper and the lower sieve sizes used for determination of biomass particle size. The sieve size average is used, because it is frequently available and for simplicity. As biomass can vary in size and shape, more complicated measures exist.[25] **Final temperature** is the final or maximum temperature of the applied reactor. **Heating rate** can be obtained, e.g., via a thermocouple in a wire mesh reactor. Otherwise, the heating rate is estimated as described in the Supporting Information. The **potassium content** is here defined as the potassium content in wt % dry basis (db) of the original biomass. In papers where the potassium content is not published, it is estimated as described in the Supporting Information. The **char yield** is defined as the percentage of ash free char from a dry ash free biomass sample.

2.2. Selection of Data Applicable for Model Development. The interest of this study is the final char yield after suspension firing; hence, only data for fully devolatilized particles have been used both for model development and model evaluation. The data set used for developing the model is obtained in a wire mesh reactor (WMR) and a drop tube reactor (DTR), originates from Trubetskaya et al.,[8,10] and will be referred to as the calibration set. Any data that fulfills the requirements indicated below will be used for independent validation of the model and is referred to as the validation set. The papers used for validation are given in Table 1. The data have been obtained in EFRs and DTRs as noted in the table. Particles were considered to have obtained full devolatilization if a paper showed consistent results for particle yield fractions over time, and/or the residence time was long compared to the particle size.[8] Data which describe the char yield for fully devolatilized particles are scarce in literature, and papers[26−32] that do not provide data on fully devolatilized particles have been omitted from the study. Likewise, papers[33,34] where the experimental conditions are outside the parameter intervals for the calibration data set are also omitted from this study. The parameter intervals are given in Table 2 for woody biomasses.

Table 2. Parameter Span for Which the Model for Wood Biomass Is Made[a]

parameter	min	max
size [mm]	0.13	0.93
final temperature [K]	873	1673
heating rate [10^3 K/s]	0.10	12*
K content [wt %db]	0.02	0.37

[a]The full data set containing 37 data points from Trubetskaya et al.[8,10] can be seen in the supplementary material. The herbaceous biomass model uses the same parameter spans except for the potassium content, where there is no upper limit; see section 3.6. *Estimated value as described in the supplementary material.

Furthermore, char yield data[35,36] obtained from reactor types (e.g., fluid bed reactors), where particle and operating conditions are vastly different from suspension firing conditions, may not be comparable and have been disregarded.

As the amount of published data describing char yield for nonwood biomass is limited, the presented model is developed based on wood biomass only. Considerations regarding expansion of the model to include herbaceous biomass char yield are presented in sections 3.5 and 3.6. The parameter spans valid for the herbaceous char yield model are identical to the ones presented in Table 2, except the potassium content, which has no upper limit for the herbaceous model.

2.3. Preprocessing. Preprocessing is performed to develop a robust model. The parameters have been preprocessed individually to ensure linearity between parameters and char yield, as PLS is a linear regression method. The reader is referred to Figures 2-4 + 6 in the paper[8] where the calibration

DOI: 10.1021/acs.energyfuels.8b02073
Energy Fuels 2018, 32, 9572−9580

set is originally presented for documentation of the correlations between the four independent parameters and char yield. For **particle size**, the correlation seems linear, so no individual preprocessing method is applied here. **Final temperature** and **heating rate** show an exponentially decreasing correlation to char yield. It is, however, possible that it can be approximated by a linear correlation in the parameter span relevant for suspension firing. Both logarithmic and no individual preprocessing (linear correlation) are tested as possibilities. The **potassium content** seems to have a linear correlation to char yield until approximately 0.5 wt %db,[8] above which the effect of the potassium levels off. As the latter is only relevant for nonwoody biomass, since no woody samples had potassium levels above 0.5 wt %db, no preprocessing of the potassium content parameter has been tested. An overview of the combinations in which the preprocessings have been tested is presented in Table 3. The data is collected in two matrices: **X** containing values for the independent variables and **Y** containing the dependent char yield values.

Table 3. Overview of Tested PLS Models for Wood Biomass[a]

model #	size	FT	HR	KC	CY	ExpVarY [%]	RMSECV [wt %points daf]
1	x	x	x	x	x	72.9	1.6
2	x	x	log(x)	x	x	81.8	1.3
3	x	log(x)	log(x)	x	x	81.7	1.4
4	x	x	log(x)	x	log(x)	81.5	1.1
5	x	log(x)	log(x)	x	log(x)	81.3	1.1
6	-	x	x	x	x	77.6	1.5
7	-	x	log(x)	x	x	88.6	1.1
8	-	x	x	x	log(x)	80.5	1.4
9	-	x	log(x)	x	log(x)	86.5	1.0
10	-	log(x)	log(x)	x	log(x)	86.5	1.0
11	-	log(x)	log(x)	x	x	88.8	1.1

[a]All models are made with one PLS component. ExpVarY and RMSECV are average values of at least 10 cross validation runs. ExpVarY = Explained variance in **Y**, FT = final temperature, HR = heating rate, KC = potassium content, CY = char yield. x = parameter is included. - = parameter not included directly as input parameter.

All parameters in the presented model have additionally been scaled to account for unit variance, to ensure that parameters contribute numerically equal regardless of the unit in which they have been measured.

2.4. Cross Validation. The cross validation performed in this study is based on the random subset method, because the information, regarding duplicates and chronology of experiments in the papers[8,10] containing the data used for the calibration set, is scarce. The random subset method is described by Dubitzky et al.[40] and ensures that the entire parameter span is used for cross validation. In this paper, the cross validation is made with six splits and six iterations, i.e., each subset consists of approximately 17% of the data set. The cross validation is performed at least 10 times for all models described in Table 3. The explained variances in **Y** and RMSECV values are averages of the performed cross validations. The calibration set contains two different types of woody biomass, pine and beech. A common cross validation approach is to remove one type of biomass to see if the remaining biomass type would give similar results. In this case, however, it could lead to dubious results, because of the differences in char yield values. In other words, as the two biomass types are primarily producing two different ranges of char yield values, using one type to predict the other would require an extrapolation of the model, which is undesirable.

3. RESULTS

3.1. Principal Component Analysis. A PCA reveals systematic behavior in a data set. Ideally, the data should be a normal distribution, but even when this is not the case, PCA can reveal some systematic behavior in a data set. In this case, only the first two principal components (PCs) are deemed to be of interest, so only these are shown in Figure 1. The loading plots for Figure 1 can be seen in the Supporting Information. In the direction of the first PC, there is a separation of the data points into biomass type. Within each biomass type, there is also a correlation to char yield in the direction of the first PC. In the direction of the second PC, the scattering due to differences in char yield is more pronounced. Since the data show systematic behavior with respect to char yield in the PCA, a PLS model is developed.

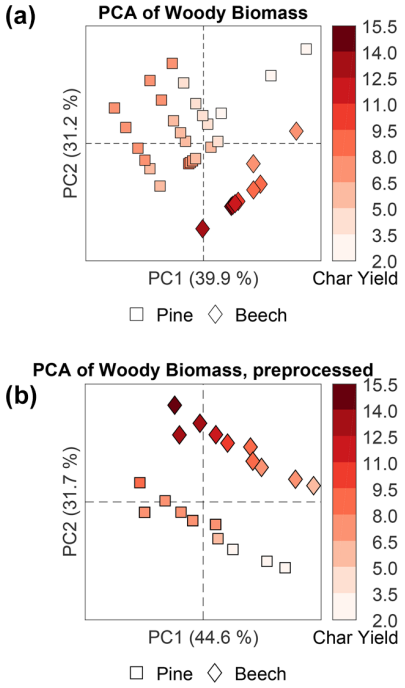

Figure 1. PCA plot for the 37 biomass data points from Trubetskaya et al.[8,10] given in the Supporting Information colored by char yield [wt %daf]. Explained variances in PC1 and PC2 are given in the parentheses on the axes. Loading plots can be seen in the Supporting Information. (a) Original variables. (b) Preprocessed variables corresponding to model 10 presented in Table 3. Some of the pine samples are located identically, which means not all are visible in this plot.

3.2. Partial Least-Squares Regression Model. The PLS model is developed to be able to predict the char yield of woody biomasses and thereby also the volatile yields. The preprocessing methods described in section 2.3 have been tested in different combinations reported in Table 3.

DOI: 10.1021/acs.energyfuels.8b02073
Energy Fuels 2018, 32, 9572−9580

On the basis of the RMSECV and explained variance in **Y**, the most well-performing models are numbers 7, 9, 10, and 11. As previously noted, a logarithmic correlation is likely between the final temperature and the char yield; hence, models 10 and 11 are preferred over models 7 and 9. All graphs presented in the paper have been inspected for both models 10 and 11, but as they are qualitatively similar, only one set will be presented. Since the RMSECV (and RMSEP given in section 3.4) are lower for model 10, it will be preferred. As stated in Table 3, the size parameter is not included in model 10, and in general, when the size parameter is included, the regression models seem to predict the char yield less accurately than when it is omitted. This will be discussed in the subsequent section 4. One PLS component is used for prediction in all of the PLS models reported here. Various plots were inspected for outlier detection, but none have been found. An example of hotelling T^2 vs Q residuals is presented in the Supporting Information.

In Figure 2, the cross validated predicted char yields have been plotted as a function of the measured char yield for model 10. The figure shows good agreement between the two, and the model has RMSECV = 1.0 wt %point and r^2 = 0.87. The model is condensed to a regression vector, which is given both for the preprocessed data and for the raw data in Table 4.

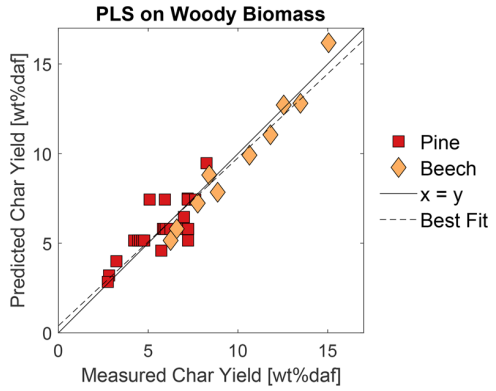

Figure 2. PLS plot of model 10 for the wood biomass calibration set.

Table 4. Regression Vectors for Model 10

parameter	reg. vec. (preprocessed)	reg. vec. (raw data)
intercept	0	3.4370
log(FT)	−0.4521	−0.6598
log(HR)	−0.6850	−0.2130
K content	0.5713	0.6852

The char yield can be predicted for new data, by converting the regression vector values back to the values they would have without the preprocessing. Thus, the char yield from wood devolatilization can be predicted for new data from eq 1.

$$CY_{wood} = 10^{3.4370+0.6852\cdot KC-0.6598\cdot\log(FT)-0.2130\cdot\log(HR)} \quad (1)$$

Here CY_{wood} is the char yield in wt %daf, KC is the potassium content in wt %db, FT is the final temperature in K, and HR is the heating rate in K/s.

3.3. General Tendencies. The general tendencies predicted by the model can be seen in Figure 3a–c. In Figure 3a, it can be seen that the char yield decreases for increasing final temperature. In Figure 3b, it can be seen that the char yield decreases rapidly with increasing heating rate in the lower end of the heating rate range and that the changes are leveling out for higher values of the heating rate. Figure 3a,b show an exponential correlation between heating rate, final temperature, and char yield. Figure 3c shows that the char yield increases as a function of increasing potassium concentrations in the biomass. All of these findings are in good agreement with the experimental observations made by Dall'Ora et al.,[7] Trubetskaya et al.,[8] and Septien et al.[9]

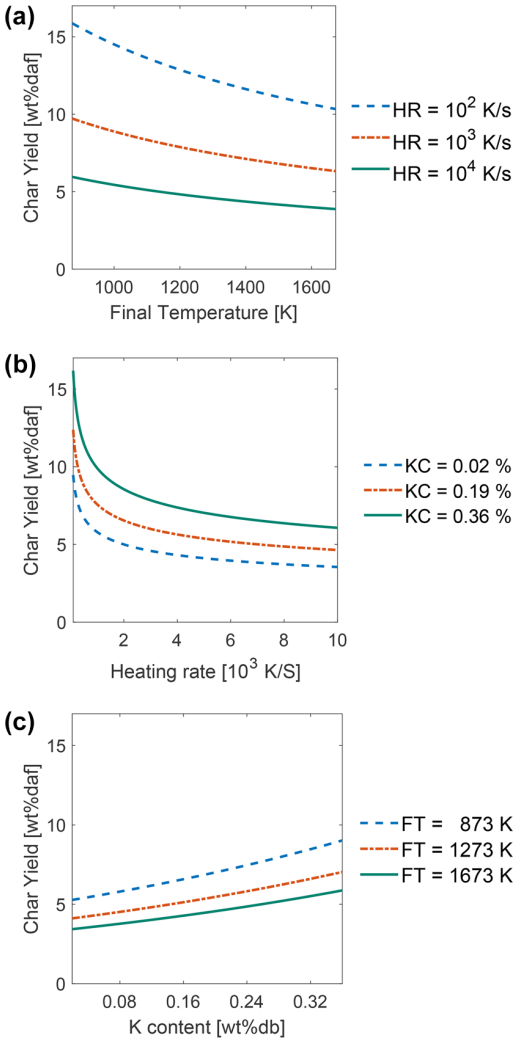

Figure 3. Model predictions for different parameters. HR = heating rate, KC = potassium content in [wt %db], FT = final temperature. (a) K content = 0.19 wt%db. (b) Final temperature = 1273 K. (c) heating rate = 5000 K/s.

3.4. Model Validation with External Data. The model has been validated with data from external experimental studies given in Table 1. The predicted and measured char yield values for the external data is depicted in Figure 4.

The figure shows predicted vs measured char yield for the validation data. There are limited data available for external validation, but in general, the data are predicted well. More data, especially in the upper char yield range, would be preferable in order to evaluate this part of the model as well. RMSEP is 0.9 wt %points for the external data. In other words,

DOI: 10.1021/acs.energyfuels.8b02073
Energy Fuels 2018, 32, 9572−9580

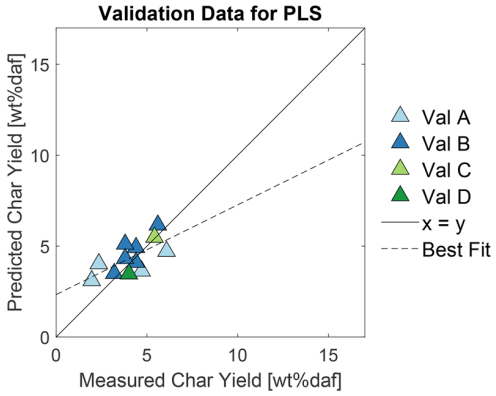

Figure 4. PLS plot for model 10 for the validation data given in Supporting Information. Best fit line is for the validation data. Val A from Dall'Ora et al.,[7] Val B from Septien et al.,[9] Val C from Chen et al.,[39] and Val D from Zhang et al.[11] The validation data are only in the lower end of the char yield range. The axes values are the same as in Figure 2 for comparability.

the average error for predicted biomass char yield for the completely independent data sets is ±0.9 wt % points, which is low and similar to the RMSECV value of 1.0 wt %points, indicating that the model is robust.

3.5. Predicting Char Yield of Straw. Straw is also a commonly used biomass fuel in suspension fired boilers. Trubetskaya et al.[8,10] have conducted experiments with wheat straw, but no additional wheat straw data obtained under suspension firing conditions applicable as validation data have been found. Consequently, a model for straw char yield has been developed by making a slope/intercept correction to the wood biomass model. An advantage of this approach is that the model is modified to give the best possible fit for the data, so biomass samples that are very similar are predicted well. Another advantage is that the slope/intercept is unbiased in determining the communal importance of the input parameters. A disadvantage of the slope/intercept is that it is not applicable for data that is different from the data used to modify the model. The following model is hence only valid for straw/herbaceous material, which has the same characteristics as the wheat straw given in the Supporting Information. The predicted vs measured wheat straw char yield can be seen in Figure 5. It can be seen that the data are approximately linear, which strengthens the validity of expanding the model by a slope/intercept correction. Slope/intercept corrections are a standard procedure described both in academia[41] and industry.[42] A more generally applicable model is presented in section 3.6.

The slope/intercept correction is further supported by the results in Figure 6a,b, which show PCA plots for the original calibration set together with validation data and straw data. Since the validation data for wood are occupying the same space in the PCA vector space as the calibration set, it is plausible that the prediction model is applicable also for the validation set, which is in good agreement with the results observed in section 3.4. The straw data are located away from the calibration set in the PCA plot, so applying the char yield model for wood directly as presented in eq 1 is not likely to yield useful results. The differences in locations in the PCA plots are primarily attributable to the potassium content being higher for straw. However, it is worth noticing that the tendency with respect to char yield in the PCA vector space is

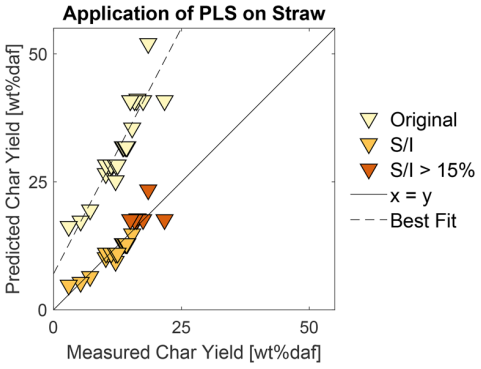

Figure 5. Predicted vs measured char yield for model 10 in [wt %daf] for straw data by Trubetskaya et al.[8,10] both for the original and the slope/intercept corrected model. The measured char yield data above 15 wt %daf are colored a darker orange to indicate which predicted values are found by extrapolation of the model. S/I = slope/intercept corrected model. The dashed best fit line is for the original model. The slope intercept corrected model has been corrected to have the best fit as the $y = x$ line. Straw data is given in the Supporting Information.

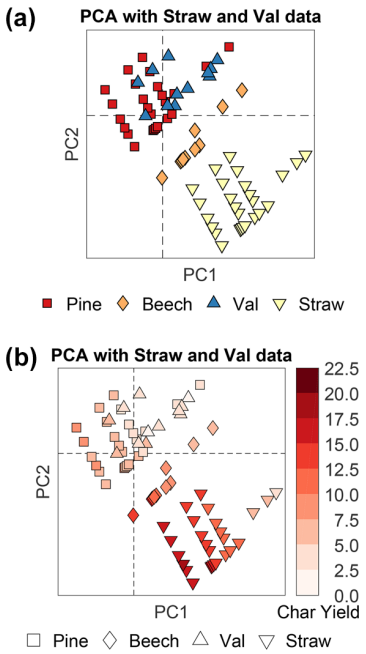

Figure 6. Validation data and straw data incorporated into the PCA first introduced in Figure 1a.

the same for straw and woody data, so a slope/intercept corrected model is appropriate. Since some of the char yields for the straw exceed the maximum char yield in the calibration set, these data points have been excluded before making the slope/intercept correction. They are removed because having to extrapolate a PLS model is generally not advisable. As can be seen in Figure 5, the removed straw data are approximately located on a straight line with the same slope as the remaining straw data, so the changes obtained by removing them are minor. A comparison of the model statistics with and without char yield data above 15 wt %daf and the original straw data can be seen in Table 5. The expression for straw char yield can be seen in eq 2. The equation has not been validated against an

DOI: 10.1021/acs.energyfuels.8b02073
Energy Fuels 2018, 32, 9572−9580

Table 5. Model Statistics for the PLS Model for the Cross Validated Calibration Set for Woody Biomass, the Validation Data for Woody Biomass, and the Straw Data[a]

included data	RMSE [wt %points daf]	r^2
woody cross validated calibration data, model 10	1.0*	0.87
woody validation data, model 10	0.9**	0.45
straw, model 10	19.8**	0.82
straw, model 10 (S/I)	1.8**	0.82
straw, model 10 (S/I), yield <15 wt %daf	0.9**	0.93

[a]The original straw model (model 10) has been reported as well as slope/intercept corrected data with and without char yield data above 15 wt %daf. *RMSECV. **RMSEP.

external validation set and should thus be used more cautiously than the model for wood biomass, especially if the potassium content is vastly different in the sample in which one wants to predict the char yield.

$$CY_{straw} = \frac{10^{(3.4370+0.6852\cdot KC-0.6598\cdot\log(FT)-0.2130\cdot\log(HR))} - 10.6603}{1.4963} \quad (2)$$

Here CY_{straw} is the char yield in wt %daf, KC is the potassium content in wt %db, FT is the final temperature in K, and HR is the heating rate in K/s.

3.6. Predicting Char Yield of Herbaceous Material.

Straw is not the only herbaceous material used for suspension firing, and a more broadly applicable char yield model would be advantageous. A possible way of modifying the model for wood presented in eq 1 in order to include additional biomass species is to determine the potassium concentration at which the catalytic effect of this compound levels off. An advantage of this approach is a more versatile model, but it comes at the cost of lower model accuracy. The cut off level for the effect of potassium is here determined from the wheat straw experimental data by Trubetskaya et al.,[8,10] and the cut off level is then tested for other herbaceous material experimental data by Trubetskaya et al.[8,10] and independent data by Jiménez et al.[37]

As previously mentioned, the linear correlation observed in the experimental data between char yield and potassium content levels off around 0.5 wt %db, so the 1.1 wt %db reported for the straw in the experiments used for model generation will likely cause an overshoot in the prediction of the char yield, if the wood model were used. However, if the wood model is used with a correction in potassium content, some of the differences between wood and herbaceous biomass can be highlighted. To determine the concentration where the effect of potassium levels off, the RMSEP for the straw is used as an optimization parameter; the lower the RMSEP, the better. For the given straw data, the potassium content, which yields the lowest squared error (RMSEP) between measured and predicted straw char yield, is 0.53 wt %db. So for biomass with a potassium content above 0.53 wt %db, the input to the model in eq 1 should be fixed at 0.53 wt %db. Figure 7 depicts the predicted vs measured straw char yield, if one uses the wood biomass model with the real straw potassium content and with a potassium content of maximum 0.53 wt %db. This indicates that the major differences in biomass char yield for wood and straw are a result of the catalytic effects of potassium in the devolatilization process. This is further strengthened

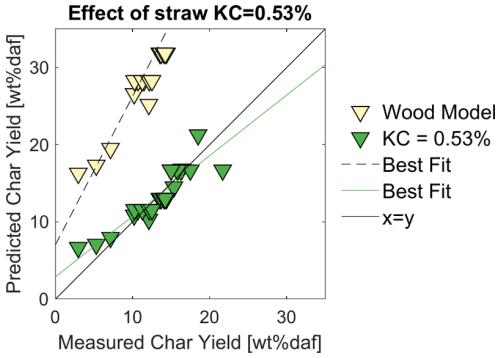

Figure 7. Predicted vs measured char yield for model 10 in [wt %daf] for the original straw data by Trubetskaya et al.[8,10] and for the wood model with a cut off value of KC = 0.53 wt %db. KC = potassium content.

when the cut off value of 0.53 wt %db is used for other herbaceous biomass, as shown in Figure 8. Using the same cut

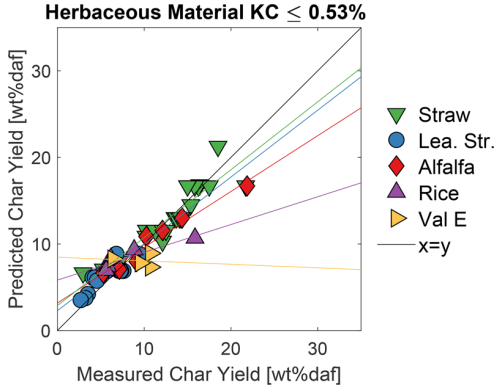

Figure 8. Predicted vs measured char yield for model 10 in [wt %daf] for leached wheat straw, rice husk, alfalfa, and wheat straw. The latter two have a cut off value of KC = 0.53 wt %db. The leached wheat straw has KC = 0.13 wt %db. Rice husk KC = 0.25 wt %db. Val E = validation data from Jiménez et al.[37] from *Cynara cardunculus* thistle with a cut off value of KC = 0.53 wt %db. KC = potassium content. Best fitted lines for all biomass types can be seen in their respective colors.

off value of 0.53 wt %db on different herbaceous biomass types shows that the change in potassium content accounts for the majority of the difference in char yield between wood and herbaceous material in general, but the potassium content cut off value of 0.53 wt %db is not equally good for all biomass types. RMSEP values and r^2 values for the herbaceous biomass can be seen in Table 6.

4. DISCUSSION

The model is generally good at predicting char yield from woody biomass from both the calibration data set and from externally sourced data with RMSECV = 1.0 wt %point and RMSEP = 0.9 wt %point, respectively. Model validity is further supported by the PCA, which shows that the char yield is correlated to one or more parameters in the data set. Expansion of the model to include wheat straw, by a slope/intercept correction, also yields good modeled results: RMSEP = 0.9 wt %point for straw with a char yield below 15 wt %daf. The model is further expanded to include different herbaceous

DOI: 10.1021/acs.energyfuels.8b02073
Energy Fuels 2018, 32, 9572−9580

Table 6. Model Statistics for Herbaceous Biomass[a]

biomass type	RMSEP [wt %points daf]	r^2
wheat straw	1.6	0.82
wheat straw, yield <15 wt %daf	1.1	0.93
leached wheat straw	1.4	0.70
alfalfa	2.2	0.95
rice husk	2.7	0.86
thistle (Val E)	2.3	0.01

[a]With a cut off value for potassium of 0.53 wt %db in model 10. The cut off value for potassium has been determined by determining the minimal possible RMSEP for the straw data, all data points included. Validation data are below dashed line.

biomass of higher potassium contents. For the versatile model, the RMSEP = 1.1 wt %daf for straw with a char yield below 15 wt %daf.

An advantage of developing a model using chemometrics is the prevention of bias in the selection of which parameters should have the most influence in the model, namely, false assumptions about how the parameters influence the char yield and which physical phenomena are more important. Parameters are only excluded from the developed model if they do not enhance the prediction accuracy of the desired dependent parameter, specifically the char yield.

In this study, the particle size is excluded as a direct input parameter to the model in the development process, because inclusion decreases the model accuracy. This can be observed by comparing the model statistics for models 1−5 with the ones for models 6−11 in Table 3, where the RMSECV and the explained variance in **Y** both increase when the size is excluded. It is possible that the reduction to a simple mean sieve size is too crude an estimate for a biomass particle distribution, as biomass particle sizes are generally difficult to determine.[25] Even when the size parameter is omitted, it is still implicit in the model as the size affects the wood particle heating rate.

The heating rate can be difficult to determine accurately. In a WMR, which was used to generate most of the calibration set data,[8] the heating rate can be controlled, but in other reactor types, it must be estimated, as seen in the Supporting Information. In the present work, a simple model is utilized to estimate particle heating rates, based on the assumption that the calculated heating rate for an isothermal particle is a reasonable approximation of the heating rate in the real particle. The larger the particle, the worse the assumption with respect to isothermicity. The assumption is justifiable, because the model yields consistent results both through the cross and external validation.

The potassium cut off value of 0.53 wt %db for biomass is useful in expanding the model to include more biomass types. It is, however, also an additional parameter, which has been fitted and which requires validation. The cut off value results in RMSEP = 2.2 wt %daf for alfalfa and RMSEP = 2.3 wt %daf for thistle, which is comparable to the RMSEP values for the herbaceous biomass with lower potassium levels. The accuracy of the model should be considered taking into account that the char yield is usually otherwise determined by proximate analysis, which overestimates the char yield for suspension firing conditions more than is the case for the model presented here.

For all models presented in this paper, there is a tendency that the char yield is slightly overpredicted for low char yields and underpredicted for high char yields as indicated by the best fit lines in Figures 2, 4, 7, and 8. This indicates that the model does not account for extreme values very well and that the PLS models do not account for all variations in the data sets. One possibility of enhancing prediction would be to develop PLS models with a higher number of input parameters, which would also allow for a higher number of PLS components in the model development phase. A disadvantage in using more input parameters is that usefulness of the model diminishes if complicated measurements are necessary to determine the char yield. For the purpose of presenting a simple model for biomass char yield as an input parameter to more complicated devolatilization models/CFD, the current compromise between complexity and accuracy has been deemed sufficient.

The model is limited by the uncertainties related to measurements in the original data, which was reported to have a measurement error of ±5 wt % within a 90% confidence interval. For a char yield of 10 wt %daf, this corresponds to a char yield of 10 ± 0.5 wt %daf. This should be compared to an RMSEP = 0.9 wt %points. The average error made by the prediction model is just shy of twice the error reported for the calibration set data, which is considered as being reasonable taking the number of parameters and data points into account, especially considering the difficulty of determining uncertainties in high heating rate experiments.

It is possible to increase the quality of the model by conducting additional devolatilization experiments in EFRs and WMRs. This should be done primarily to explore the design space more systematically but also to increase the amount of experimental data. In the design space covered by the experiments for the calibration set, the input parameters are correlated to the degree seen in the correlation coefficient chart in Figure 9. The chart gives the correlation (negative or positive) between the input parameter values chosen in the experiments. The higher the absolute value in the coefficient chart, the more the two parameters are correlated in the conducted experiments. It is advantageous not to have a high correlation between parameters in order to be able to

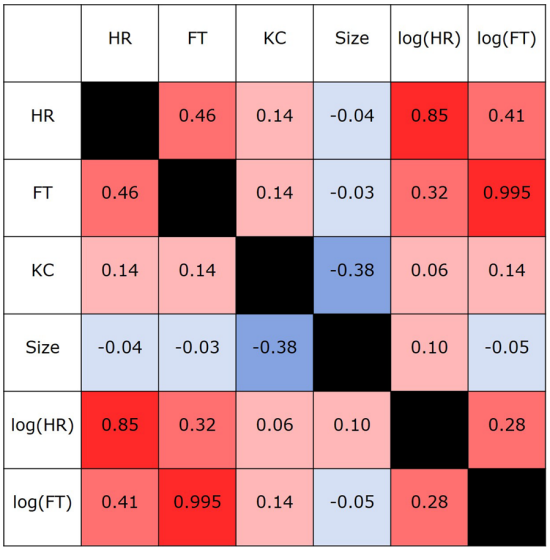

Figure 9. Correlation coefficient chart for the parameters used to obtain the calibration set of wood biomass data.

DOI: 10.1021/acs.energyfuels.8b02073
Energy Fuels 2018, 32, 9572−9580

determine the effects of the individual parameters. Despite being generally good, the chart still suggests that variations in the particle size have not been tested equally for the two wood types, which would have been optimal. The correlation between heating rate and final temperature might be more difficult to separate as they are physically linked, but more WMR experiments could decouple these two parameters.

5. CONCLUSION

Often a proximate analysis is used to determine the char yield for a biomass sample; however, for suspension firing combustion conditions with high heating rates and high final temperatures, the char yields are lower. The models presented in this paper can be used to more accurate estimations of char yield under suspension firing conditions.

Through PCA and PLS, experimental char yield data from woody biomass particles have been used to develop a simple model for predicting the char yield of woody biomass with an RMSECV = 1.0 wt %daf. The input parameters for the model are final temperature, heating rate, and potassium content. Validation of the model has been carried out using experimental data from four different studies, which gave an RMSEP = 0.9 wt %daf. The model has been expanded to include wheat straw by applying a slope/intercept correction, which yielded an RMSEP = 0.9 wt %daf. At a slight cost in model accuracy, the model is further expanded to include all herbaceous biomass. This gives RMSEP = 1.1 wt %daf for straw and slightly higher RMSEP values for other herbaceous biomass. The expansion is conducted by determining the potassium content, where the catalytic effects of potassium on the devolatilization process levels off. The value is determined to be 0.53 wt %db. Thus, the char yield of biomass can be determined from eq 1 repeated below.

$$CY_{biomass} = 10^{3.4370+0.6852\cdot KC-0.6598\cdot\log(FT)-0.2130\cdot\log(HR)}$$

Here $CY_{biomass}$ is the char yield in wt %daf, FT is the final temperature in K, HR is the heating rate in K/s, and KC is the potassium content in wt %db; if KC > 0.53 wt %db, then KC = 0.53 in the above equation. The model is relevant for suspension firing conditions.

■ ASSOCIATED CONTENT

Supporting Information

The Supporting Information is available free of charge on the ACS Publications website at DOI: 10.1021/acs.energyfuels.8b02073.

Raw data for chemometric analysis, supplementary plots from the analysis, and a model for estimating missing parameters in char yield data (PDF)

■ AUTHOR INFORMATION

Corresponding Author

*E-mail: paj@kt.dtu.dk.

ORCID

Anna Leth-Espensen: 0000-0001-8183-4928

Peter Glarborg: 0000-0002-6856-852X

Notes

The authors declare no competing financial interest.

■ ACKNOWLEDGMENTS

The authors gratefully acknowledge the financial and advisory support received from Ørsted A/S, Burmeister and Wain Scandinavian Contractors A/S, and Rambøll A/S. We also thank the Nordic Five Tech (N5T) alliance for financial support.

■ NOMENCLATURE

Abbreviations

CFD = computational fluid dynamics
CY = char yield
daf = dry ash free base
db = dry base
DTR = drop tube reactor
EFR = entrained flow reactor
FT = final temperature
HR = heating rate
KC = potassium content
LV = latent variables
PC = principal component
PCA = principal component analysis
PLS = partial least-squares regression
RMSE = root mean squared error
TGA = thermogravimetric analysis
WMR = wire mesh reactor
wt = weight

Greek Characters

ϵ = emissivity coefficient [-]
μ = dynamic viscosity [Pa·s]
ρ = density [kg/m^3]
σ = Stefan−Boltzmann constant [J/(s·m·^{2}K^4]

Roman Characters

C_p = specific heat capacity [J/(kg·K)]
D = diameter [m]
g = gravity acceleration constant [m^2/s]
h = convective heat transfer coefficient [J/(s·m·^{2}K]
k = thermal conductivity [J/(s·m·K)]
n = number of data points
Nu = Nusselt Number
Pr = Prandtl Number
Re = Reynolds Number
T = temperature [K]
v = velocity [m/s]
y = measured char yield value for experiment i [wt %]
$\hat{y}$ = predicted char yield value for experiment i [wt %]
X = matrix of independent parameters
Y = matrix of dependent parameters

Sub- and Superscripts

p = particle
CV = cross validation
end = final or maximum value of, e.g., the temperature
g = gas
i = index number
ini = initial value
P = prediction

■ REFERENCES

(1) Lu, Z.; Jian, J.; Jensen, P. A.; Wu, H.; Glarborg, P. Influence of Torrefaction on Single Particle Combustion of Wood. *Energy Fuels* **2016**, *30*, 5772−5778.

DOI: 10.1021/acs.energyfuels.8b02073
Energy Fuels 2018, 32, 9572−9580

(2) Lu, Z.; Jian, J.; Arendt Jensen, P.; Wu, H.; Glarborg, P. Impact of KCl impregnation on single particle combustion of wood and torrefied wood. *Fuel* **2017**, *206*, 684−689.
(3) Ström, H.; Thunman, H. CFD simulations of biofuel bed conversion: A submodel for the drying and devolatilization of thermally thick wood particles. *Combust. Flame* **2013**, *160*, 417−431.
(4) Johansen, J. M.; Jensen, P. A.; Glarborg, P.; Mancini, M.; Weber, R.; Mitchell, R. E. Extension of apparent devolatilization kinetics from thermally thin to thermally thick particles in zero dimensions for woody biomass. *Energy* **2016**, *95*, 279−290.
(5) *ANSYS Fluent 17.2 Theory Guide*. https://www.sharcnet.ca/Software/Ansys/17.2/en-us/help/flu_th/flu_th_sec_disp_law4.html, Accessed: Feb 21, 2018.
(6) Priyanto, D. E.; Ueno, S.; Hashida, K.; Kasai, H. Energy-efficient milling method for woody biomass. *Adv. Powder Technol.* **2017**, *28*, 1660−1667.
(7) Dall'Ora, M.; Jensen, P. A.; Jensen, A. D. Suspension Combustion of Wood: Influence of Pyrolysis Conditions on Char Yield, Morphology, and Reactivity. *Energy Fuels* **2008**, *22*, 2955−2962.
(8) Trubetskaya, A.; Jensen, P. A.; Jensen, A. D.; Steibel, M.; Spliethoff, H.; Glarborg, P. Influence of fast pyrolysis conditions on yield and structural transformation of biomass chars. *Fuel Process. Technol.* **2015**, *140*, 205−214.
(9) Septien, S.; Valin, S.; Dupont, C.; Peyrot, M.; Salvador, S. Effect of particle size and temperature on woody biomass fast pyrolysis at high temperature (1000 - 1400 °C). *Fuel* **2012**, *97*, 202−210.
(10) Trubetskaya, A.; Jensen, P. A.; Jensen, A. D.; Garcia Llamas, A. D.; Umeki, K.; Glarborg, P. Effect of fast pyrolysis conditions on biomass solid residues at high temperatures. *Fuel Process. Technol.* **2016**, *143*, 118−129.
(11) Zhang, Y.; Kajitani, S.; Ashizawa, M.; Miura, K. Peculiarities of Rapid Pyrolysis of Biomass Covering Medium- and High-Temperature Ranges. *Energy Fuels* **2006**, *20*, 2705−2712.
(12) NikAzar, M.; Hajaligol, M. R.; Sohrabi, M.; Dabir, B. Mineral matter effects in rapid pyrolysis of beech wood. *Fuel Process. Technol.* **1997**, *51*, 7−17.
(13) Acquah, G. E.; Via, B. K.; Fasina, O. O.; Adhikari, S.; Billor, N.; Eckhardt, L. G. Chemometric modeling of thermogravimetric data for the compositional analysis of forest biomass. *PLoS One* **2017**, *12*, e0172999.
(14) Kim, K.; Labbé, N.; Warren, J. M.; Elder, T.; Rials, T. G. Chemical and anatomical changes in *Liquidambar styraciflua* L. xylem after long term exposure to elevated CO_2. *Environ. Pollut.* **2015**, *198*, 179−185.
(15) Toscano, G.; Rinnan, Å.; Pizzi, A.; Mancini, M. The Use of Near-Infrared (NIR) Spectroscopy and Principal Component Analysis (PCA) to Discriminate Bark and Wood of the Most Common Species of the Pellet Sector. *Energy Fuels* **2017**, *31*, 2814−2821.
(16) Mancini, M.; Rinnan, Å.; Pizzi, A.; Mengarelli, C.; Rossini, G.; Duca, D.; Toscano, G. Near infrared spectroscopy for the discrimination between different residues of the wood processing industry in the pellet sector. *Fuel* **2018**, *217*, 650−655.
(17) Neves, D.; Thunman, H.; Matos, A.; Tarelho, L.; Gómez-Barea, A. Characterization and prediction of biomass pyrolysis products. *Prog. Energy Combust. Sci.* **2011**, *37*, 611−630.
(18) Trubetskaya, A.; Surup, G.; Shapiro, A.; Bates, R. B. Modeling the influence of potassium content and heating rate on biomass pyrolysis. *Appl. Energy* **2017**, *194*, 199−211.
(19) Wold, S.; Esbensen, K.; Geladi, P. Principal Component Analysis. *Chemom. Intell. Lab. Syst.* **1987**, *2*, 37−52.
(20) Jackson, J. E. *A user's guide to principal components*; John Wiley & Sons, Inc., 1991.
(21) Eriksson, L.; Byrne, T.; Johansson, E.; Trygg, J.; Wikström, C. *Multi- and Megavariate Data Analysis: Basic Principles and Applications*, 3rd ed.; Umetrics Academy, 2013; p 71.
(22) Kjeldahl, K.; Bro, R. Some common misunderstandings in chemometrics. *J. Chemom.* **2010**, *24*, 558−564.
(23) Bro, R.; Smilde, A. K. Principal component analysis. *Anal. Methods* **2014**, *6*, 2812−2831.
(24) Zachariassen, C. B. *Process Analytical Chemistry and Technology in Pectin Production*. Ph.D. Thesis, University of Copenhagen, 2007.
(25) Trubetskaya, A. *Fast pyrolysis of biomass at high temperatures*. Ph.D. Thesis, Technical University of Denmark, 2016.
(26) Dupont, C.; Commandré, J.-M.; Gauthier, P.; Boissonnet, G.; Salvador, S.; Schweich, D. Biomass pyrolysis experiments in an analytical entrained flow reactor between 1073 and 1273 K. *Fuel* **2008**, *87*, 1155−1164.
(27) Lewis, A. D.; Fletcher, T. H. Prediction of Sawdust Pyrolysis Yields from a Flat-Flame Burner Using the CPD Model. *Energy Fuels* **2013**, *27*, 942−953.
(28) Niemelä, N. P.; Tolvanen, H.; Saarinen, T.; Leppänen, A.; Joronen, T. CFD based reactivity parameter determination for biomass particles of multiple size ranges in high heating rate devolatilization. *Energy* **2017**, *128*, 676−687.
(29) Nunn, T. R.; Howard, J. B.; Longwell, J. P.; Peters, W. A. Product Compositions and Kinetics in the Rapid Pyrolysis of Sweet Gum Hardwood. *Ind. Eng. Chem. Process Des. Dev.* **1985**, *24*, 836−844.
(30) Umeki, K.; Kirtania, K.; Chen, L.; Bhattacharya, S. Fuel Particle Conversion of Pulverized Biomass during Pyrolysis in an Entrained Flow Reactor. *Ind. Eng. Chem. Res.* **2012**, *51*, 13973−13979.
(31) Zanzi, R.; Sjöström, K.; Björnbom, E. Rapid high-temperature pyrolysis of biomass in a free-fall reactor. *Fuel* **1996**, *75*, 545−550.
(32) Zanzi, R.; Sjöström, K.; Björnbom, E. Rapid pyrolysis of agricultural residues at high temperature. *Biomass Bioenergy* **2002**, *23*, 357−366.
(33) Johansen, J. M.; Gadsbøll, R.; Thomsen, J.; Jensen, P. A.; Glarborg, P.; Ek, P.; De Martini, N.; Mancini, M.; Weber, R.; Mitchell, R. E. Devolatilization kinetics of woody biomass at short residence times and high heating rates and peak temperatures. *Appl. Energy* **2016**, *162*, 245−256.
(34) Johansen, J. M. *Power Plant Burners for Bio-Dust Combustion*. Ph.D. Thesis, Technical University of Denmark, 2015.
(35) Anastasakis, K.; Kitsiou, I.; de Jong, W. Fast devolatilization characteristics of 'low cost' biomass fuels, wood and reed. Potential feedstock for gasification. *Fuel Process. Technol.* **2016**, *142*, 157−166.
(36) Asadullah, M.; Zhang, S.; Li, C.-Z. Evaluation of structural features of chars from pyrolysis of biomass of different particle sizes. *Fuel Process. Technol.* **2010**, *91*, 877−881.
(37) Jiménez, S.; Remacha, P.; Ballesteros, J. C.; Giménez, A.; Ballester, J. Kinetics of devolatilization and oxidation of a pulverized biomass in an entrained flow reactor under realistic combustion conditions. *Combust. Flame* **2008**, *152*, 588−603.
(38) Solano, M. L.; Manzanedo, E.; Concheso, R.; Curt, M. D.; Sanz, M.; Fernández, J. Potassium fertilisation and the thermal behaviour of Cynara cardunculus L. *Biomass Bioenergy* **2010**, *34*, 1487−1494.
(39) Chen, L.; Dupont, C.; Salvador, S.; Grateau, M.; Boissonnet, G.; Schweich, D. Experimental study on fast pyrolysis of free-falling millimetric biomass particles between 800 and 1000 °C. *Fuel* **2013**, *106*, 61−66.
(40) Dubitzky, W., Granzow, M., Berrar, D. P., Eds. *Fundamentals of Data Mining in Genomics and Proteomics*; Springer, 2007; p 178.
(41) Eskildsen, C. E.; Hansen, P. W.; Skov, T.; Marini, F.; Nørgaard, L. Evaluation of Multivariate Calibration Models Transferred between Spectroscopic Instruments: Applied to near Infrared Measurements of Flour Samples. *J. Near Infrared Spectrosc.* **2016**, *24*, 151−156.
(42) Winning, H. *Standardization of FT-IR instruments*; Foss A/S: Hillerød, Denmark, 2014.

DOI: 10.1021/acs.energyfuels.8b02073
Energy Fuels 2018, 32, 9572−9580

A Biomass Experimental Data

Table S1: wood biomass data for generation of model. HR = heating rate. Estimated values marked with orange.

Biomass	**Equip.**	**Size** mm	**final T** K	**HR** K/s	**K content** wt % daf	**Char yield** wt % daf	**Reference**
Pinewood	DTF	0.3125	1273	5747	0.02	3.2	S1
Beechwood	DTF	0.3125	1273	4382	0.37	7.8	S1
Pinewood	DTF	0.3125	1523	9336	0.02	2.8	S1
Beechwood	DTF	0.3125	1523	7093	0.37	6.6	S1
Pinewood	DTF	0.3125	1673	12208	0.02	2.8	S1
Beechwood	DTF	0.3125	1673	9259	0.37	6.3	S1
Pinewood	WMR	0.125	873	1000	0.02	7.5	S2
Beechwood	WMR	0.125	873	1000	0.36	12.6	S2
Pinewood	WMR	0.125	1273	1000	0.02	5.9	S2
Beechwood	WMR	0.125	1273	1000	0.36	10.6	S2
Beechwood	WMR	0.125	1523	1000	0.36	8.4	S2
Pinewood	WMR	0.125	1273	100	0.02	8.3	S2
Beechwood	WMR	0.125	1273	100	0.36	15.1	S2
Pinewood	WMR	0.125	1273	300	0.02	7.2	S2
Beechwood	WMR	0.125	1273	300	0.36	13.5	S2
Pinewood	WMR	0.125	1273	600	0.02	7.0	S2
Beechwood	WMR	0.125	1273	600	0.36	11.8	S2
Pinewood	WMR	0.125	1273	3000	0.02	5.7	S2
Beechwood	WMR	0.125	1273	3000	0.36	8.9	S2
Pinewood	WMR	0.125	873	1000	0.02	5.1	S2
Pinewood	WMR	0.3025	873	1000	0.02	5.9	S2
Pinewood	WMR	0.39	873	1000	0.02	7.6	S2
Pinewood	WMR	0.5125	873	1000	0.02	7.2	S2
Pinewood	WMR	0.725	873	1000	0.02	7.6	S2
Pinewood	WMR	0.925	873	1000	0.02	7.6	S2
Pinewood	WMR	0.125	1273	1000	0.02	5.8	S2
Pinewood	WMR	0.3025	1273	1000	0.02	5.9	S2
Pinewood	WMR	0.39	1273	1000	0.02	6.0	S2
Pinewood	WMR	0.5125	1273	1000	0.02	6.2	S2
Pinewood	WMR	0.725	1273	1000	0.02	7.0	S2
Pinewood	WMR	0.925	1273	1000	0.02	7.2	S2
Pinewood	WMR	0.125	1523	1000	0.02	4.2	S2
Pinewood	WMR	0.3025	1523	1000	0.02	4.4	S2
Pinewood	WMR	0.39	1523	1000	0.02	4.6	S2
Pinewood	WMR	0.5125	1523	1000	0.02	4.7	S2
Pinewood	WMR	0.725	1523	1000	0.02	4.8	S2
Pinewood	WMR	0.925	1523	1000	0.02	7.2	S2

Table S2: Biomass data for evaluation of model. Estimated values marked with orange. Woody biomass above dashed line. Herbaceous biomass below dashed line.

Biomass	Equip.	Size [mm]	final Temp. K	HR K/s	K content wt % daf	Char Yield wt % (daf)	Reference
Pinewood	EFR	0.3025	1273	6040	0.0332	2.4	S3
Beechwood sawdust	EFR	0.3025	1273	4604	0.0955	6.1	S3
Pinewood	EFR	0.3025	1573	10721	0.0332	2.0	S3
Beechwood sawdust	EFR	0.3025	1573	8138	0.0955	4.7	S3
Beech for food smoking	DTF	0.3565	1273	3601	0.090	3.9	S4
Beech for food smoking	DTF	0.815	1273	1183	0.082	5.2	S4
Beech for food smoking	DTF	0.3565	1473	5349	0.090	3.8	S4
Beech for food smoking	DTF	0.815	1473	1811	0.082	3.3	S4
Beech for food smoking	DTF	0.3565	1673	7704	0.090	2.4	S4
Beech for food smoking	DTF	0.815	1673	2689	0.082	3.3	S4
Hinoki cypress sawdust	DTR	0.25	1273	11997	0.03	4.0	S5
beech wood	DTR	0.35	1073	2393	0.05	5.4	S6
Cynara Cardunculus thistle	EFR	0.35	1073	10000	>0.53	15.3	S7
Cynara Cardunculus thistle	EFR	0.35	1203	10000	>0.53	11.8	S7
Cynara Cardunculus thistle	EFR	0.35	1313	10000	>0.53	14.3	S7
Cynara Cardunculus thistle	EFR	0.35	1448	10000	>0.53	15.3	S7

B Estimating the Missing Parameters

Table S4: The experimentally specific variables necessary for estimating the Heating Rate.

Symbol	Description	Unit
D_p	Diameter of particle	m
T_{end}	Final Temperature of particle	K

Table S5: The parameters to be calculated for estimating the Heating Rate.

Symbol	Description	Unit
$C_{p,g}$	Specific heat capacity of gas	$J/(kg \cdot K)$
k	Thermal conductivity	$J/(s \cdot m \cdot K)$
T	Half way Temperature in particle	K
v_{slip}	slip velocity	m/s
μ	Dynamic Viscosity	$Pa \cdot s$
ρ_g	Density of carrier gas	kg/m^3

Table S3: wood biomass data for evaluation of model. Estimated values marked with orange.

Biomass	**Equip.**	**Size** [mm]	**final Temp.** K	**HR** K/s	**K content** wt % daf	**Char Yield** wt % (daf)	**Reference**
Straw	DTF	0.3125	1273	10000	1.1	7.14	S1
Straw	DTF	0.3125	1523	10000	1.1	5.29	S1
Straw	DTF	0.3125	1673	10000	1.1	2.96	S1
Straw	WMR	0.125	873	1000	1.1	21.7	S2
Straw	WMR	0.125	1273	1000	1.1	14.26	S2
Straw	WMR	0.125	1523	1000	1.1	11.49	S2
Straw	WMR	0.125	1673	1000	1.1	10.21	S2
Straw	WMR	0.125	1273	100	1.1	18.51	S2
Straw	WMR	0.125	1273	300	1.1	16.41	S2
Straw	WMR	0.125	1273	600	1.1	15.37	S2
Straw	WMR	0.125	1273	3000	1.1	12.12	S2
Straw	WMR	0.125	873	1000	1.1	15.83	S2
Straw	WMR	0.3025	873	1000	1.1	16.25	S2
Straw	WMR	0.39	873	1000	1.1	17.5	S2
Straw	WMR	0.5125	873	1000	1.1	15.83	S2
Straw	WMR	0.725	873	1000	1.1	15	S2
Straw	WMR	0.925	873	1000	1.1	15	S2
Straw	WMR	0.125	1273	1000	1.1	13.56	S2
Straw	WMR	0.3025	1273	1000	1.1	13.56	S2
Straw	WMR	0.39	1273	1000	1.1	13.73	S2
Straw	WMR	0.5125	1273	1000	1.1	14.41	S2
Straw	WMR	0.725	1273	1000	1.1	14.07	S2
Straw	WMR	0.925	1273	1000	1.1	14.24	S2
Straw	WMR	0.125	1523	1000	1.1	10.71	S2
Straw	WMR	0.3025	1523	1000	1.1	10.26	S2
Straw	WMR	0.39	1523	1000	1.1	11.28	S2
Straw	WMR	0.5125	1523	1000	1.1	12.18	S2
Straw	WMR	0.725	1523	1000	1.1	12.18	S2
Straw	WMR	0.925	1523	1000	1.1	12.52	S2

Table S6: The constants necessary for estimating the heating rate. Values assumed from literature.

Symbol	Description	Value	Unit	Reference
$C_{p,p}$	Specific heat capacity of particle	$1500 + T_i$	$J/(kg \cdot K)$	S8
g	gravity acceleration constant	9.81	m/s^2	
R	Gas constant	$8.206 \cdot 10^{-5}$	$m^3 \cdot atm\ /(K \cdot mol)$	
ρ_{hinoki}	Density hinoki cypress	400	kg/m^3	S9
ρ_{pine}	Density pine wood	600	kg/m^3	S10
ρ_{beech}	Density beech	800	kg/m^3	S10
σ	Stefan-Boltzmann constant	$5.670367 \cdot 10^{-8}$	$J/(s \cdot m^2 \cdot K^4)$	S11
ϵ	Emissivity Coefficient	0.85	-	S12

B.1 Assumptions

The estimate of the heating rate is based on a number of assumptions given in the list below.

A The heating rate can be represented by a single value even though it varies with time and location in the particle.

B Particles are spherical

C Particle size can be approximated with average of the sieve sizes.

D Particles are uniform, i.e. no pores.

E Particles are isothermal.

F Particle properties as for example density are uniform throughout the particle.

G No chemical reaction adds to the energy balance.

H All gasses are inert and ideal.

I The temperature around the particle can be approximated as the average between the initial and the final temperatures.

J Initial gas temperature is 298 K.

B.2 Temperature Dependent Properties of Nitrogen

From NIST[S13] the properties are collected as temperature dependent properties if nothing else is noted. The carrier gas is nitrogen for all relevant biomass data given in table S1 and S2. Correlation and calculations analogue to the ones presented below can be found for other gasses if relevant. The properties of the carrier gas are temperature dependent. Here the temperature for the estimation is defined in equation (1).

$$T = T_{ini} + \frac{T_{end} - T_{ini}}{2} \tag{1}$$

B.2.1 Density of Nitrogen

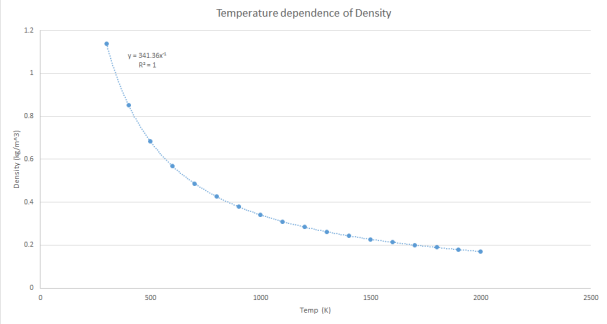

Figure S1: The correlation between Density and Temperature for N_2. Data from NIST.[S13]

The density temperature correlation is given in equation (2).

$$\rho_{N_2} = 341.36\frac{1}{T_g} \tag{2}$$

B.2.2 Heat capacity of Nitrogen

$$C_p = A + B \cdot \frac{T_g}{1000} + C \cdot \left(\frac{T_g}{1000}\right)^2 + D \cdot \left(\frac{T_g}{1000}\right)^3 + E \cdot \left(\frac{1000}{T_g}\right)^2 \tag{3}$$

Where the constants are given in table S7.

Table S7: Constants for the Shomate Equation for Nitrogen in the interval 500-2000 K.

A	B	C	D	E
19.50583	19.88705	-8.598535	1.369784	0.527601

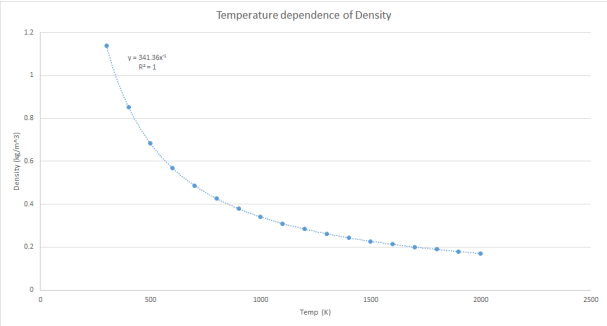

Figure S2: The correlation between Heat Capacity and Temperature for N_2. Data from NIST.[S13]

B.2.3 Viscosity of Nitrogen

Data from NIST. A third degree polynomial is fitted to the data, which yields $R^2 = 1$. Gives the correlation given in equation (4). As this polynomial is fitted to the given data it is only valid in the temperature range 300-2000 K.

$$\mu_g = 3 \cdot 10^{-9} \cdot T_g^3 - 2 \cdot 10^{-5} \cdot T_g^2 + 0.0508 \cdot T_g + 4.2787 \tag{4}$$

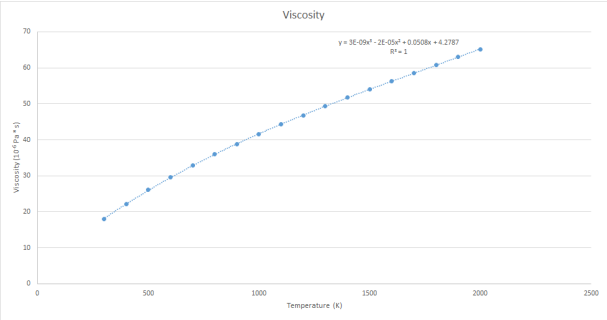

Figure S3: The correlation between Viscosity and Temperature for N_2. Data from NIST.[S13]

B.2.4 Thermal Conductivity of Nitrogen

Data from NIST. A second degree polynomial is fitted to the data, which yields $reg^2 = 1$. Gives the correlation given in equation (4). As this polynomial is fitted to the given data it is only valid in the temperature range 300-2000 K.

$$k = -7 \cdot 10^{-9} \cdot T_g^2 + 7 \cdot 10^{-5} \cdot T_g + 0.0069 \tag{5}$$

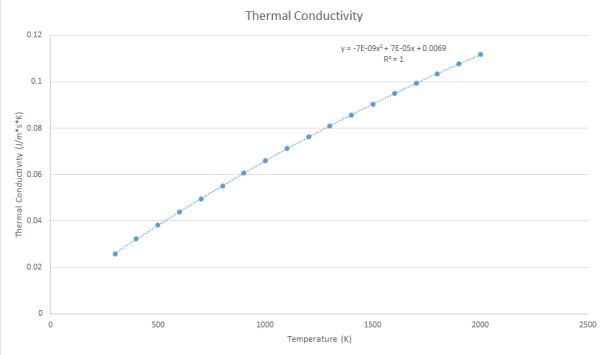

Figure S4: The correlation between Conductivity and Temperature for N_2. Data from NIST.[S13]

B.3 Calculating the Reynolds Number and Prandtl Number

The Reynolds Number for a sphere in a fluid is given by equation (6).[S14]

$$Re_p = \frac{\rho_g \cdot v_p \cdot D_p}{\mu} \tag{6}$$

Where ρ_g is the density of the carrier gas (here N_2), v_p is the particle velocity as calculated in equation (7) or (8),[S15*]. D_p is the particle diameter, and μ is the dynamic viscosity of the carrier gas.

$$v_p = \frac{D_p^2 \cdot g \cdot (\rho_p - \rho_g)}{18 \cdot \mu} \tag{7}$$

Where g is the gravitational acceleration constant. Equation (7) is only valid for $10^{-4} < Re_p < 1$. Within this limit the flow is in the Stokes regime. I.e. it is assumed that the flow is strictly laminar. This must be checked by calculating he Reynolds number. An example can be seen in section B.5. For Reynolds number in the range 2 to 400 equation (8) can be used instead. Here the Reynolds number must likewise be tested

*In Kemiske Enhedsoperationer by Clement et al.[S15] the correlations are given in equation (7.8)

to see if it is within the given range. For flow with a Reynolds number between 1 and 2 the correlation given by Oseen[S15†] can be used. They are not relevant for the data used here, so the reader is encouraged to seek more information if relevant.

$$v_p = 0.153 \cdot \left(\frac{(\rho_p - \rho_g) \cdot D_p^{1.6} \cdot g}{\mu^{0.6} \cdot \rho_g^{0.4}} \right)^{0.714} \tag{8}$$

The Prandtl Number is given in equation (9).

$$Pr = \frac{C_{p,g} \cdot \mu}{k} \tag{9}$$

B.4 Calculating the Heating Rate

The Nusselt number is approximately 2 for very small particles,[S16] but it has an increasing influence the larger the particles. To ensure consistency it is here calculated regardless of particle size. Numerous numerical correlations between Nu, Re, and Pr exist.[S17,S18‡] A simple and widely used[S19] correlation to calculate the averaged nusselt number for flow around a sphere was presented by Ranz and Marshall[S17,S20§] and is given in equation (10).

$$Nu = 2 + 0.6 \cdot Re^{1/2} \cdot Pr^{1/3} \tag{10}$$

Furthermore the Nusselt number is defined as in equation (11).

$$Nu = \frac{h \cdot D_p}{k} \Leftrightarrow h = \frac{Nu \cdot k}{Dp} \tag{11}$$

Heat transfer through thermal conduction is described in chapter 14.1 in Transport Phenomena, equation 14.1-1.[S17] Heat transfer through radiation is described in section 16.5. From these the heating rate of a solid sphere can be calculated assuming the sphere is uniform and isothermal. The equation for calculating the heating rate is given in equation (12).

$$HR = \frac{1}{C_{p,p} \cdot \rho_p \cdot \frac{4}{3} \cdot \pi (\frac{D_p}{2})^3} \cdot 4 \cdot \pi \cdot (\frac{D_p}{2})^2 \cdot ((T - T_i) \cdot h + \epsilon\sigma(T_g^4 - T^4)) \tag{12}$$

B.5 Example of Estimating the Heating Rate

Usually the given parameters in papers and for experiments are the chemical composition of carrier gas, biomass type, biomass particle diameter, final temperature of reactor system (assuming particle has same final temperature), diameter and volumetric flowrate at normal conditions for the reactor. From this the heating rate should be estimated. The example given here is based on data from DallOra et al.[S3] The necessary data are given in table S8. All numbers in the following subchapter have been rounded due to practical reasons. The calculations are made with all available decimals.

Table S8: Example of data for calculating the heating rate. From Dall'Ora et al.[S3]

Variable	Value	Unit
D_p	$0.1075 \cdot 10^{-3}$	m
T_{end}	1073	K
Biomass Type	Pine Wood	

The temperature is the first thing to calculate. It is assumed that the appropriate temperature is the average between the initial and the final temperature as given in equation (1). For the example given here it is calculated in equation (13).

$$T = 298K + \frac{1073K - 298K}{2} = 686\,K \tag{13}$$

†Information is give on page 185

‡In Transport Phenomena by Bird et al.[S17], the corelations are given in table 14.2-1

§Tn the book Transport Phenomena by Bird et al.[S17] the correlation in presented on page 439, eq. 14.4-5

Since the carrier gas is Nitrogen gas, N_2, the correlations given in equation (2) through (5) can be used to calculate the gas parameters. As these are necessary for subsequent calculations, they are calculated in equation (14) through (17) for convenience.

$$\rho_g = \frac{341.36}{686} = 0.498\, kg/m^3 \tag{14}$$

$$\mu = 3 \cdot 10^{-15} \cdot 686^3 - 2 \cdot 10^{-11} \cdot 686^2 + 0.0508 \cdot 10^{-6} \cdot 686 + 4.2787 \cdot 10^{-6} = 30.7 \cdot 10^{-6}\, Pa \cdot s \tag{15}$$

$$C_{p,g} = 19.50583 + 19.88705 \cdot 0.686 - 8.598535 \cdot 0.686^2 + 1.369784 \cdot 0.686^3 + 0.527601 \cdot (\frac{1000}{686})^2 = 30.7\, J/(kg \cdot K) \tag{16}$$

$$k = -7 \cdot 10^{-9} \cdot 686^2 + 7 \cdot 10^{-5} \cdot 686 + 0.0069 = 0.0516\, J/(s \cdot m \cdot K) \tag{17}$$

If $10^{-4} < Re < 1$ then equation (18) is valid. It is here assumed to be correct and the Reynolds number is then subsequently checked to verify.

$$v_p = \frac{(0.1075 \cdot 10^{-3} m)^2 \cdot 9.81 m/s^2 \cdot (600 kg/m^3 - 0.498 kg/m^3)}{18 \cdot 30.7 \cdot 10^{-6} Pa \cdot s} = 0.123\, m/s \tag{18}$$

Checking the Reynolds Number is done in equation (19).

$$Re = \frac{0.498 kg/m^3 \cdot 0.123 m/s \cdot 0.1075 \cdot 10^{-3} m}{30.7 \cdot 10^{-6} Pa \cdot s} = 0.215 \tag{19}$$

Since the Reynolds number check holds up, the equation chosen to calculate the velocity is appropriate. The Prandtl Number is calculated in equation (20) by using equation (9).

$$Pr = \frac{30.7 J/kg \cdot K) \cdot 30.7 \cdot 10^{-6} Pa \cdot s}{0.0516 J/(s \cdot m \cdot K)} = 0.0182 \tag{20}$$

When the Reynold Number and the Prandtl Number have been calculated the Nusselt Number can be calculated from equation(10). For this example the Nusselt Number is given in equation (21).

$$Nu = 2 + 0.6 \cdot 0.215^{1/2} \cdot 0.0182^{1/3} = 2.07 \tag{21}$$

Using equation (11) the convective heat transfer coefficient can be calculated as in equation (22).

$$h = \frac{2.07 \cdot 0.0516 J/(s \cdot m \cdot K)}{0.1075 \cdot 10^{-3} m} = 995\, J/(s \cdot m^2 \cdot K) \tag{22}$$

And finally the heating rate can be calculated from equation (12) as shown in equation (23).

$$HR = \frac{4 \cdot \pi \cdot (\frac{0.1075 \cdot 10^{-3} m}{2})^2}{1798 J/(kg \cdot K) \cdot 600 kg/m^3 \cdot \frac{4}{3}\pi(\frac{0.1075 \cdot 10^{-3}}{2})^3} \cdot \left((686K - 298K) \cdot 995 J/(s \cdot m^2 \cdot K) + 0.85 \cdot 5.670367 \cdot 10^{-8} J/(S \cdot m^2 \cdot K^4) \cdot ((1073K)^4 - (686)^4) \right) = 22703\, K/s \tag{23}$$

C Estimating the Potassium Content

The potassium content is rarely given in papers and must consequently be estimated. This estimation is here only done when the fraction of ash in the biomass used for experiments is known in order to ensure at least some accuracy. In that case the percentage of potassium in a biomass sample of the same species can be found in literature and this fraction is then assumed to be reasonably close to the real value. The reason for using the original ash fraction to estimate the potassium content is to minimize the potential error due to estimation.

C.1 Example of Estimating the Potassium Content

Dupont et al.[S21] have made high heating rate experiments, where the potassium content for the biomass is not stated. The biomass is a mixture of sylvester pine and spruce. The fraction of the two is not given, so the potassium content for sylvester pine stem wood is found in in a paper by Filbakk et al.[S22] and it is assumed to be representative. According to Filbakk et al the potassium content in sylvester pine is 76 g/kg ash. Using Dupont et al.[S21] as example the necessary parameters are given in table S9.

Table S9: Example of parameters for estimating the potassium content.

Parameter	Value	Unit	Source
Potassium Content in sylvester pine	76	g/kg ash	[S22]
Ash content in original biomass	2.1	wt% db	[S21]

The potassium content in wt% daf is calculated in equation (24).

$$c_K = \frac{76 g/kg\, ash}{1000 g\, ash/kg\, ash} \cdot \frac{2.1 g\, ash}{100 g\, biomass\,(db)} \cdot \frac{100 g\, biomass\,(db)}{(100-2.1) g\, biomass\,(daf)} = 0.163 wt\% daf \qquad (24)$$

D PCA

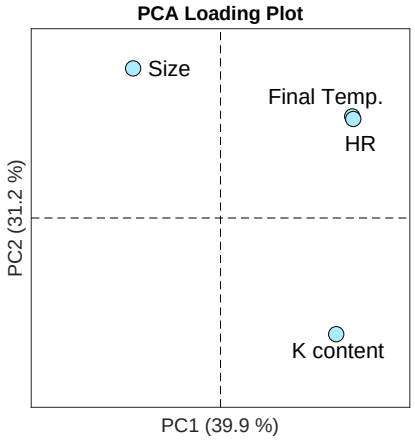

Figure S5: The loading plot for figure 1a. Final temperature and heating rate are positioned almost identically in the loading plot, because they are strongly correlated. HR = Heating rate.

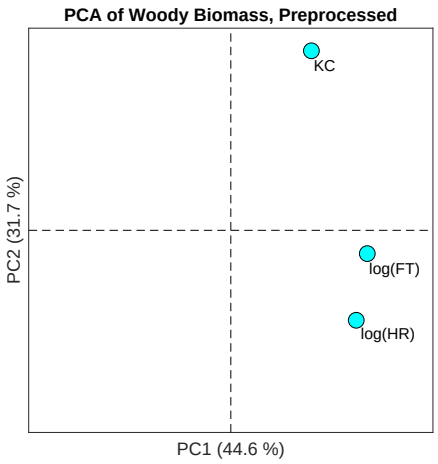

Figure S6: The loading plot for figure 1b. HR = Heating rate, FT = Finalt temperature, KC = potassium content.

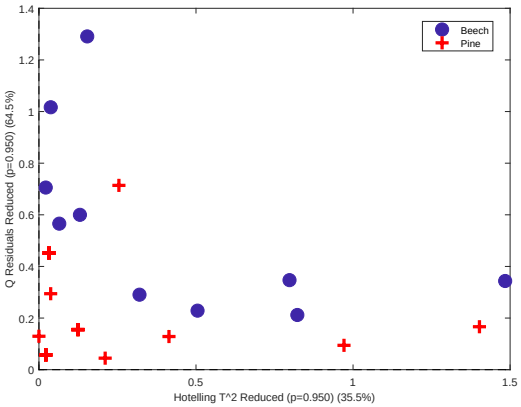

Figure S7: The Q residuals as a function of Hotelling's T^2 for model 10. No outliers are identified. Some pine data points are located identically, which is why only ten points can be seen in the plot.

References

[S1] Anna Trubetskaya, Peter Arendt Jensen, Anker Degn Jensen, Angel David Garcia Llamas, Kentaro Umeki, and Peter Glarborg. Effect of fast pyrolysis conditions on biomass solid residues at high temperatures. *Fuel Process. Technol.*, 143:118–129, 2016. ISSN 03783820. doi: 10.1016/j.fuproc.2015.11.002.

[S2] Anna Trubetskaya, Peter Arendt Jensen, Anker Degn Jensen, Markus Steibel, Hartmut Spliethoff, and Peter Glarborg. Influence of fast pyrolysis conditions on yield and structural transformation of biomass chars. *Fuel Process. Technol.*, 140:205–214, 2015. ISSN 03783820. doi: 10.1016/j.fuproc.2015.08.034.

[S3] Michelangelo Dall'Ora, Peter Arendt Jensen, and Anker Degn Jensen. Suspension Combustion of Wood: Influence of Pyrolysis Conditions on Char Yield, Morphology, and Reactivity. *Energy Fuels*, 22(5):2955–2962, 2008.

[S4] Santiago Septien, Sylvie Valin, Capucine Dupont, Marine Peyrot, and Sylvain Salvador. Effect of particle size and temperature on woody biomass fast pyrolysis at high temperature (1000 - 1400 °C). *Fuel*, 97:202–210, 2012. ISSN 0016-2361. doi: 10.1016/j.fuel.2012.01.049. URL `http://dx.doi.org/10.1016/j.fuel.2012.01.049`.

[S5] Yan Zhang, Shiro Kajitani, Masami Ashizawa, and Kouichi Miura. Peculiarities of Rapid Pyrolysis of Biomass Covering Medium- and High-Temperature Ranges. *Energy Fuels*, 20(6):2705–2712, 2006.

[S6] L. Chen, C. Dupont, S. Salvador, M. Grateau, G. Boissonnet, and D. Schweich. Experimental study on fast pyrolysis of free-falling millimetric biomass particles between 800 °c and 1000 °c. *Fuel*, 106:61 – 66, 2013. ISSN 0016-2361.

[S7] Santiago Jiménez, Pilar Remacha, Juan C Ballesteros, Antonio Giménez, and Javier Ballester. Kinetics of devolatilization and oxidation of a pulverized biomass in an entrained flow reactor under realistic combustion conditions. *Combust. Flame*, 152(4):588–603, 2008. doi: 10.1016/j.combustflame.2007.10.001.

[S8] M.G. Grønli. *A theoretical and experimental study of the thermal degredation of biomass*. PhD thesis, NTNU, 1996.

[S9] Yoshio Kijidani and Yoshimitsu Fujii. Microfibril angle and density of hinoki (Chamaecyparis obtusa) trees in 15 half-sib families in a progeny test stand in Kyushu, Japan. *Journal of Wood Science*, 58 (3):195–202, 2012. doi: 10.1007/s10086-011-1240-8.

[S10] EngineeringToolbox. Densities of wood species. `http://www.engineeringtoolbox.com/wood-density-d\_40.html`, 2016. Accessed: 2018-02-23, Last Modified: 2016-06-03.

[S11] P. J. Linstrom and W. G. Mallard, editors. *"Fundamental Physical Constants, Stefan Boltzmann constant" in NIST Chemistry WebBook, NIST Standard Reference Database Number 69*. National Institute of Standards and Technology, Gaithersburg MD, 20899, 2014. URL `https://physics.nist.gov/cgi-bin/cuu/Value?sigma`.

[S12] Morten G. GrÃ¸nli and Morten C. Melaaen. Mathematical model for wood pyrolysiscomparison of experimental measurements with model predictions. *Energy & Fuels*, 14(4):791–800, 2000. doi: 10.1021/ef990176q.

[S13] M.O. McLinden E.W. Lemmon and D.G. Friend. *"Thermophysical Properties of Fluid Systems" in NIST Chemistry WebBook, NIST Standard Reference Database Number 69*. National Institute of Standards and Technology, Gaithersburg MD, 20899, 2005. URL `http://webbook.nist.gov`.

[S14] Osborne Reynolds. Xxix. an experimental investigation of the circumstances which determine whether the motion of water shall he direct or sinuous, and of the law of resistance in parallel channels. *Philosophical Transactions of the Royal Society of London*, 174:935–982, 1884. doi: 10.1098/rstl.1883.0029. URL `http://rstl.royalsocietypublishing.org/content/174/935.short`.

[S15] K.H. Clement, P. Fangel, A.D. Jensen, and K. Thomsen. *Kemiske Enhedsoperationer*, volume 5. Polyteknisk Forlag, 2 edition, 2009. ISBN 8750209418.

[S16] Zhipeng Duan, Boshu He, and Yuanyuan Duan. Sphere Drag and Heat Transfer. *Nature Publishing Group*, pages 1–7, 2015. doi: 10.1038/srep12304. URL http://dx.doi.org/10.1038/srep12304.

[S17] R.B. Bird, W.E. Stewart, and E.N. Lightfoot. *Transport Phenomena*, volume 1. John Wiley & sons, Inc., rev. 2nd edition, 2007. ISBN 9780470115398.

[S18] Andreas Richter and Petr A Nikrityuk. International Journal of Heat and Mass Transfer Drag forces and heat transfer coefficients for spherical , cuboidal and ellipsoidal particles in cross flow at sub-critical Reynolds numbers. *International Journal of Heat and Mass Transfer*, 55(4):1343–1354, 2012. ISSN 0017-9310. doi: 10.1016/j.ijheatmasstransfer.2011.09.005. URL http://dx.doi.org/10.1016/j.ijheatmasstransfer.2011.09.005.

[S19] Kentaro Umeki, Kawnish Kirtania, Luguang Chen, and Sankar Bhattacharya. Fuel Particle Conversion of Pulverized Biomass during Pyrolysis in an Entrained Flow Reactor. *Ind. Eng. Chem. Res.*, 51(43): 13973–13979, 2012.

[S20] W.E. Ranz and W.R. Marshall. Evaporation from Drops: Part 2. *Chemical Engineering Progress*, 48 (4):173–180, 1952.

[S21] Capucine Dupont, Jean-Michel Commandré, Paola Gauthier, Guillaume Boissonnet, Sylvain Salvador, and Daniel Schweich. Biomass pyrolysis experiments in an analytical entrained flow reactor between 1073 K and 1273 K. *Fuel*, 87(7):1155–1164, 2008. doi: 10.1016/j.fuel.2007.06.028.

[S22] Tore Filbakk, Raida Jirjis, Juha Nurmi, and Olav Høibø. The effect of bark content on quality parameters of Scots pine (Pinus sylvestris L .) pellets. *Biomass and Bioenergy*, 35(8):3342–3349, 2010. ISSN 0961-9534. doi: 10.1016/j.biombioe.2010.09.011. URL http://dx.doi.org/10.1016/j.biombioe.2010.09.011.

Appendix C Paper C: Supplementary Material

This chapter in the appendix is the supplementary material for Paper C.

Table C.1: Model input and output parameters.

ρ	T_g	AR	R	$\Upsilon*$	$t_{devo,2D}$	A(fit)	E_a(fit)	A(PLS)	E_a(PLS)	$t_{devo,0D}$
kg/m^3	K	-	µm		s	s^{-1}	J/mol	s^{-1}	J/mol	s
700	1300	1.01	39.4	96.9	0.016	$1.13{\cdot}10^{8}$	$1.05{\cdot}10^{5}$	$2.39{\cdot}10^{8}$	$1.15{\cdot}10^{5}$	0.017
700	1300	1.01	1560	90.1	4.4	$1.49{\cdot}10^{2}$	$3.44{\cdot}10^{4}$	$5.96{\cdot}10^{1}$	$2.78{\cdot}10^{4}$	5.5
700	1300	3	39.4	96.9	0.019	$5.55{\cdot}10^{8}$	$1.27{\cdot}10^{5}$	$2.03{\cdot}10^{8}$	$1.13{\cdot}10^{5}$	0.016
700	1300	3	1560	90.1	6.0	$1.84{\cdot}10^{1}$	$2.58{\cdot}10^{8}$	$5.06{\cdot}10^{1}$	$2.59{\cdot}10^{4}$	4.9
700	1900	1.01	39.4	98.0	0.0081	$8.86{\cdot}10^{5}$	$6.64{\cdot}10^{4}$	$1.13{\cdot}10^{6}$	$7.77{\cdot}10^{4}$	0.0092
700	1900	1.01	1560	94.2	1.9	1.70	$4.52{\cdot}10^{-11}$	$2.82{\cdot}10^{-1}$	$-9.47{\cdot}10^{3}$	6.2
700	1900	3	39.4	98.0	0.010	$6.52{\cdot}10^{5}$	$7.16{\cdot}10^{4}$	$9.60{\cdot}10^{5}$	$7.58{\cdot}10^{4}$	0.010
700	1900	3	1560	94.2	2.6	1.17	$1.72{\cdot}10^{-6}$	$2.39{\cdot}10^{-1}$	$-1.14{\cdot}10^{4}$	5.0
1300	1300	1.01	39.4	96.5	0.026	$2.19{\cdot}10^{8}$	$1.12{\cdot}10^{5}$	$2.39{\cdot}10^{8}$	$1.15{\cdot}10^{5}$	0.026
1300	1300	3	39.4	96.5	0.031	$8.98{\cdot}10^{8}$	$1.34{\cdot}10^{5}$	$2.03{\cdot}10^{8}$	$1.13{\cdot}10^{5}$	0.026
1300	1900	1.01	39.4	97.7	0.013	$8.72{\cdot}10^{5}$	$6.81{\cdot}10^{4}$	$1.13{\cdot}10^{6}$	$7.77{\cdot}10^{4}$	0.014
1300	1900	1.01	1560	93.4	3.4	$9.29{\cdot}10^{-1}$	$1.00{\cdot}10^{-9}$	$2.82{\cdot}10^{-1}$	$-9.47{\cdot}10^{3}$	3.6
1300	1900	3	39.4	97.7	0.015	$4.68{\cdot}10^{5}$	$7.09{\cdot}10^{4}$	$9.60{\cdot}10^{5}$	$7.58{\cdot}10^{4}$	0.014
1300	1900	3	1560	93.4	4.8	$6.32{\cdot}10^{-1}$	$9.83{\cdot}10^{-8}$	$2.39{\cdot}10^{-1}$	$-1.14{\cdot}10^{4}$	1.6
1000	1600	2.005	799.7	93.2	1.5	7.12	$8.67{\cdot}10^{3}$	$4.64{\cdot}10^{1}$	$2.23{\cdot}10^{4}$	1.8
700	1600	1.01	39.4	97.6	0.011	$5.93{\cdot}10^{6}$	$8.25{\cdot}10^{4}$	$1.28{\cdot}10^{7}$	$9.46{\cdot}10^{4}$	0.011
700	1600	2	39.4	97.6	0.012	$6.63{\cdot}10^{6}$	$8.99{\cdot}10^{4}$	$1.18{\cdot}10^{7}$	$9.36{\cdot}10^{4}$	0.011
700	1600	3	39.4	97.6	0.012	$7.80{\cdot}10^{6}$	$9.38{\cdot}10^{4}$	$1.08{\cdot}10^{7}$	$9.27{\cdot}10^{4}$	0.011
700	1600	5	39.4	97.6	0.014	$9.52{\cdot}10^{6}$	$9.78{\cdot}10^{4}$	$9.20{\cdot}10^{6}$	$9.07{\cdot}10^{4}$	0.011
700	1600	8	39.4	97.6	0.014	$1.10{\cdot}10^{7}$	$1.00{\cdot}10^{5}$	$7.19{\cdot}10^{6}$	$8.78{\cdot}10^{4}$	0.011
700	1600	1.01	400	94.8	0.33	$2.17{\cdot}10^{4}$	$5.26{\cdot}10^{4}$	$8.82{\cdot}10^{2}$	$3.97{\cdot}10^{4}$	0.54
700	1600	2	400	94.8	0.39	$3.47{\cdot}10^{3}$	$4.40{\cdot}10^{4}$	$8.14{\cdot}10^{2}$	$3.87{\cdot}10^{4}$	0.54
700	1600	3	400	94.8	0.41	$2.10{\cdot}10^{3}$	$4.18{\cdot}10^{4}$	$7.49{\cdot}10^{2}$	$3.77{\cdot}10^{4}$	0.54
700	1600	5	400	94.8	0.43	$1.54{\cdot}10^{3}$	$4.08{\cdot}10^{4}$	$6.36{\cdot}10^{2}$	$3.58{\cdot}10^{4}$	0.54
700	1600	8	400	94.8	0.44	$1.35{\cdot}10^{3}$	$4.05{\cdot}10^{4}$	$4.97{\cdot}10^{2}$	$3.29{\cdot}10^{4}$	0.53
700	1600	1.01	755	93.8	0.81	$7.50{\cdot}10^{1}$	$1.85{\cdot}10^{4}$	$6.39{\cdot}10^{1}$	$2.46{\cdot}10^{4}$	1.7
700	1600	2	755	93.8	1.0	$1.70{\cdot}10^{1}$	$1.15{\cdot}10^{4}$	$5.89{\cdot}10^{1}$	$2.37{\cdot}10^{4}$	1.6
700	1600	3	755	93.8	1.0	$1.27{\cdot}10^{1}$	$1.05{\cdot}10^{4}$	$5.43{\cdot}10^{1}$	$2.27{\cdot}10^{4}$	1.6
700	1600	5	755	93.8	1.1	$1.07{\cdot}10^{1}$	$1.00{\cdot}10^{4}$	$4.60{\cdot}10^{1}$	$2.07{\cdot}10^{4}$	1.5
700	1600	8	755	93.8	1.1	9.97	$9.94{\cdot}10^{3}$	$3.60{\cdot}10^{1}$	$1.78{\cdot}10^{4}$	1.5
700	1600	1.01	1560	92.6	2.5	1.64	$2.31{\cdot}10^{3}$	3.18	$7.43{\cdot}10^{3}$	4.0
700	1600	2	1560	92.6	3.2	1.00	$1.13{\cdot}10^{3}$	2.93	$6.46{\cdot}10^{3}$	3.9
700	1600	3	1560	92.6	3.5	$8.85{\cdot}10^{-1}$	$1.00{\cdot}10^{3}$	2.70	$5.49{\cdot}10^{3}$	3.8
700	1600	5	1560	92.6	3.7	$8.17{\cdot}10^{-1}$	$1.01{\cdot}10^{3}$	2.29	$3.53{\cdot}10^{3}$	3.6
700	1600	8	1560	92.6	3.8	$7.87{\cdot}10^{-1}$	$1.06{\cdot}10^{3}$	1.79	$6.05{\cdot}10^{2}$	3.3

{2.7182818284}ϑφερτυθιοπσδφγηξκλ